Stability of Elastic Grid Shells

by

Romain Mesnil

Diplôme d'ingénieur
École Nationale des Ponts et Chaussées, 2013

Submitted to the Department of Civil and Environmental Engineering
in Partial Fulfillment of the Requirements for the Degree of

Master of Engineering

at the

Massachusetts Institute of Technology

June 2013

Signature of Author: _____

Department of Civil and Environmental Engineering
May 10, 2013

Certified by: _____

John A. Ochsendorf
Professor of Building Technology and Civil and Environmental Engineering
Thesis Supervisor

Certified by: _____

Cyril Douthe
Researcher and Structural Engineer at IFSTTAR, Institut français des sciences et
technologies des transports, de l'aménagement et des réseaux
Thesis Supervisor

Accepted by: _____

Heidi Nepf
Chair, Departmental Committee for Graduate Students

Stability of Elastic Grid Shells

by

Romain Mesnil

Submitted to the Department of Civil and Environmental Engineering
in May 10, 2013 in Partial Fulfillment of the Requirements
for the Degree of Master of Engineering in Civil and Environmental Engineering

Abstract

The elastic grid shell is a solution that combines double curvature and ease of mounting. This structural system, based on the deformation of an initially flat grid without shear stiffness was invented more than fifty years ago. The apparition of new materials such as GFRP increased the potential of such structures whose properties depend on the deformation, or equivalently pre-stress of an initial structure. Elastic grid shells seem particularly promising as shelters, lightweight roofs, or kinetic structures.

Although fundamental to the behavior of the strucure, the influence of the pre-stress on the stability of elastic grid shells has yet to be studied. Understanding this phenomenon could allow engineers to design more efficiently elastic grid shells.

This thesis studies the influence of pre-stress on the stability of elastic grid shells. The research conducts a parametric study that focuses both a pre-buckled arch and initially flat circular elastic grid shells with different grid spacing and levels of pre-stress. Realistic values of the parameters are determined from existing projects. The buckling analysis as well as the form-finding of the different structures are performed using finite element analysis. The tools are validated with comparison of the shape and buckling capacity of a pre-buckled arch with existing experiments. The parametric studies lead to recommendations aiming to facilitate the design of elastic grid shells.

Keywords Elastic grid shell, Low-Speed Dynamics, form-finding, linear buckling analysis

Thesis Supervisor: John A. Ochsendorf
Title: Professor of Building Technology Civil and Environmental Engineering

Thesis Supervisor: Cyril Douthe
Title: Researcher and Structural Engineer at IFSTTAR, Institut français des sciences et technologies des transports, de l'aménagement et des réseaux

Stabilité des Grid Shells Élastiques

par

Romain Mesnil

Présentée au Département de Génie Civil et Environnemental
le 10 Mai 2013 dans le cadre de l'obtention du
Diplôme de Master of Engineering in Civil and Environmental Engineering

Résumé

Les grid shells élastiques sont une solution présentant le double avantage de la double courbure et de la facilité de montage. Cette typologie de structure, fondée sur la déformation élastique d'une grille plane sans raideur en cisaillement, a été inventée il y a plus de cinquante ans. L'apparition de nouveaux matériaux, tels les matériaux composites à base de fibre de verre ont accru le potentiel de ces structures dont les propriétés dépendent de la déformation, ou de façon équivalente de la pré-contrainte du matériau. Les grid shells élastiques semblent particulièrement prometteurs en tant que constructions temporaires, abris, ou couvertures légères.

Bien qu'essentielle au comportement de la structure, l'influence de la pré-contrainte sur la charge ultime de flambement des grid shells élastiques n'a pas encore été étudiée en détail. La compréhension de ce phénomène pourrait permettre aux ingénieurs de dimensionner plus efficacement les grid shells élastiques.

Cette thèse étudie l'influence de la pré-contrainte sur la stabilité au flambement des grid shells élastiques. Le travail de recherche consiste en une étude paramétrique d'une poutre flambée utilisée comme une arche et de grid shells élastiques construits à partir de grilles initialement circulaires avec des niveaux de pré-contrainte différents. Des valeurs réalistes des paramètres sont déterminées à partir de projets précédents. L'analyse de flambement linéarisée ainsi que la recherche de forme sont effectuées à l'aide d'un logiciel d'éléments finis. Les outils utilisés sont validés grâce à la comparaison avec de précédents résultats théoriques et expérimentaux. Les études paramétriques aboutissent à des recommandations visant à faciliter le dimensionnement de grid shells élastiques.

Mots-clé: Grid shell élastique, Low-Speed Dynamics, recherche de forme, analyse de flambement linéarisée

Co-directeur de thèse: Cyril Douthe
Titre: Chercheur et ingénieur à l'IFSTTAR

Co-directeur de thèse: John A. Ochsendorf
Titre: Professeur de Génie Civil et Architecture

Acknowledgments

Table of Contents

List of Figures

Chapter 1

Introduction

The aim of this work is to evaluate the buckling capacity of some elastic grid shells. These structures are made out of an initially flat deformed grid, which implies that a pre-stress due to the deformation exists in the structure. A parametric study is conducted by varying different geometries and grid topologies. The study focuses on two practical structures: pre-buckled arch and to domes. Quantifying the influence of this pre-stress provides guidelines for preliminary design.

1.1 Motivation

1.1.1 Force and form

When designing a building the architect and the engineer have to come up with a physical object to address a specific problem. This problem has countless aspects: urban integration, structural efficiency, environmental performance, aesthetics, cost, etc. The design of the final object involves the choice of shape, a form taken by the structure. A structural engineer will focus on the balance between shape, cost and structural efficiency.

Straight elements have been proven to be less efficient than curved elements in terms of pure structural performance. In a simple experiment (Figure 1.1), Heinz Isler (1926-2009) has shown that a curved plastic element can carry up to 30 times the load that the same element would carry if flat.

This property was known by master builders and designers, who came up with different curved structural systems along the ages. With the creation of new materials, the improvement of theories and calculations methods, new solutions were found.
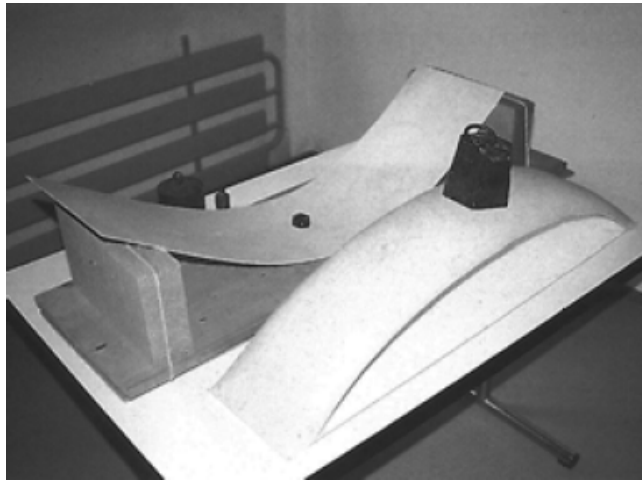
Figure 1.1: Experiment proving the efficiency of double curved structures *source: [11]*

1.1.2 Double curved structures in history

The use of curved structures is an universal component of vernacular architecture, and builders did not wait for the development of theories and computational tools to build daring structures. The largest unreinforced concrete structure today is still the Pantheon in Rome (Figure 1.2). Built two thousand years ago, this spherical dome spans $43.3m$ with a thickness-to-span ratio of 2.8% [15].

Beyond their structural efficiency, curved structures can have a dramatic presence. In the *Memoirs of Hadrian*, Marguerite Yourcenar's description of the Pantheon expresses all the poetry of this design [43].

"My intention had been that this sanctuary of All Gods should reproduce the likeness of the terrestrial globe and of the stellar sphere, that globe wherein are enclosed the seeds of eternal fire, and that hollow sphere containing all. Such was also the form of our ancestors' huts where the smoke of man's earliest hearths escaped through an orifice at the top. The cupola, constructed of a hard but lightweight volcanic stone which seemed still to share in the upward movement of flames, revealed the sky through a great hole at the center, showing alternately dark and blue. This temple, both open and mysteriously enclosed, was conceived as a solar quadrant. The hours would make their round on that caissoned ceiling, so carefully polished by Greek artisans; the disk of daylight would rest suspended there like a shield of gold; rain would form its clear pool on the pavement below; prayers would rise like smoke toward that void where we place the gods."

Marguerite Yourcenar (1903-1987), Memoirs of Hadrian

Figure 1.2: Pantheon in Rome, 126 AD *(photo: Romain Mesnil)*

There is no surprise that this form of construction was used for many churches during the Renaissance. The oculus, made possible by compressive hoop stresses, is a typical architectural feature of italian churches of the Renaissance, such as the dome of San Peter's Basilica. During a period where the antic culture was praised, it is interesting to notice that religious buildings did not used the characteristics of the Parthenon, the other great example of antic religious architecture.

The oldest double curved structures still existing are either concrete structures from the Antic Rome or masonry structures. The catalan vault is a great example of lightweight structure in masonry. The most emblematic figure of this technique is probably Antonio Gaudí (1852-1926), who used impressive hanging chain models as seen in Figure 1.3 and based on the principle described by Robert Hooke (1635-1703):

> *As hangs the flexible line, so but inverted will stand the rigid arch.*
> *Robert Hooke 1675*
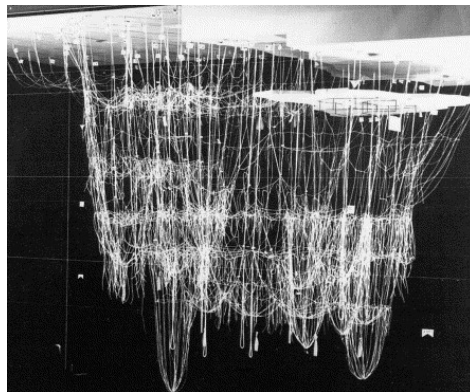
Figure 1.3: Reconstruction of one of Gaudi's hangin chain models *(photo: Institute for Lightweight Structures, Stuttgart)*

With the introduction of reinforced concrete, that can handle both tension and compression, thin shells appeared (Figure 1.4). Pioneers such as Heinz Isler (1926-2009), Eduardo Torroja (1881-1961), Felix Candela (1910-1997) or Nicolas Esquillan (1902-1989) developed impressive and efficient structures, a few of which are on Figure 1.4. The thinness of shells like Isler's Tennis Court (Figure 1.4a), Candela's "Los Manantiales" Café (Figure 1.4b) or Torroja's Zarzuela Hippodrome (Figure 1.4c) is still striking today, and their performance often overcomes the one of more recent buildings. For example, the shell of the CNIT, which was built in 1958 in La Défense still holds the record of span for a concrete structure (218m) and of surface area carried by one point $(7,500m^2)$ for a thickness of only 6cm at the crown (Fig 1.4d). These buildings also illustrate the variety of shapes offered by thin shells.

(a) Tennis Court (Heinz Isler, 1982)
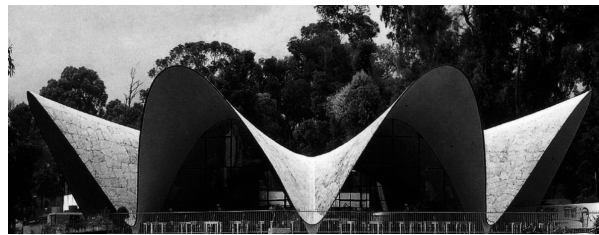
(b) Café "Los Manantiales" (Felix Candela, 1951)*(Foto: Universidad Politécnica de Madrid)*
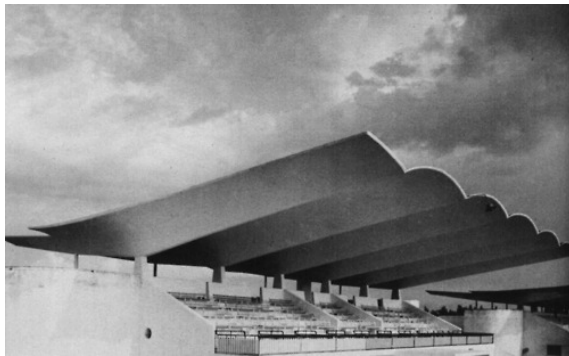
(c) Zarzuela Hippodrome (Eduardo Torroja, Madrid, 1935)

(d) CNIT (Nicolas Esquillan, 1958)

Figure 1.4: Examples of thin concrete shells

Despite their elegance and efficiency, these constructions did not spread widely. One of the reasons explaining this is the cost of manwork which has taken over the cost of material during the twentieth century. Building a concrete shell requires to build a curved and complex formwork that can be used for one particular structure only and therefore a consequent amount of manual labor. Material optimization is not economically efficient if it involves a lot of manual work, making thin shell structures more difficult to build today.

Two paradigms can overcome the question of economical efficiency of double-curved structures. The first one has been introduced by Frei Otto in the 1960's and uses the transformation of a simple geometry into a complex one thanks to the elastic deformation of the material. The second one is related to the development of the digital tools that enable manufacturing of components with an unique geometry for an acceptable cost. They are both commonly labelled as "grid shells".

1.1.3 What is a grid shell?

In the 1960's, Frei Otto and the *Institut für leichte Flächentragwerke* Stuttgart (or Institute for Lightweight Structures) developed an innovative structural system. The grid shell is described by Edmund Happold as a "doubly curved surface formed from a lattice of timber bolted together [...]. When flat, the lattice is a mechanism with one degree of freedom." [20]. This definition involves a particular mounting mechanism which overcomes the complexity of the final shape thanks to the simplicity of the undeformed structure.

This idea to use deformation of the material to obtain curvature has actually been used before by other cultures. The Madan people used this technique to build mudhif, a large communal house with a curved roof [1]. The main structural material used is straw: soft columns are first erected and are then deformed to become arches, as seen in Figure 1.5.

(a) Construction of a mudhif house (b) Inside of a mudhif house
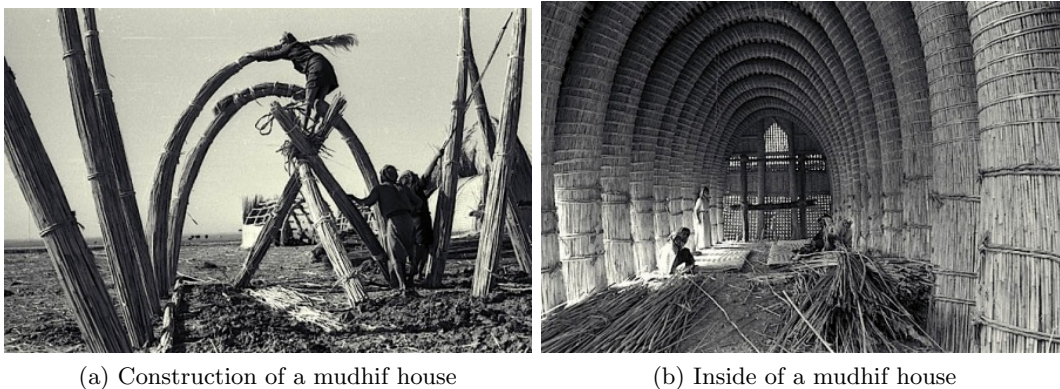
Figure 1.5: Mudhif house *(photo: Catarina Stewart)*

The potential for this structure was fully demonstrated with the contruction of the Multihalle of the Bundesgartenschau in Mannheim in 1976, as seen in Figure 1.6. The timber grid shell spans 55 meters for self-weight of only 20kg.m^{-2}. It took only three weeks to mount the 9,500m^2 of the roof.

---

[1] http://booksnbuildings.tumblr.com/post/26145618940/catrinastewart-ma-adan-iraq-the-marsh

Figure 1.6: Mannheim Multihalle

In the 1990's, Hans Schober and Jörg Schlaich developed glazed steel grid shells. In this case, the structure acts as a discrete shell, and the mounting sequence does not involve deformation (equivalently: pre-stress) of the grid. Several difficulties occured for the design of such structures, and especially the glazing. Because four points are not necesseraly in the same plane, specific precautions have to be taken if one wants to create a grid shell with a quadrangular grid and avoid huge cost increase implied by the fabrication of curved glass panels. One of the solutions for this issue is the generation of translational surfaces that do not necessarily match with the funicular shape [19].

Built in 1989, the roof of a swimming in Neckarsulm (Figure 1.7) is one of the first examples of steel grid shells and of the techniques developed by Jörg Schlaich and Hans Schober. The grid shell is made out of elements with the same length, except on the borders. The shape is a portion of a sphere, which implied that all the glass panels have the same curvature. Because the quadrangular was not able to carry the loads by its own, diagonal pre-stressed cables were introduced to brace the structure [24].

Figure 1.7: Roof of a swimming pool in Neckarsulm *(photo: `www.sbp.de`)*

Digital design and fabrication techniques have made these structures acceptable from an economical point of view [29]. The difficulty of the cladding is often overcome by using triangular panels, as it can be seen in some recent examples of Figure 1.8.

(a) British Court Museum

(b) Milano Trade Fair

(c) MyZeil in Frankfurt

Figure 1.8: Recent examples of steel grid shells

The term "grid shell" is often used without distinction on the mounting process. This work actually focuses on the grid shells introduced by Frei Otto. The grid, initially flat, and without any in-plane shear stiffness, is deformed elastically to create a double-curved surface. The deformed grid is then braced to gain in-plane shear stiffness and increase the buckling capacity. For more clarity, the term *"elastic grid shell"* will be used when this mounting sequence is employed, and the term *"grid shell"* will be used to describe other structures acting as discrete shells.

1.1.4 Why lightweight structures?

With self-weight from $7kg.m^{-2}$ to $20kg.m^{-2}$ elastic grid shells can legitimately be considered as lightweight structures. It is necessary to identify the purpose of lightweight structures. In *Leicht Weit*, Jörg Schlaich lists three main reasons that justify the construction of lightweight structures [37]:

- the first one is ecological: by reducing the amount of material, one reduces the environmental impact of a building. Moreover, these structures are often easy to deconstruct and recycle;

- the second one is economical: building lightweight structures require engineers and qualified workers and thus more added value for the society;

- the last one is cultural: lightness and transparency are often better considered as heavyness.

These arguments show that lightweight structures in general, and particularly elastic grid shells can have a real place in the construction industry. Their properties allow to list other advantages and potential. Moreover, elastic grid shells and grid shells are a way to combine lightness and free-form, and therefore have the ability to adress more comprehensive and complex designs.

Grid shells also create beautiful spaces and iconic shapes. Their lightness allows a great transparency and different use. They can be used to cover existing spaces (like the roof of the Odeon, see Figure 1.9), or new spaces (like the Savill Building).

Figure 1.9: Roof of the Odeon in Munich *(photo: Jens Weber)*

1.2 Potential of pre-stressed structures

1.2.1 Ease of use

Each structure has to be considered as the result of the interaction between a site, a program and the technical capacities of the local industry. For the design of the Second Hooghly

Bridge in Kolkata, the engineers of *Schlaich Bergermann und Partner* had to design rivet connections, because of the difficulty to weld on site in India [38]. The engineers had to take the capacity of the local industry in their design, and they had to look for solutions that woud not be viable in Europe.

It seems unlikely that digital design spreads quickly in the developing countries. Therefore using a simple method such as the deformation of soft elements to create efficient shapes has a great potential in these areas. As seen in Figure 1.10, the construction detail of the Multihalle are extremely simple compared to the typical connections used for steel grid shells.
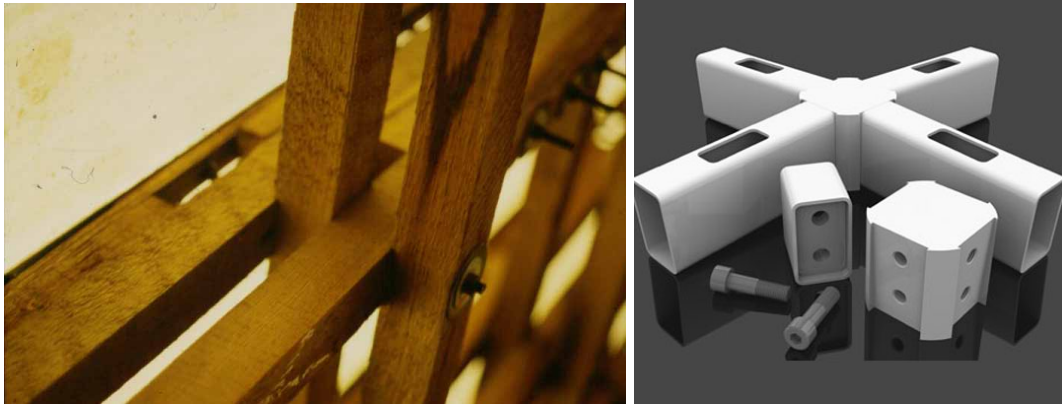
(a) Elastic grid shell: Mannheim Multihalle

(b) Grid shell: Milano Trade Fair (source: Novum GmbH)

Figure 1.10: Comparison of typical construction details

1.2.2 Temporary structures

Buildings are culturally considered as static and permanent objects. Temporary structures are often confined to specific usage, such as shelters, mobile structures or pavilions for specific events like the Olympics. The main reason for that is that construction techniques and materials were not suited to kinetic structures because of their heaviness. The cladding materials, such a glass, were also sensitive to differential motions.

Because of a combination of ease of erection and extreme lightness that allow cheap transportation, elastic grid shells open the door to new ways of thinking our buildings. As an example, an experimental grid shell in GFRP of approximately 150 m^2 has been designed for a weight inferior to $10 kg \cdot m^{-2}$ [17]. That means that a truck could transport several houses at once without any problem.

Elastic grid shells have recently used as temporary structures. A temporary Forum of $500 m^2$

for the festival Solidays' in Paris has been mounted in less than one week and unmounted in a few days [5]. A temporary cathedral has been recently built in Créteil with an elastic grid shell seen in Figure 1.11. The structure is supposed to be used during the two years of renovation of the cathedral of Créteil.

Figure 1.11: Temporary cathedral in Créteil - engineers: UR Navier and T/E/S/S *(photo: Yves Mernier)*

1.2.3   Kinetic structures

Elastic grid shells combine lightness and low stiffness before the final shape is found . These characteristics could open new perspectives for the design of kinetic structures. A fine example of the application of pre-stress to generate kinetic structures is the Pavilion One Ocean [23]. In this project, the façade can actually move and "breathe" thanks to actuator provoking buckling of slender composite shells (concept and facade can be seen on Figure 1.12). Inspiration from plants guided the initial design [30].
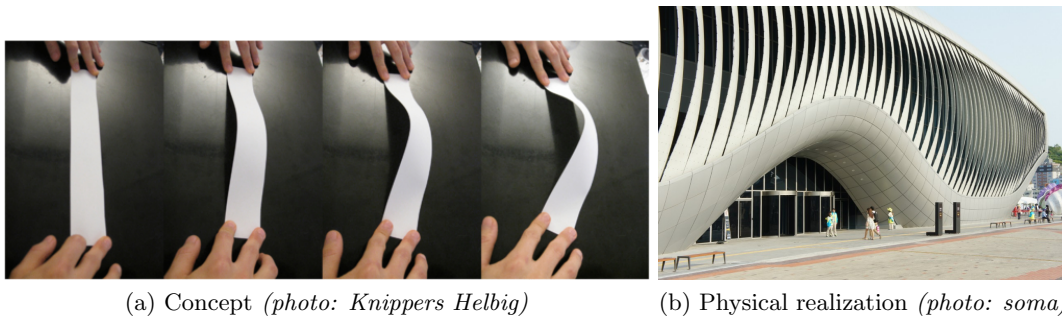
(a) Concept *(photo: Knippers Helbig)*　　　(b) Physical realization *(photo: soma)*

Figure 1.12: An example of pre-stressed kinetic structure: the Pavilion One Ocean

Since pre-stressed structures like elastic grid shells store strain energy, they have potential to release it through large displacements if the boundary conditions are controlled. If the cladding is compatible with deformation, one can imagine structures that could change their shapes to adapt weather conditions or programs.

1.3 Problem statement

1.3.1 Unresolved questions and design of elastic grid shells

Despite their advantages, elastic grid shells did not spread and they remain quite rare. The Mannheim grid shell is still the largest elastic grid shell ever built and only a dozen of elastic grid shells have been built so far[2]. This rarity can be explained to a certain extent by technical difficulties and also by cultural reasons. The main factor that limits the design possibilities in the first steps of the design is the lack of knowledge on these structures and the computation time necessary to perform complex nonlinear analysis.

The form-finding was an important issue for the first elastic grid shells. As for his cable nets or membrane structures, Frei Otto worked with hanging chains models. The limits of this approach lays in the precision of the measurement of the final shape. Developments in numerical methods, and expecially the Dynamic Relaxation made this issue less critical recently [18],[3].

Buckling often governs the design of grid shells [10] : engineers must be involved early enough in the design to propose different alternatives compatible with the architectural view and the good behavior of the structure. If some guidelines already exist for grid shells [34], there is no information allowing conceptual design of elastic grid shells for buckling. For example, it is known that increasing the curvature of an arch or a shell will increase its buckling capacity. But in the example of an elastic grid shell, increasing the curvature of the element means also increasing the moment due to the initial deformation. Thus, there is a "competition" between the positive effect of geometry, and the negative effect of pre-stress.

1.3.2 Thesis goal

There is a theoretical gap on the mechanical properties of pre-stressed structures. The competing effects of geometry and pre-stress are not fully quantified yet. It prompts heavy analysis for the structural engineers, and makes the design process of elastic grid shells complex. The development of the first elastic grid shells involved significant computational efforts. This work proposes to focus on a technical issue, with the hope to reduce the calculation intensity for the designer, allowing more efficient and diverse design. This idea is developed on Figure

---

[2]For more details on previous examples of elastic grid shells, see A

1.13, which takes inspiration from a diagram explaining the development of new structural solutions.

Solution for a new structural problem
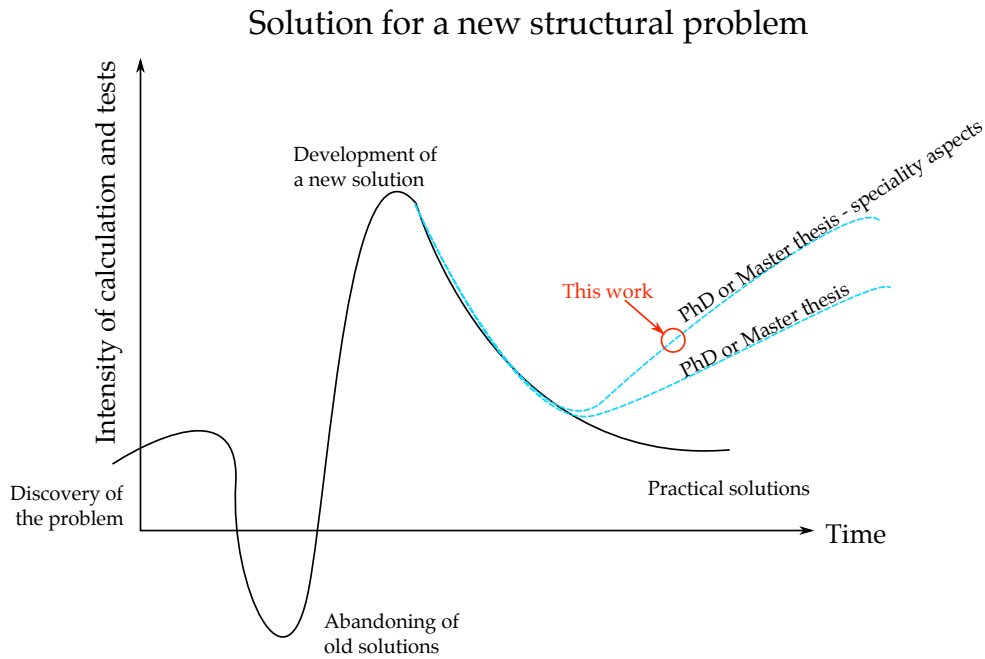
Figure 1.13: Diagram illustrating the purpose of this work (reproduced from [40])

The thesis goals can be summed up as follows:

- Establish a methodology for the analysis of pre-stressed structures in general and elastic grid shells in particular;

- Provide a first rigorous set of data on the buckling capacity of elastic grid shells;

- Expand the knowledge on buckling of grid shells to elastic grid shells.

This thesis proposes to answer these three questions:

- Does the pre-stress influence the shape of the buckling modes?

- How does the pre-stress affect the bearing capacity of elastic grid shells?

- It is possible to draw parallels between the behavior of elastic grid shells and grid shells?

1.3.3 Approach

The approach used in this thesis is to conduct a parametric study varying different levels of pre-stress for a unique grid topology: an initially flat circular grid. The bearing capacity of both pre-stressed and unstressed structures are calculated using the finite element program ADINA. Since the aim of this work is to identify trends in the behavior of pre-stressed structures.

1.4 Outline of Chapters

In Chapter 2, relevant publications on the stability of grid shells and pre-stressed structures are presented. This literature review recalls the background of this dissertation on design and mechanics of grid shells and pre-stressed structures.

The methodology used in this work is discussed in Chapter 3. The tool chosen to perform form-finding and buckling analysis is presented, and the validation of the Finite Element Software ADINA is performed on simple examples.

The first parametric study is presented in Chapter 4. The problem studied is the buckling of a pre-buckled beam used as an arch. Results of the finite element analysis are compared to both analytical results and previous experiments or numerical calculations. The derivation of theoretical formulæ gives an understanding of the behavior of the pre-stressed structure.

The parametric study of elastic grid shells made out of circular grids is presented in Chapter 5. Their bearing capacity is compared to rigid grid shells with the same geometry. The influence of the pre-stress on the buckling capacity of elastic grid shells is discussed. Chapter 6 concludes with the original contributions of the thesis.

Chapter 2

Literature review

2.1 Introduction

The objective of this chapter is to present major contributions in the field of grid shells design. Since this thesis aims to compare elastic grid shells and grid shells, literature on both fields is presented. There is a variety of publications focusing on different aspects, from the conceptual design to nonlinear analysis of structures. If both designers and scientists have published on grid shells, it seems that pre-stressed structures is a topic studied only by the structural mechanics community.

2.2 Design of elastic grid shells

2.2.1 Overview

Only few elastic grid shells have been built in the past fifty years. Their design, far from being a standard procedure, is a case by case study. The very first examples were developed with "hanging nets" models [20], [22]. Frei Otto saw in grid shells an equivalent to the hanging chain in three dimensions, a concept that is ilustrated in the Deubau grid shell in Essen shown in Figure 2.1. As for his membranes or cable nets structures, he worked closely with the *Institut für Anwendungen der Geodäsie im Bauwesen* (the institute for the application of geodesy in construction) for the design of his first grid shells.

Up to now, the design of elastic grid shells involved the creation of specific programs to generate the geometry or do the structural analysis. The first work of the *Institut für leichte Flächentragwerke* is closely related to the development of computational methods. The force density method was developed at the same time as Frei Otto's structures, and the development of the computational tools is closely linked to the birth of the new forms that appeared in the

1970's. The elastic grid shells built since the 1990's also involved significant computational effort for the form-finding and optimization of the mesh.

(a) Hanging chain model   (b) Elastic grid shell in Essen (1962)
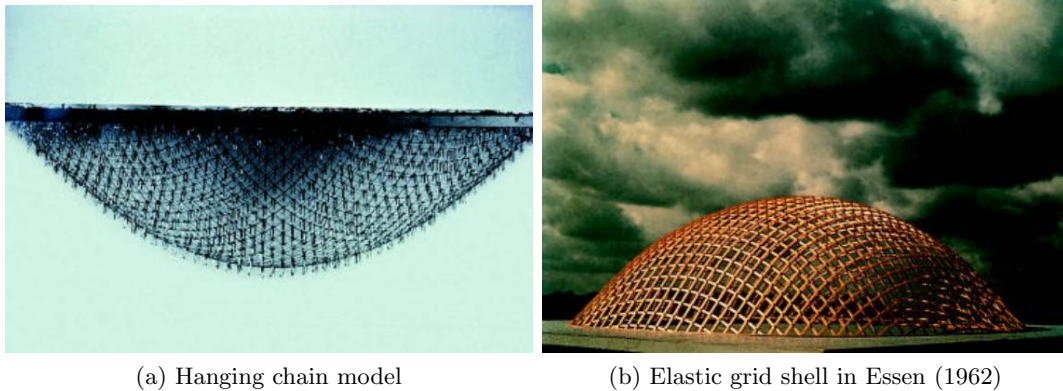
Figure 2.1: Elastic grid shell in Essen (1962)*(photo: `http://www.freiotto.com`)*

The Table 2.1 summarizes the most significant elastic grid shells built. A wide variety of spans and materials appear in these examples. Timber is the most common solution, however other materials, such as GFRP or even cardboard have also been used successfully.

Name	Year	Span	Number of layers	Material
Essen	1963	15m×15m	2	Timber
Mannheim	1976	60m×60m	4	Timber (hemlock)
Polydôme	1991	25m×25m	2	Timber
Earth Centre	1998	6m×6m	4	Timber (oak)
EXPO 2000	2000	72m×35m	2	Cardboard
Downland	2002	48m×15m	4	Timber (oak)
Savill	2004	90m×25m	4	Timber (larch)
Chiddingstone Orangerie	2007	12m × 5m	4	Timber (oak)
Grid shell UR Navier	2007	6m×23.6m	2	GFRP
Solidays'	2011	10m×35m	2	GFRP
Créteil temporary cathedral	2013	15m	2	GFRP

Table 2.1: Significant previous elastic grid shells

It is interesting to notice that the number of elastic grid shells built has increased significantly in the 2000's. It actually reflects the progress of the industry in the design of complex structures in the last decade.

2.2.2 Simple and double layers

Another interesting property to be considered is the number of layers used in the elastic grid shells. Most of the timber elastic grid shells have four layers and not two. This choice is guided by a structural purpose: when deformed, the grid is subject to a bending moment proportional to the curvature:

$$M = EI\kappa \tag{2.1}$$

The maximal bending stress in the beam is given by following equation:

$$\sigma = \frac{Mh}{2I} \tag{2.2}$$

Where M is the bending moment, I is the moment of inertia and h is the height of the cross-section. From a practical point of view, the designer decided of a maximal curvature κ_{max} in the structure and has to maintain a reasonable stress:

$$\sigma < \sigma_d \tag{2.3}$$

which leads to:

$$h < \frac{2\sigma_d}{E\kappa} \tag{2.4}$$

It is noticed that a limitation on the height (and thus on the inertia if one considers practical aspects) of the sections exists. On the other hand, once the shape is found, the inertia should be maximized to resist buckling. This competition between these two objectives was solved by using different layers. When the structure is flat, it is possible to juxtapose two grids on top of each other without stiff connection. The bending stiffness of the structure is the double of the stiffness of one grid. Once the final shape is reached, the layers are rigidly connected to each other. The bending stiffness increases significantly, the grids acting like a three-dimensional Vierendeel truss.
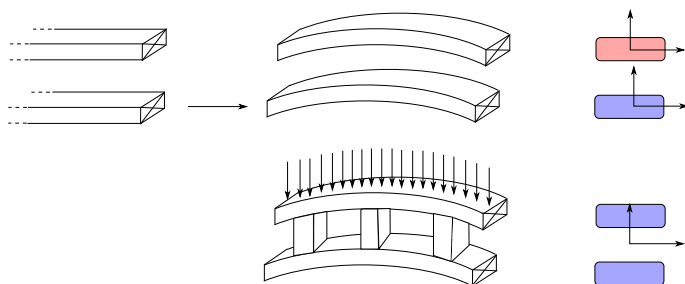
Figure 2.2: Interest of the double layer: influence on the equivalent bending stiffness

This principle has been used extensively for timber grid shells [22], [21], but not for GFRP grid shells. The mechanical model of multiple layers is a complex issue that is still not

fully modelled. Competing models exist, from the Gamma method developed by Möhler and Schelling (explained in the Appendix B. of the Eurocode 5 [16]) to finite element models. The main complexity remains in the model of the rigidity of the connections between the different layers [35].

In order to study one unique effect (the pre-stress), this work focuses on single-layered elastic grid shells. Since the literature review shows that single-layered grid shells are in GFRP, the characteristics of the cross-sections chosen in this work are typical of GFRP pultruded profiles.

2.3 Mechanics of grid shells

2.3.1 Form-finding

The first difficulty in the study of grid shells, as for many lightweight structures is the form-finding procedure. In this thesis, form-finding of elastic grid-shells is performed, therefore, it is necessary to recall the main methods used up to now.

Force density

The first numerical method allowing the generation of cable nets was actually developed during the planning of the roof of the Olympic Stadium in Munich. Linkwitz and Schek [33] developed an equilibrium method that linearizes the equations called force-density method (*Kraft-Dichte Methode*). This method is still used extensively for the form-finding of cable nets or membranes. A modified procedure called the "constrained force density method" by Milos Dimcic is used to design steel grid shells. To learn more about this method and its application, the reader can refer to [15].

Dimcic took the recent example of two projects designed by the office *Knippers Helbig*: the Sun Valley of the Shanghai EXPO (2010) and MyZeil in Frankfurt. Both grid shells present a triangular grid and particular features. The funnel-shaped grid shells of the EXPO (Figure 2.3a) are carrying huge point loads coming from the membranes attached to them: a refinement of the mesh around these points were necessary to avoid huge cross-sections. The shopping mall MyZeil (Figure 2.3b) is a good example of free-form grid shell. The geometry was first given by the architects to the engineers, who had first to optimize the shape and then optimize the mesh [29]. In both cases, the so-called "relaxation" of the mesh led to a smooth grid, appealing to the eye, despite the complexity of the shapes or the loads.
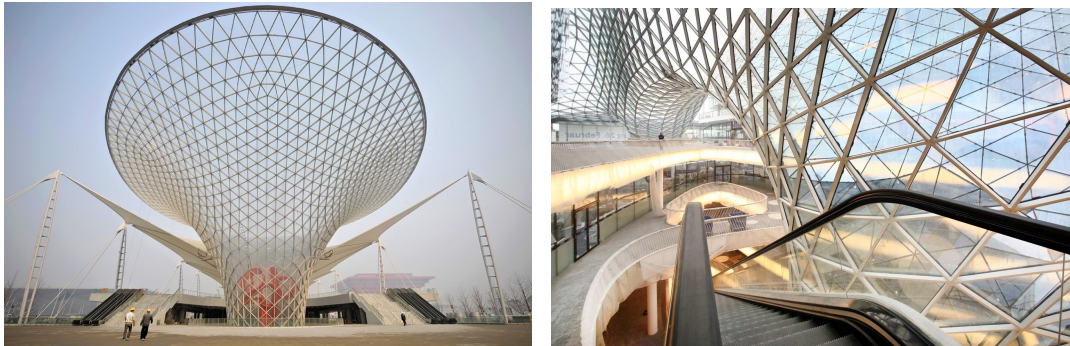
(a) One of the six Sun Valley, Shangai EXPO 2010 (SBA Architects) *(photo: AFP)*

(b) MyZeil (Arch: Massiliamo Fuksas) *(photo: Photographs +)*

Figure 2.3: Two steel grid shells using the contrained force density method (structural engineers: Knippers Helbig Advanced Engineering)

Newton-Raphson

The force-density method assumes no bending rigidity for the elements. Elastic grid shells require other methods because the determination of the bending stresses is key for the structural analysis. A first approach could be to use a typical nonlinear scheme, such as Newton-Raphson. It appears that this method is not very stable in the case of elastic grid shells [18]. This might explain why another method has spread during the last years in the form-finding of elastic grid shells.

Dynamic relaxation

In the past years, efforts have been made in the formulation of Dynamic-Relaxation method [17]. This method is based on a simple idea: in the physical world, a structure subject to a load will start oscillating and the damping effect will stabilize the structure to its equilibrium position. The damping introduced can take either be a *viscous damping* or a *kinetic damping*. The first one has a physical sense from the material point of view, the second one is based on an energy principle detailed below.

The mechanical energy E_{tot} is the sum of the kinetic energy E_K and of the potential energy E_p.

$$E_{tot} = E_K + E_p \tag{2.5}$$

In order to understand the principle of the kinetic damping, we can do the assumption that the system is subject to conservative forces, in this case, the mechanical energy is conserved.

Deriving equation 2.5 with respect to time leads to:

$$\frac{dE_{tot}}{dt} = \frac{dE_K}{dt} + \frac{dE_p}{dt} = 0 \tag{2.6}$$

In a static approach, the equilibrium corresponds to a minimum of the potential energy. Since the mechanical energy is constant, it means that the kinetic energy necessarily reaches a maximum when the system is at the equilibrium position. The kinetic damping consists of looking for maxima of the kinetic energy to a structure subject to an artificial dynamic motion. When an approximate value for maximum is found, the structure is stopped and set to the approximate equilibrium position. From there, a new approximation of the maximum of the kinetic energy can be found. This iterative procedure converges to the equilibrium position.

In the case of elastic grid shells, it appears that the results predicted by the dynamic relaxation are different from the models neglecting bending stiffness of the elements [18]. The method has been employed for the construction of modern grid shells.

2.3.2 Free-form

The main method used to generate geometry was initially a method of trial and error combined with physical models and numerical methods such as dynamic relaxation. This requires the involvement of the structural engineer from the very beginning of the design. Moreover, the structural efficiency is not the only criterion in the design of the skin of a building. The environmental impact and the energy efficiency become an important concern: buildings are responsible for 40 percent of the global energy use and one third of the global greenhouse gas emissions [26]. Grid shells and elastic grid shells give the possibility to build shapes that are different from the funicular shapes.

Because shapes are often governed by other requirements that the structural efficiency, some methods such as the compass method have been developed to map double curved surfaces [7], [8]. The advantage of this method is that it can be scripted and included into drawing tools such as Rhino [5], providing an interface with the user. Other methods based on the minimization of the strain energy of the grid has been proposed [32].

2.3.3 Buckling of grid shells

Buckling of grid shells has been studied both by the design community and the scientific community. Different methods were proposed to respond to the needs of designers, who need to explore different solutions in the early stages of design, and need precise analysis tools in the development stage. Analytical methods respond to the first need whereas numerical methods can address more complex considerations.

Overview

As pointed out in numerous papers, buckling is a fundamental consideration in the design and analysis of grid shells. Grid shells combines different main types of buckling, as described in [10].

a) Member buckling: a single member buckles without affecting the rest of the structure;

b) Local instability: snap-through of one or several nodes;

c) Global instability: the structure buckles as a whole;

d) A combination of the above mentioned modes.

Analytical approach

This complexity and variety of possible modes makes approaches based on equivalent shells difficult, because they omit the member buckling or the local instabilities [10]. However, some methods have been developed to make model of equivalent shells. The interest of these methods is that they can provide workable formulæ for designers. These methods are listed in [34], where the concept of equivalent stiffness has been applied for spherical domes and barrel vaults.

The importance of analytical or pseudo-analytical formulations in the developement of new structures cannot be ignored. The development of the thin-shells theory led Franz Dischinger (1888-1943) and Ulrich Finsterwalder (1897-1998) to design new shapes, such as the 76m span (a record at that time) *Markethalle* in Leipzig (1929) [6]. The analytical methods developed for grid shells can help the designer in the first steps of the design process. However, they are limited to simple geometries and might not reflect all the possibilities available to the designer.

Numerical approach

To this day, finite element analysis is the prefered tool to analysis the buckling of grid shells. The improvement of computation power makes the nonlinear analysis easier. The available computational power is such that it is now possible to couple finite element analysis with optimization methods such a search heuristic algorithm like *Genetic Algorithms* to explore different mesh topologies optimizing the performance of grid shells [15].

Complete incremental nonlinear analysis of structure up to collapse and beyond remain computationally expensive. For that reason, linear buckling analysis is an efficient method to

estimate the collapse load of a structure. This method is based on the solving of an eigenvalue problem which is a linearization of the initial nonlinear problem. The theory as well as the considerations exposed in this part can be found in [4].

Let $^{t-\Delta t}\mathbf{R}$ and $^t\mathbf{R}$ be the vector of applied loads at time $t - \Delta t$ and t. The stiffness matrix at time $t - \Delta t$ and t are $^{t-\Delta t}\mathbf{K}$ and $^t\mathbf{K}$. In the linearized buckling analysis problem, the stiffness matrix at any time τ is defined by equation (2.7):

$$^\tau\mathbf{K} = {}^{t-\Delta t}\mathbf{K} + \lambda \left({}^t\mathbf{K} - {}^{t-\Delta t}\mathbf{K} \right) \tag{2.7}$$

and,

$$^\tau\mathbf{R} = {}^{t-\Delta t}\mathbf{R} + \lambda \left({}^t\mathbf{R} - {}^{t-\Delta t}\mathbf{R} \right) \tag{2.8}$$

Where λ is a scaling factor, the linear buckling problem is an eigenvalue problem. At collapse of buckling, the stiffness matrix becomes singular:

$$^\tau\mathbf{K} \cdot \boldsymbol{\phi} = \mathbf{0} \tag{2.9}$$

Where $\boldsymbol{\phi}$ is a non-zero vector. From this, we get the eigenvalue problem described by equation (2.10). Let λ_1 be the smallest eigenvalue of this problem and $\boldsymbol{\phi}_1$ be a corresponding normalized eigenvector.

$$^t\mathbf{K} \cdot \boldsymbol{\phi} = \frac{\lambda - 1}{\lambda} {}^{t-\Delta t}\mathbf{K} \cdot \boldsymbol{\phi} \tag{2.10}$$

Finally, we get the buckling load from equation (2.8):

$$\mathbf{R}_{buckling} = {}^{t-\Delta t}\mathbf{R} + \lambda_1 \left({}^t\mathbf{R} - {}^{t-\Delta t}\mathbf{R} \right) \tag{2.11}$$

Equations (2.7) and (2.8) correspond to a linearization of the initial problem. It is assumed that the stiffness of the element and the applied load varies linearly during the interval Δt. For that reason, the linear buckling analysis is efficient only if the pre-buckling displacements are relatively small. Specific precautions must be taken when analyzing arch or shell-like structure, which can exhibit relatively important displacement before collapse. The hypothesis can be verified if the difference between $^{t-\Delta t}\mathbf{R}$ and $^t\mathbf{R}$ is small enough, i.e. if the applied load is close to the "real" buckling load.

It has been shown that grid shells are sensitive to imperfections [10]. It is possible to add imperfections expressed as a displacement vector proportional to the first eigenvector $\boldsymbol{\phi}_1$. For grid shells, it is possible to consider several buckling modes in this kind of consideration. However, this topic remains a specific question treated by confirmed designers because no building code discusses this possibility.

2.4 Mechanics of pre-stressed structures

2.4.1 Overview

Pre-stressed structures are mostly studied by the structural mechanics community. The complexity of these structures often prevents the derivation of analytical solutions. Therefore, studies on pre-stressed structures involve heavy use of finite element analysis.

2.4.2 Stability of 2D structures

The simplest pre-stressed structure where the pre-stress is linked to gain a geometrical stiffness is the pre-buckled arch. Although apparently simple, no analytical closed form solution seems to have been derived for the buckling capacity. This problem has been studied both numerically with nonlinear finite element analysis [25] and experimentally [41], [12]. The studies focused on both shallow arches, where the geometry of the pre-buckled arch can be approximated by a half-sine wave, but also for steep arches. Thompson and Hunt proposed a simple relation between the buckling capacity of a pre-buckled strut used as an arch and the bearing capacity of an unstressed arch. As a rule of thumb, the buckling capacity of pre-stressed arch is equal to 75% of the one of an unstressed arch with the same geometry.

The numerical methods used for the study of pre-buckled beams were fully nonlinear and did not use linear buckling. Because of the full nonlinearity, these method are computationally expensive. The stability of 3D pre-stressed structures such as elastic grid shells has still to be developed.

2.5 Summary

In this chapter, some major contributions in the field of grid shells design have been exposed. The design of these structures has come to a certain maturity illustrated by an increasing number of constructions in the past decade. If methods of form-finding are correctly used by designers, it appeared that stability analysis involved more complications. Analytical formulations were derived for few geometries only and numerical methods must be used with precautions. The stability of pre-stressed structures is not yet deeply studied by the designers community. Comparisons of the buckling capacity of elastic grid shells with grid shells have still to be performed.

The designers use the finite element method for the analysis of structures. In order to develop a workable method, this work presents a parametric study on buckling capacity of grid shells.

Chapter 3

Methodology

This chapter presents the methodology used to answer the questions posed in the Chapter 1 and stated again below:

- Does the pre-stress influence the shape of the buckling modes?

- How does the pre-stress affect the bearing capacity of elastic grid shells?

- It is possible to draw parallels between the behavior of elastic grid shells and grid shells?

3.1 Procedure for a parametric study

Because of the extensive use of finite element analysis by the design and structural mechanics communities, it has been chosen to implement a numerical procedure using this method. It is used both for form-finding and buckling analysis.

3.1.1 Procedure for the finite-element analysis

The analysis of elastic grid shells proposed in this thesis is described by six steps:

a) The grid is initially flat. It is made out of beam elements connected together with links (Master/Slave nodes). The ends of the beams can slide in the initial plane;

b) Form-finding procedure: *Statics Solver* in ADINA use of the *Slow Dynamics* option for stabilization. The load applied is a uniform line load;

c) The ends of the beams are restrained with pin connections, the bracing is added, the initial load is taken away;

d) Another nonlinear calculation is performed in order to determine the equilibrium posi-tion of the stabilized structure;

e) A load is added: it can be either symmetrical or not, and it can be projected (e.g.: snow) or not (e.g.: self-weight of the grid shell or cladding);

f) Linearized buckling calculation.

The same procedure can be adapted to a structure that would have the same geometry, but without any pre-stress. The buckling capacity of the two structures will be compared and discussed.

The geometry found here does not correspond to the geometry that would be found using force density, as it is currently done for steel grid shell [15] [1]. A grid shell without initial pre-stress would have a different geometry, since the bending stiffness of the elements is neglect when using force-density method. Furthermore, since the connections between elements can be rigid, different meshes such a quadrangular, triangular, or even Voronoi meshes can be applied to steel grid shells without pre-stress [15]. This is a limitation of the comparison of the influence of pre-stress.

3.1.2 Choice of the parameters

Every physical phenomenon is represented by the means of a mathematical model. In the case of structures, engineers often use the theory of elasticity. This mathematical model uses a certain number n of parameters and p units. The Buckingham Π Theorem guarantees that an equivalent mathematical model with $n - p$ dimensionless parameters can be constructed. This theorem has been used in this work for the estimation of the buckling load of grid shells.

3.2 2D validation of computational method: example of a pre-buckled arch

3.2.1 Form-finding

The approach of this thesis was to combine form-finding and buckling analysis in the same computing environment, therefore a finite element package has been used. Statics solvers using Newton-Raphson method are generally not efficient for the calculation of grid shells. For that reason, explicit dynamics have been used in previous works [7]. However, since

---

[1] *MyZeil* or *Shanghai Expo 2010* both designed by Knippers Helbig are cited as examples of structures designed with a relaxed mesh, a hybrid version of the force-density method

dynamic explicit methods are conditionally stable even in linear cases [4], the parameters have to be adjusted. In this work, the final shape of elastic grid shells is obtained thanks to the statics solver of ADINA. The Newton-Raphson method is combined with a Low-Speed Dynamics stabilization scheme. The philosophy of this method remains close to the dynamic relaxation: the dynamic response of the structure is calculated for a load applied very slowly, a damping matrix is introduced and the structure eventually comes to an equilibrium position [1].

The system solved by ADINA is basically:

$$\mathbf{M}^{t+\Delta t}\ddot{\mathbf{U}}^{(i)} + \mathbf{C}^{t+\Delta t}\dot{\mathbf{U}}^{(i)} + \mathbf{K}^{(i-1)t+\Delta t}\mathbf{U}^{(i)} = {}^{t+\Delta t}\mathbf{R} - {}^{t+\Delta t}\mathbf{F}^{(i-1)} \tag{3.1}$$

Where:

$$\mathbf{C} = \beta\mathbf{K} \tag{3.2}$$

and β is a parameter that can be changed by the user. It has been chosen to keep the default value of $\beta = 10^{-4}$. The modeling guide of ADINA recommends a minimal value for the time step defined by following equation:

$$\Delta t > \beta \cdot 10^5 \tag{3.3}$$

Derivation of the equilibrium equation

The form-finding was performed by using the nonlinear static solver in ADINA. Translations were enforced at the boundaries, the deflected beam has to take the shape of a curve known as *Elastica*. Theoretical solutions for this problem come from Jacques Bernoulli and Leonhard Euler [31] and can be confrounted with the results from ADINA.
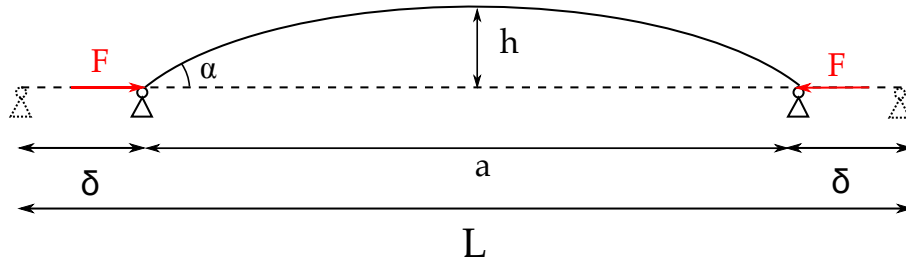
Figure 3.1: Parameters describing the form-finding problem

Once the buckling load is reached, the equation of motion for the beam has to take the large displacements into account and can be written[2]:

$$EI\kappa + Fv = 0 \tag{3.4}$$

Once the buckling load is reached one has to take into acount the large displacements hypothesis. It follows that $\kappa = \frac{d\theta}{ds}$ and that $\frac{dv}{ds} = sin\,(\theta)$.

$$EI\frac{d^2\theta}{ds^2} = -Fsin\,(\theta) \tag{3.5}$$

If we multiply both terms by $\frac{2d\theta}{ds}$, integrate with respect to θ and notice that $\frac{d\theta}{ds}\,(s = 0) = 0$ by symmetry it yields:

$$EI\left(\frac{d\theta}{ds}\right)^2 = 2 \cdot F \cdot [cos\,(\theta) - cos\,(\alpha)] \tag{3.6}$$

We introduce the parameter k such as $k = \sqrt{\frac{F}{EI}} = \frac{\pi}{L}\sqrt{\frac{F}{F_c}}$ where F_c is the critical load for buckling $F_c = \frac{\pi^2 EI}{L^2}$.

$$ds = \frac{-d\theta}{k\sqrt{2\,(cos\,(\theta) - cos\,(\alpha))}} \tag{3.7}$$

$$ds = \frac{-d\theta}{2k\sqrt{sin^2\left(\frac{\alpha}{2}\right) - sin^2\left(\frac{\theta}{2}\right)}} \tag{3.8}$$

Horizontal Force

We can integrate over the all beam, and notice that:

$$L = \int_{s_{min}}^{s_{max}} \mathrm{d}s \tag{3.9}$$

Which can be written equivalently as:

$$L = \int_0^{\alpha} \frac{\mathrm{d}\theta}{k\sqrt{sin^2\left(\frac{\alpha}{2}\right) - sin^2\left(\frac{\theta}{2}\right)}} \tag{3.10}$$

We introduce the variable ϕ such as $sin\left(\frac{\theta}{2}\right) = sin\left(\frac{\alpha}{2}\right) \cdot sin\,(\phi)$, this implies $\mathrm{d}\theta = 2 \cdot tan\left(\frac{\alpha}{2}\right) \cdot cos\,(\phi)\,\mathrm{d}\phi$:

$$kL = 2 \cdot \int_0^{\frac{\pi}{2}} \frac{\mathrm{d}\phi}{\sqrt{1 - sin^2\left(\frac{\alpha}{2}\right) \cdot sin^2\,(\phi)}} \tag{3.11}$$

---

[2]the solution of this problem can be found in many books including [17]

At this stage, Legendre's first elliptic integral $I\left[sin\left(\frac{\alpha}{2}\right)\right]$ is introduced. There are tables giving values for this integral following different values of α.

$$I\left[sin\left(\frac{\alpha}{2}\right)\right] = \int_0^{\frac{\pi}{2}} \frac{\mathrm{d}\phi}{\sqrt{1 - sin^2\left(\frac{\alpha}{2}\right) \cdot sin^2\left(\phi\right)}} \tag{3.12}$$

Finally,

$$kL = 2 \cdot I\left[sin\left(\frac{\alpha}{2}\right)\right] \tag{3.13}$$

Rise at mid-span

The rise h of the beam can be found by noticing that $\mathrm{d}v = \mathrm{d}s \cdot sin\left(\theta\right)$ and by plugging this result in (3.8), the same substitution can be used:

$$\frac{h}{L} = \frac{sin\left(\frac{\alpha}{2}\right)}{I\left[sin\left(\frac{\alpha}{2}\right)\right]} \tag{3.14}$$

Projected length

The projected length of the beam over a can be found when one notices that $\mathrm{d}x = \mathrm{d}s \cdot cos\left(\theta\right)$:

$$\frac{a}{L} = \frac{J\left[sin\left(\frac{\alpha}{2}\right)\right]}{I\left[sin\left(\frac{\alpha}{2}\right)\right]} \tag{3.15}$$

where :

$$J\left[sin\left(\frac{\alpha}{2}\right)\right] = \int_0^{\frac{\pi}{2}} \sqrt{1 - sin^2\left(\frac{\alpha}{2}\right) \cdot sin^2\left(\phi\right)} \left(\frac{1 - 2 \cdot sin^2\left(\frac{\alpha}{2}\right) \cdot sin^2\left(\phi\right)}{1 - sin^2\left(\frac{\alpha}{2}\right) \cdot sin^2\left(\phi\right)}\right) \mathrm{d}\phi \tag{3.16}$$

3.2.2 Consistency of the Finite Element Model

Influence of the mesh density

Before comparing Finite Element Method with the theory, it was necessary to determine a mesh density that would guarantee reliable results both for the estimation of the displacements and for the buckling load of the buckled arch. The influence of the mesh density has been studied for a particular set of values. The initial length of the beam is of 15 meters. The enforced displacement δ at each node is of 0.5 meter.

The reference value was a model meshed with 1024 elements. It appears that the results both for displacements and buckling load are very accurate for a mesh with 32 elements. This density has been chosen for the comparison of Finite Element results and theory.
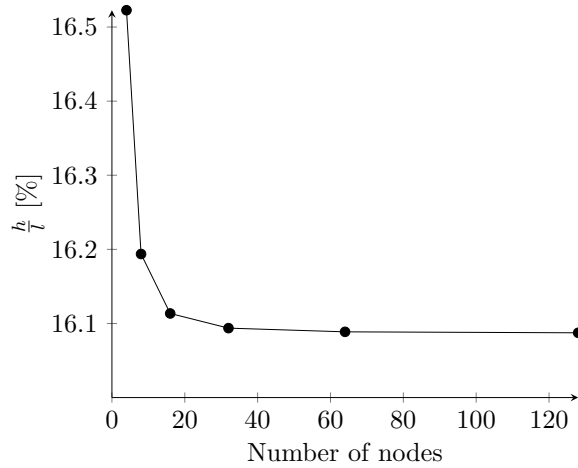
Figure 3.2: Evolution of $\frac{h}{l}$ with the number of nodes
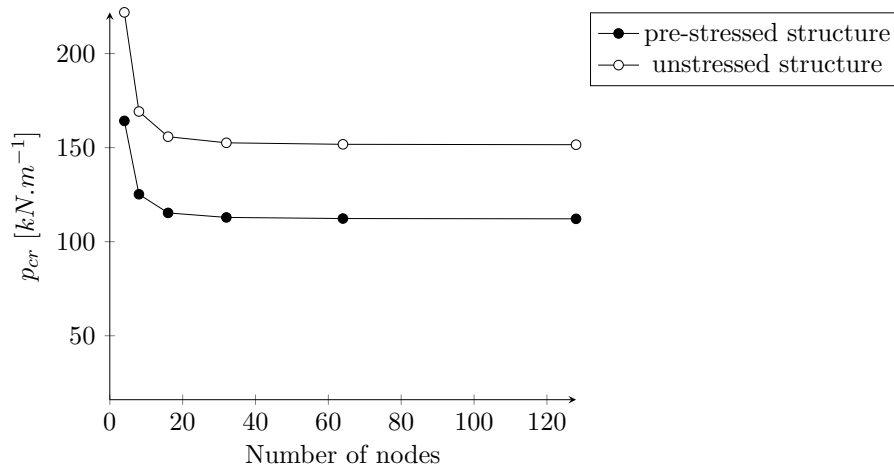
Figure 3.3: Evolution of the buckling load with the number of nodes - $\delta = 0.5m$

Imposed displacements

An imposed displacement has been applied to each boundary of a model with 32 elements in ADINA. The values of imposed displacement is equal to the theoretical value, the horizontal reaction force and the rise of the beam are compared. It has been chosen to vary α between 0° and 90°.

α $[°]$	$\frac{F}{F_c}$	$\frac{h}{L}$	$\frac{a}{L}$
10	1.00382	0.0553795	0.992397
20	1.0154	0.109707	0.969731
30	1.03512	0.16195	0.932432
40	1.06366	0.21112	0.881204
50	1.10204	0.256288	0.817003
60	1.15172	0.296604	0.74102
70	1.21472	0.331309	0.654637
80	1.29389	0.359749	0.559396
90	1.3932	0.38138	0.456947

Table 3.1: Theoretical values for the *Elastica*

The Figure 3.4 illustrates the results of the nonlinear statics solver from ADINA for different values of prescribed displacements of the boundaries δ. The theoretical results and the results from ADINA have been compared for values of α between 0° and 90°, which covers the range of real structures.

(a) Result from ADINA - $\frac{\delta}{L} = \frac{1}{30}$

(b) Result from ADINA - $\frac{\delta}{L} = \frac{7}{15}$

(c) Result from ADINA - $\frac{\delta}{L} = \frac{2}{3}$
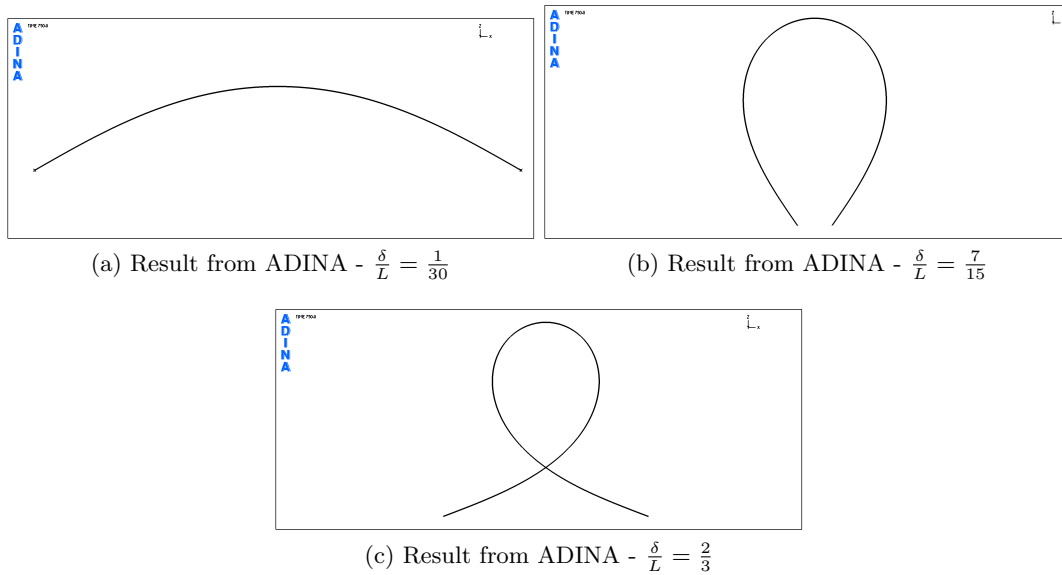
Figure 3.4: Different results for the buckling of a simply supported beam

The error on both displacements and horizontal force in the structure remains small (inferior to 0.1%). Therefore, we can conlude that the mesh chosen describes accurately both the final geometry and the forces in the structures resulting from the imposed displacements.
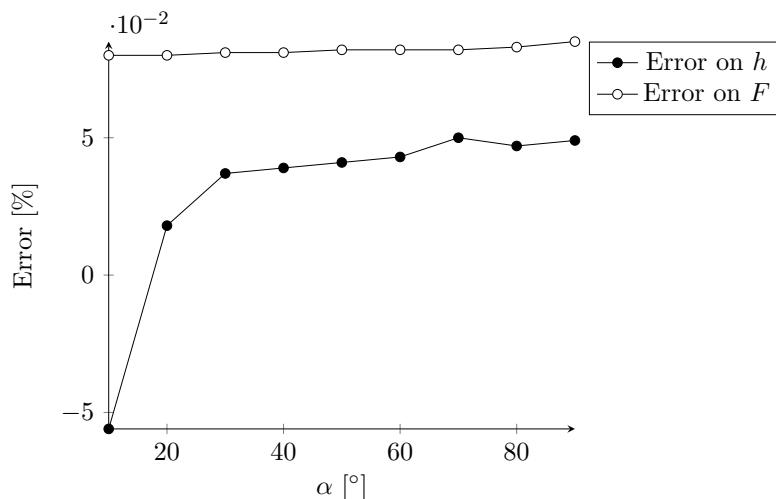
Figure 3.5: Error between ADINA and the theoretical solution

3.2.3   Buckling analysis

It has already been pointed out in the Section 2.3.3 that linear buckling analysis could lead to some imprecisions because of relatively large pre-buckling displacements. The sensibility to the value of the applied load has been studied. In equation (2.11), the value of $^t\mathbf{R}$ can have an influence on the value of $\mathbf{R}_{buckling}$ because the linearization is an approximation of the real structural behavior. By chosing different values of the applied load $^t\mathbf{R}$, it is possible to quantify this phenomenon.

An arch with a rise-over-span ratio of 0.25 has been studied. This example has been studied by Chini and Wolde-Tinsae with a nonlinear algorithm [13]. The values of this previous study are used as reference. The arch is slender, as the structures that will be studied in the rest of this thesis, but the rise-over-span ratio is big enough so that the arch will be subject to buckling and not snap-through. This geometrical stiffness is typical of the elastic grid shells built up to now, it limits the displacements before buckling. The results are shown in Figure 3.6.
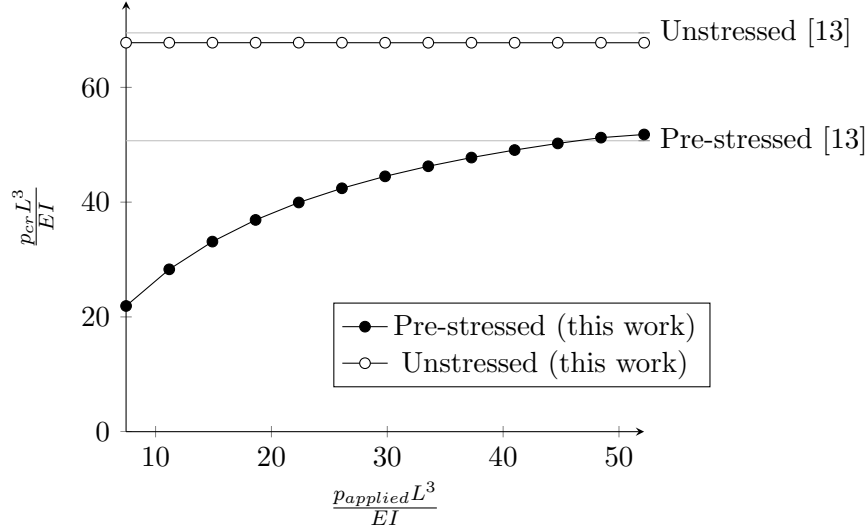
Figure 3.6: Influence of the applied load on the buckling load calculated for $\frac{h}{L'} = 0.25$

The unstressed arch is not sensitive to the value of the load applied. It is probably due to the relatively high rise-over-span ratio. It demonstrates the interest of using linear buckling analysis for unstressed arches. The pre-stressed structure however is very sensitive to the value of the load applied initially. The buckling load calculated is an increasing function of the applied load. It eventually converges to a value extremely close to the reference value, as seen in Figure 3.6. The Table 3.2 sums up the results and demonstrates the accuracy of the linear buckling analysis when the applied load is close enough of the collapse load.

Quantity	Chini and Wolde-Tinsae [13]	ADINA	Error
$\dfrac{p_{cr}L^3}{EI}$, pre-stressed arch	50.7	51.7	$+1.9\%$
$\dfrac{p_{cr}L^3}{EI}$, unstressed arch	69.5	67.8	-1.2%

Table 3.2: Accuracy of ADINA compared to [13] for $\frac{h}{L'} = 0.25$

The fact that the applied load has to be close to the actual collapse to get accurate result is a difficulty of the linear buckling analysis method. To solve this issue, an iterative method based has been implemented, as seen in Figure 3.7. It is possible to start the calculation with a small applied load. This will lead to the evaluation of a critical $p_{cr,1}$. Because the calculated buckling load is inferior to the real buckling load on Figure 3.6, the stiffness matrix will remain definite positive if the load $p_{cr,1}$ is applied. Therefore, it is possible to apply the load $p_{cr,1}$ and from there, get a second load $p_{cr,2}$. By repeting this procedure, it is possible

to build a sequence $(p_{cr,n})_{n \in \mathbb{N}}$.

$$\forall n \in \mathbb{N}, p_{applied,n+1} = p_{cr,n} \tag{3.17}$$

and

$$\forall n \in \mathbb{N}, p_{cr,n+1} = f\left(p_{applied,n+1}\right) \tag{3.18}$$

Where f is an increasing function (it is the result of the linear buckling analysis in ADINA). The property of the sequence $(p_{cr,n})_{n \in \mathbb{N}}$ are recalled below. The sequence is increasing:

$$\forall n \in \mathbb{N}, p_{cr,n+1} > p_{cr,n} \tag{3.19}$$

It is possible to find an upper bound P

$$\forall n \in \mathbb{N}, p_{cr,n} < P \tag{3.20}$$

The sequence $(p_{cr,n})_{n \in \mathbb{N}}$ is an increasing sequence and has an upper bound. Therefore it converges to a certain value p_{cr}:

$$\forall \varepsilon > 0, \exists n_0 / \forall n > n_0, \mid p_{cr} - p_{cr,n} \mid < \varepsilon \tag{3.21}$$
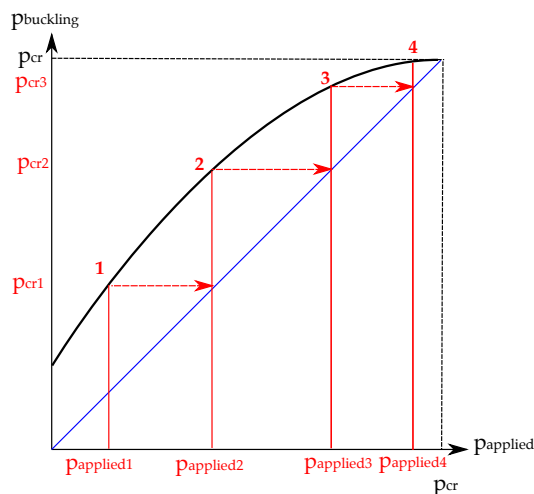
Figure 3.7: Method employed to guarantee accuracy

It is clear that the higher $p_{applied,1}$ is, the closer one will get to the critical load. The convergence criterion can be set by choosing a specific value of ε in equation (3.21). The convergence criterion has been set at $\mid \frac{p_{cr,n+1}L^3}{EI} - \frac{p_{cr,n}L^3}{EI} \mid < 0.1$, which represents generally 1% of the buckling load. It appeared that the procedure converged quickly (around four or five iterations).

3.3   3D validation of computational method

The example of a square grid has been used to validate the numerical method proposed in this work at the Section 3.2.1. The beams are circular hollow sections with an external diameter of 50mm, a thickness of 2mm and a Young Modulus of 35GPa. These properties are quite typical of GFRP pultruded profiles. The beams are supported on end rollers allowing displacements in the plane (XY). Upwards forces of 200N are applied to each connection point. This example has been studied by Cyril Douthe [18], which gives points of comparison.
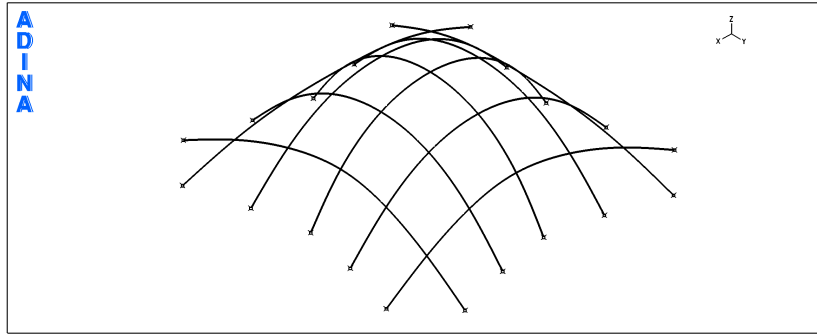
Figure 3.8: Form-finding of an initially flat square grid - 48 elements per beam

The mesh density has been varied from 12 to 60 elements per beam. It is remarkable to notice that the mesh density has a very low impact on the maximal displacements $U_{x,max}$, $U_{z,max}$ and maximal vertical force $R_{z,max}$ of the structure. The finite-element method with the Low-Speed Dynamics converges even if each beam is made out of 12 elements. The consistency of the different models tends to validate the numerical method used for the form-finding in this work: the model is in accordance with the previous finite element studies within a range inferior to 1%.

Model	Nb. of elements	$U_{x,max}$ (in m)	$U_{z,max}$ (in m)	$R_{z,max}$ (in N)
DR [18]	6	1.42	3.41	434
	12	1.37	3.33	450
	24	1.35	3.3	458
	60	1.34	3.29	458
FEM [18]	60	1.36	3.31	459
FEM-Low-Speed Dynamics (this work)	12	1.36	3.32	460
	24	1.36	3.31	462
	48	1.36	3.31	461
	60	1.36	3.31	460

Table 3.3: Comparison of different form-finding methods

The computation time shows the Low-Speed Dynamics method to be stable. The time required to reach convergence increases with the mesh density and remains consistent if the applied is doubled. However, to reach that result, some intermediate steps have been added to guarantee stability. All the models use 20 time-steps of 5 seconds (the Δt in Eq.(3.3)). If this precaution is not taken, the computation time can increase significantly when the applied loads are increased. As for Newton-Raphson scheme, the optimization of the time steps (or of the load factor) is a complex issue and requires experience from the user. The purpose of this work is not to present the optimization of the Low-Speed Dynamics method for the form-finding of grid shells. Based on this example, the form-finding performed during the parametric study was made using several time-steps, the number of steps being increased when convergence seemed to be problematic.

Nb. of elements	Time for $P = 200N$ [s]	Time for $P = 400N$ [s]
12	2.74	3.83
24	3.30	3.55
48	7.05	5.33
60	8.48	6.28

Table 3.4: Computation time for different mesh densities

3.4   Summary

This chapter presented the methodology used for the form-finding and buckling analysis of pre-stressed structure. The comparison with previous studies builds confidence for the rest of this work. We notice that in particular:

- a mesh with a length of $\frac{1}{50}$ of the arc lenth is sufficient to describe both form-finding and buckling load;

- the Low-Speed Dynamics solver is a robust alternative to the form-finding methods presented in Chapter 2;

- a linear buckling analysis is sufficient to predict the collapse load of structures without imperfections;

- some precautions have to be taken to obtain satisfying results with the linear buckling analysis.

The method presented in the Chapter will be used in the next Chapter on the example of a pre-buckled beam used as an arch and will be extended in Chapter 5

Chapter 4

Application to a 2D Arch

This Chapter applies the methodology introduced in the Chapter 3 to a pre-buckled beam used as an arch. The buckling load of the pre-stressed and unstressed structures are compared and discussed. The respective roles of the bending moments and of the compressive axial forces on the stability of the pre-stressed structure are compared.

4.1   Description of the problem and choice of the parameters

Before tackling complex problems, the simple example of the form-finding and buckling analysis of a buckled beam used as an arch has been studied. The shape taken by the arch is one of the rare closed form solutions for nonlinear analysis of beams and is known as the *Elastica*.

The problem of the buckling of the arch is represented on Figure 4.1 and can be described by four quantities:

a) The initial length of the beam L $[m]$;

b) the enforced displacements of each support δ $[m]$;

c) the bending stiffness of the beam EI $[N.m^2]$;

d) the critical line load p_{cr} $[kN.m^{-1}]$.

The model in ADINA uses Hermitian beam elements (finite element formulation of Euler-Bernoulli elements). This means that the shear deformations are supposed to be small, which can be justified by the high slenderness of beams in grid shells. Therefore GA_s is not a parameter in this study. The geometry is fully described by the first two parameters (there is one curve that minimizes the potential energy), the height of the arch for example

can be determined with these parameters. It has to be noticed that EA can play a role for very shallow arches, where snap-through is an issue, but in the case of $\alpha > 10°$, the buckling governs the stability of the structure.

There are four parameters and two different units describing the system (force and length). The application of the Vaschy-Buckingham Π Theorem assures that the system can be described with two dimensionless numbers [9], which simplifies the parametric study of this problem.

$$\Pi_1 = \frac{p_{cr}L^3}{EI} \tag{4.1}$$

$$\Pi_2 = \frac{\delta}{L} \tag{4.2}$$

This theorem assures that the equation describing the physical model can be reduced to the following form:

$$\phi_1\left(\Pi_1, \Pi_2\right) = 0 \tag{4.3}$$

From a practical point of view, this equation can theoretically put into the following form, as explained in [9]:

$$\Pi_1 = \phi_2\left(\Pi_2\right) \tag{4.4}$$

This can be summed up as follows, the function ϕ_2 can change following the boundary conditions.

$$\frac{p_{cr}L^3}{EI} = \phi_2\left(\frac{\delta}{L}\right) \tag{4.5}$$
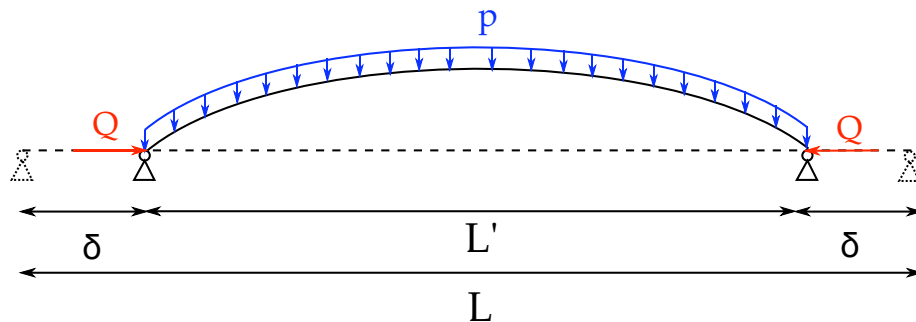
Figure 4.1: Parameters describing the buckling of the arch

To guarantee that the behavior is governed by in-plane buckling, a circular-hollow section has been chosen. The external diameter is of 42mm and the wall thickness is of 3mm. The analysis conducted was a 3D analysis, the out-of-plane rotations were restrained at the supports.
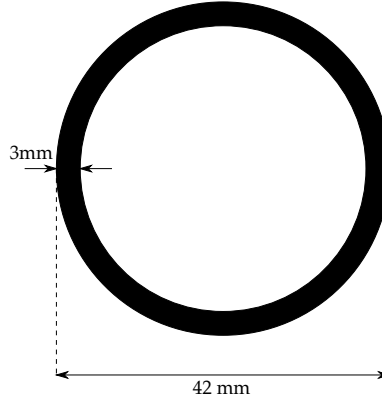
Figure 4.2: Cross-section used in the parametric study

4.2 Comparison of the pre-stressed and unstressed state

4.2.1 Shape of the buckling modes

The first concern before comparing the value of the critical load is to know whether the prestress affects the shape of the buckling modes or not. The first four buckling modes of the unstressed arches have been studied for different values of $\frac{\delta}{L}$. The modes remain qualitatively the same and are summed up in Table 4.1

Mode No.	Description
1	Out of plane
2	In plane
3	Out of plane
4	In plane

Table 4.1: Description of the first buckling modes for the unstressed arches

4.2.2 Influence of the prestress on the buckling capacity

The influence of prestress on stability has been studied for different values of $\frac{\delta}{L}$. Based on estimations of the rise and span of existing projects, it has been estimated that the practical

range for $\frac{\delta}{L}$ is to be between 8% and 17%. It corresponds to a rise of 30% and 50%, which is a typical value observed in prestressed grid shells.

The buckling load for the arch under a line load is compared with a theoretical formula for the buckling of circular arches under normal pressure derived by Timoshenko in [42]. No simple theoretical formula exists for the buckling of the *Elastica*, but it can be expected the approximation by a circular arch to be accurate for low rise, as the variation of curvature of the *Elastica* would be small. The theoretical formulæ for the buckling of a circular arch derived by Timoshenko are read:

$$p_{cr,buckling} = \frac{EI}{R^3}\left(\frac{\pi^2}{\alpha^2} - 1\right)$$ (4.6)

$$p_{cr,snap-through} = \frac{384EIh}{5L^4}\left(1 + \sqrt{\frac{4\left(1-\frac{4I}{Ah^2}\right)^3}{27\left(\frac{4I}{Ah^2}\right)^2}}\right)$$ (4.7)

The Figure 4.3 displays the non-dimensional buckling load $\frac{p_{cr}L^3}{EI}$ for the first in-plane mode in function of the ratio $\frac{L'}{h}$. It reveals that the buckling capacity of a pre-buckled beam used as an arch is lower than an arch with the same geometry and without pre-stress.
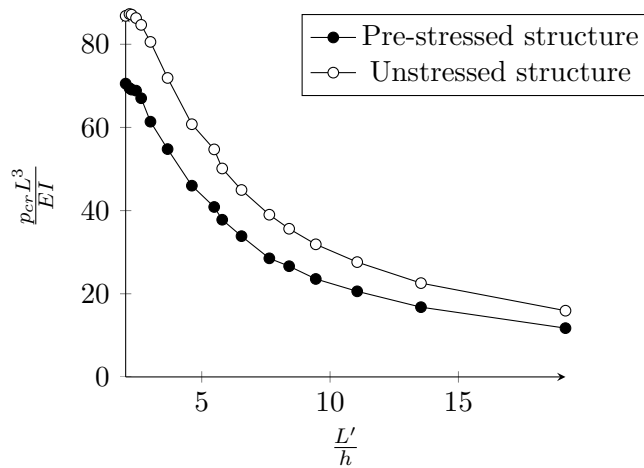
Figure 4.3: Buckling capacity of the *Elastica*: influence of the pre-stress

The buckling load of the unstressed structure calculated with ADINA has been compared to equation 4.6. The Figure 4.4 shows a very good correlation between theory and finite element model for high values of $\frac{L}{h}$ (shallow arches). For $\frac{L}{h} > 6$, the error remains inferior to 1%, and the maximal relative error inferior to 6%.

The bigger difference observed for deep arches can be explained by several factors. First, the theoretical formula proposed is valid for circular arches. The geometry studied is different from a circular arch. For shallow arches, the approximation of the geometry might be satisfying, but as the arch gets deeper, the two geometries become more and more distinct [13]. Secondly, the equation 4.6 assumes a small slope at the base and is only an approximation in the case of deep arches. Despite these small aproximations, it can be considered that for engineering purpose, the accuracy of the finite element is satisfying.
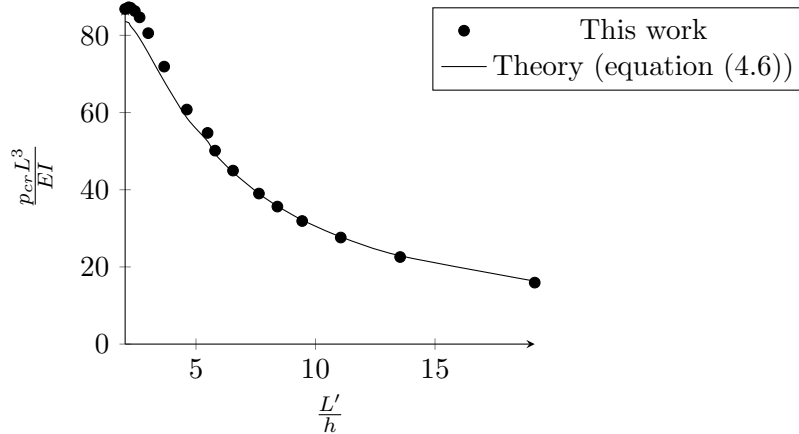
Figure 4.4: Comparison of ADINA and theory - unstressed structure

No analytical solution has been derived for the buckling load of a pre-buckled arch. The validation of the finite element has been made by comparing the results from ADINA with previous experiment [12] and numerical analysis [11]. These previous studies provide few points of comparison, but they all match with the study performed here, as seen in Figure 4.5.
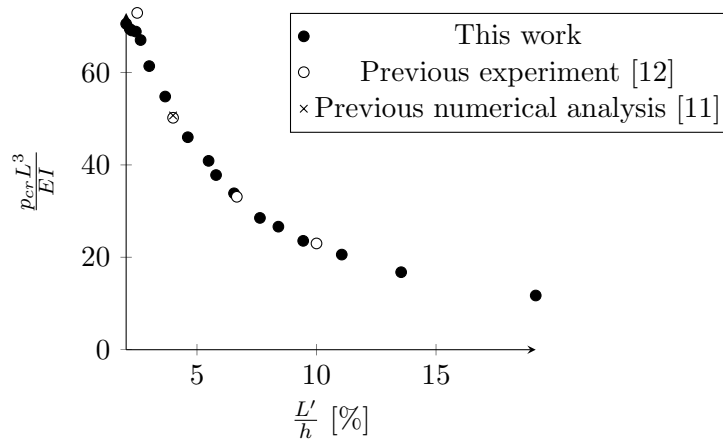
Figure 4.5: Comparison of ADINA with previous works

4.3 Discussion

4.3.1 Buckling capacity of pre-stressed arch

It has been seen that the pre-stress decreases the buckling capacity of arches. In order to quantify this effect, the ratio of the critical line load or the pre-stressed and unstressed structures against the ratio $\frac{\delta}{L}$ has been plotted in Figure 4.6. In one article, Thompson proposed an approximate value of $\frac{p_{cr,pre-stressed}}{p_{cr,unstressed}} = 75\%$ [41]. The results of this study confirms that this approximation is valid for shallow arches (up to $\frac{\delta}{L} = 10$, which corresponds to $\frac{L'}{h} = 3.0$). The data created thanks to the finite element analysis allows to refine the study. A linear regression has been performed, the correlation is of $R^2 = 0.926$, which can lead us to draw some trends.

$$\frac{p_{cr,pre-stressed}}{p_{cr,unstressed}} = 0.4156 \cdot \frac{\delta}{L} + 0.7356 \tag{4.8}$$

The linear regression described by equation 4.8 shows that the ratio $\frac{p_{cr,pre-stressed}}{p_{cr,unstressed}}$ is an increasing function of $\frac{\delta}{L}$. This result runs a bit against intuition: since the pre-stress decreases the buckling capactiy of an arch, one could have expected the linear regression to be a decreasing function of $\frac{\delta}{L}$.
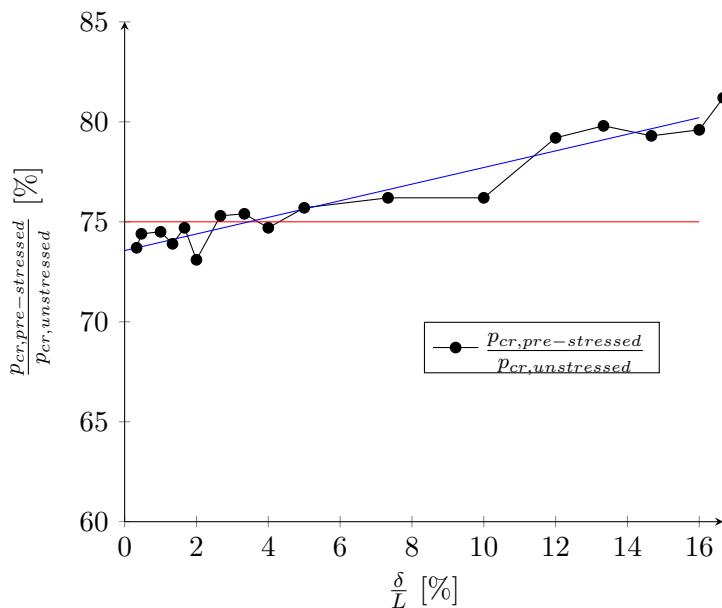
Figure 4.6: Ratio of the critical load - linear regression (blue) and previous approximation [41] (red)

4.3.2 Influence of the initial axial load

To understand this result, the ultimate axial load in the arch has been studied. For that purpose, a uniform load of $p = 1N \cdot m^{-1}$ has been applied to each arch. The axial force at the crown and at the supports induced by this load $N_{p=1,crown}$ and $N_{p=1,support}$ have been measured. The axial force at the crown and supports induced by the prestress $N_{pre-stress,crown}$ and $N_{pre-stress,support}$ have been measured as well. The ultimate axial forces are given by equations 4.9 ans 4.10:

$$N_{cr,pre-stressed} = \frac{p_{cr,pre-stressed}}{1N \cdot m^{-1}} \cdot N_{p=1N \cdot m^{-1}} + N_{pre-stress} \qquad (4.9)$$

$$N_{cr,unstressed} = \frac{p_{cr,unstressed}}{1N \cdot m^{-1}} \cdot N_{p=1N \cdot m^{-1}} \qquad (4.10)$$

As seen in Figure 4.7, the ultimate axial force at the crown is higher for the pre-stressed structure. For high levels of pre-stress (high $\frac{\delta}{L}$), the ultimate axial load at the crown can be 45% higher for the pre-stress structure.
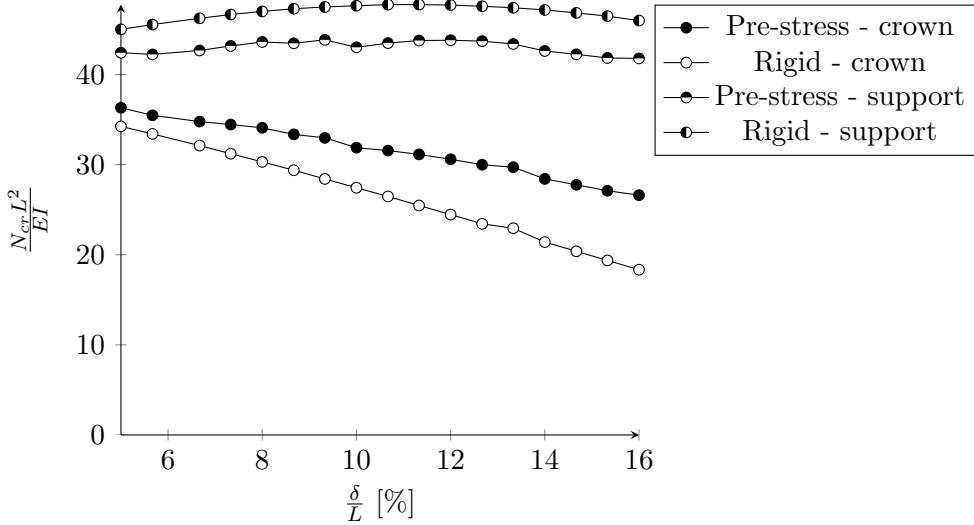
Figure 4.7: Critical axial force at crown and support

The theoretical critical axial force for an unstressed circular arch is given by following formula, which has been derived in [14]:

$$N_{cr,support} = p_{cr}R\left(\alpha \sin \alpha + \frac{\cos \alpha}{2}\left(\frac{(9 - 4\alpha^2)\sin 2\alpha - 10\alpha \cos 2\alpha - 8\alpha}{2\alpha - 3sin2\alpha + 4\alpha \cos^2 \alpha}\right)\right) \qquad (4.11)$$

$$N_{cr,crown} = \frac{p_{cr}R}{2}\left(\frac{(9-4\alpha^2)\sin 2\alpha - 10\alpha\cos 2\alpha - 8\alpha}{2\alpha - 3sin2\alpha + 4\alpha\cos^2\alpha}\right) \tag{4.12}$$

Using (4.6) and noticing that $R = \frac{L}{2\sin\alpha}$, we get:

$$N_{cr,support} = \frac{4EI\sin^2\alpha}{L^2}\left(\frac{\pi^2}{\alpha^2}-1\right)\left(\alpha\sin\alpha + \frac{\cos\alpha}{2}\left(\frac{(9-4\alpha^2)\sin 2\alpha - 10\alpha\cos 2\alpha - 8\alpha}{2\alpha - 3sin2\alpha + 4\alpha\cos^2\alpha}\right)\right) \tag{4.13}$$

$$N_{cr,crown} = \frac{2EI\sin^2\alpha}{L^2}\left(\frac{\pi^2}{\alpha^2}-1\right)\left(\frac{(9-4\alpha^2)\sin 2\alpha - 10\alpha\cos 2\alpha - 8\alpha}{2\alpha - 3sin2\alpha + 4\alpha\cos^2\alpha}\right) \tag{4.14}$$

When the arch is shallow ($\alpha \longleftrightarrow 0$), then we get:

$$N_{cr,crown} = N_{cr,support} = \frac{4\pi^2 EI}{L^2} \tag{4.15}$$

It is noticed that in this case, the axial force due to pre-stress represents 25% of the total buckling of an unstressed arch, as seen in equation (4.16).

$$1 - \frac{F_c}{N_{cr,crown}} = 75\% \tag{4.16}$$

This equation can be compared to the ratio of the buckling load discussed in Section 4.3.1. The relation found in equation (4.16) is identical to the relation discussed by Thompson and Hunt [41]. We can conclude that the majority of the loss of bearing capacity of the pre-buckled arch is due to the initial axial force.

It has already been noticed in Table 3.1 that the axial force does not vary much ($+30\%$ between $\alpha = 0°$ and $\alpha = 90°$) whereas the buckling capacity of the unstressed arch described by Figure 4.3 increases significantly. It explains why the ratio $\frac{p_{cr,pre}}{p_{cr,uns}}$ increases with $\frac{\delta}{L}$: the effect of the initial axial force does not vary as much as the geometrical stiffness.

4.4 Summary

This chapter presented a comprehensive study of the first in-plane mode of a pre-buckled beam used as an arch. The correlation between analytical results and previous experiments confirms the accuracy of the method used. Some trends can be drawn out of the results:

- pre-stressed arches have a lower bifurcation point than unstressed arches with the same geometry;

- this reduction of bearing capacity is due to the axial force induced by the pre-stress;

- the effects of the initial axial force are dominant compared to the one of the initial moment;

- the geometrical stiffness increases faster with respect to the pre-stress than the negative term in the stiffness due to this pre-stress. In other terms, increasing the rise-over-span ratio of a buckled beam will always lead to an improvement of its bearing capacity.

Chapter 5

Application to pseudo-funicular grid shells

This chapter presents the results of the parametric study performed on pseudo-funicular grid shells. Because of the will to provide design guidelines for elastic grid shells, it is important to study realistic values of parameters that could lead to a design. The initial topology of the grid and the coherence of its choice is discussed.

5.1 Expectations

A linearized buckling analysis will give a piece of information on the load where strong nonlinearities occur. However, it does not provide information on the stiffness redistribution in the structure beyond the buckling load. Eventually, a member instability can be a very restrained phenomenon, but it can also influence a global collapse mechanism.

It makes sense to study the influence of the initial stresses in the structure with regard to the different types of buckling modes. Two broad questions can be asked at this stage:

- How does the pre-stress affect the ultimate buckling load of the structure?

- Does the pre-stress change the buckling mode?

(a) Local buckling mode   (b) Global mode
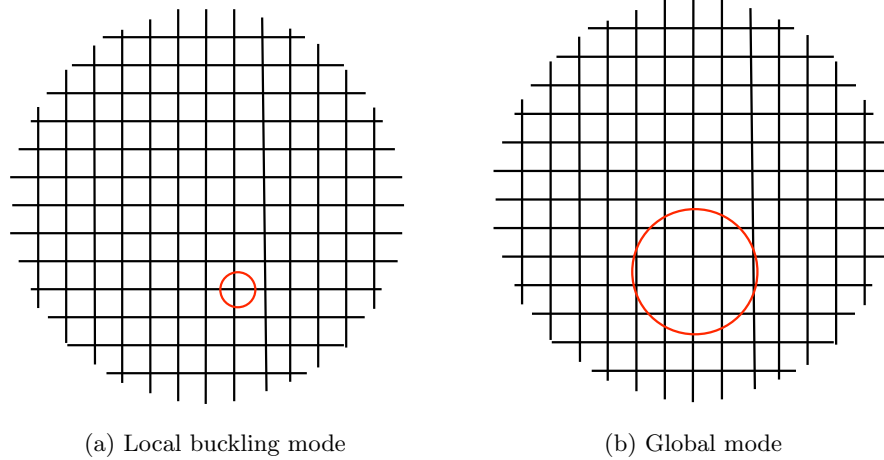
Figure 5.1: Different buckling modes for a circular grid

5.2 Background of the parametric study

5.2.1 Introduction

The intent of this work was to provide results that could be used as guidelines for designers of elastic grid shells. Given the fact that it has been chosen to model single-layer grid shells, it was natural to take inspiration from the previous designs. As already pointed out in Section 2.2.2, this characteristic is typical of composite grid shells. Therefore, typical characteristics of composite materials were used in the finite element model.

The cross-section of the beam elements is identical to the one of the composite grid shells designed by *UR Navier*. The beam are modelled with Hermitian elements with a circular hollow section. The external diameter of the tube is 42mm, the thickness 3mm, the Young's Modulus is taken equal to 25 GPa [17]. Based on a typical span of the composite grid shells of 7m-15m, a typical size of 15m has been chosen for the flat grid.

An important point in the design of elastic grid shells is of course the ultimate stress in the structure during the erection, but also during service. One has to guarantee that the stress does not exceed a specified stress. We refer here to the example of the first grid shell in composite materials, where following design values were considered [17]:

$$\sigma_{erection} < 275 MPa \tag{5.1}$$

$$\sigma_{service} < 110 MPa \tag{5.2}$$

The purpose of this dissertation is not to propose perfect designs of elastic grid shells, but rather explore a variety reasonable possibilities. Therefore, the equations 5.1 and 5.2 were used as guidelines, but we allowed an overcome up to 30% the real design stress in order to generate more solutions.

5.2.2 Form

As it has already been pointed out, grid shells allow a great variety of shapes. The question of the topology of the grids to be calculated during the parametric studies is important, because it should reflect both the formal possibilities offered by elastic grid shells and provide a somewhat generic type of shape. The two main typologies of grid shells that can be identified are the dome and the barrel vault.

It has been shown in previous studies that the buckling capacity of barrel vaults is very sensitive to the curvature introduced in the longitudinal direction (or corrugation) [34]. Barrel vaults seem also to be much more sensitive than regular domes to the mesh orientation. This statement is illustrated by the Figure 5.2. The surface to be covered is generally long (red rectangle), the designer can decide on a form, for example, a cylindrical shape. One dispose of several solutions to mesh the grid shell surface. The first one (on top) reproduces a typology of arches with secondary members. In this case, the pre-stress will be very uneven in the grid: in the case of a cylindrical shape, half of the elements are not curved at all. The stresses in the "arches" will be the limiting factor to the form-finding procedure and the bucking modes are likely to be close to the buckling modes of arches. A more efficient scheme would be to have a grid that is skewed compare to the main span (bottom). In this case, there is no clear hierarchy between the members and the structure will effectively act as a shell.

Plan   Perspective

Plan   Perspective
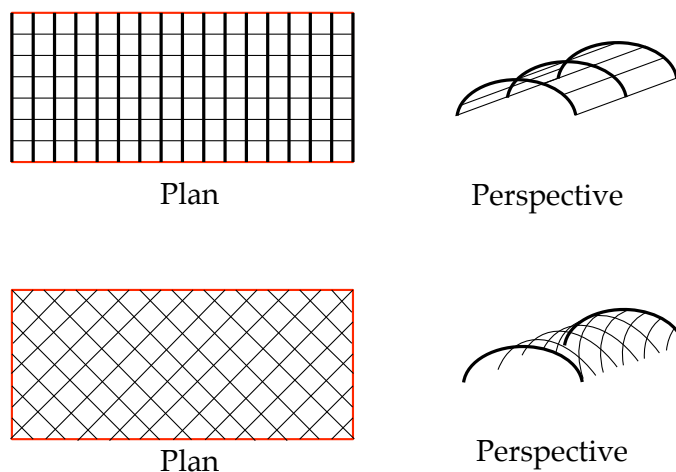
Figure 5.2: Different grid topologies for a same global geometry

These two considerations: sensititivity to corrugation and sensitivity to mesh orientation are not present in regular domes. For circular domes, the orientation has no influence at all on the pre-stress in the elements. Studying domes requires less parameters than the barrel vaults which allows a better understanding of the role of the pre-stress in the results. For that reason, the parametric study focus on regular domes.

Two simple grid shapes have been compared: the first one is the square grid and the second one is the cicular grid.

Square grid

An initially flat square grid gives a regular dome, which was the goal in the choice of the grid topology. However, it appeared in preliminary studies that the shape was not without some problems. The grid remains flat near the corners, giving an unpleasant aspect to the grid shell, as seen in Figure 5.3. Moreover, the bending moment near the corners was limiting the height that could be reached by deforming the grid.
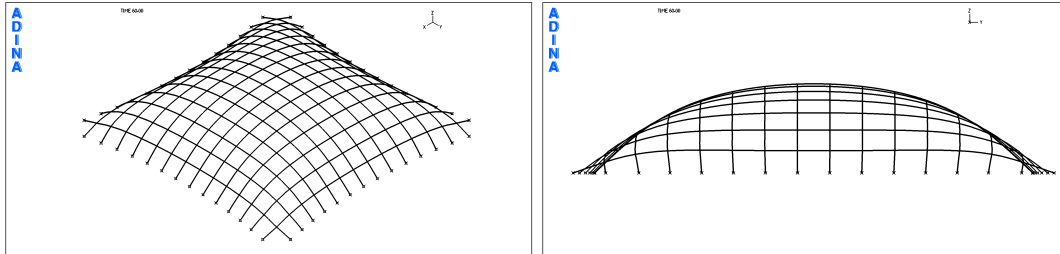
(a) Perspective   (b) Elevation

Figure 5.3: Square grid deformed before stabilization

To understand this problem, one can consider the governing of a membrane supported on a square. The curvature tensor can be described as follows in a moderately large displacement theory.

$$\kappa_{\alpha\beta} = -\frac{\partial^2 w}{\partial\alpha\partial\beta} \tag{5.3}$$

The general membrane equilibrium equation is written as follows:

$$N_{xx}\kappa_{xx} + 2N_{xy}\kappa_{xy} + N_{yy}\kappa_{yy} = p \tag{5.4}$$

where $N_{\alpha\beta}$ is the membrane force tensor, $\kappa_{\alpha\beta}$ is the curvature tensor, and p is the applied load normal to the surface. When the membrane lays over a square, because the edges are

straight, the curvature at the edges is given by:

$$\kappa_{xx}|_{x=\pm x_0} = \kappa_{yy}|_{y=\pm y_0} = \kappa_{xy}|_{y=\pm y_0 or x=\pm x_0} = 0 \tag{5.5}$$

This means that the equation of equilibrium 5.4 is not valid at the corners. The membrane theory only does not describe properly what occurs at the corners. A "membrane" will actually rely on bending deformation near the corners. It explains why wrinkles appear at the corners of inflated structures and why the bending stresses were concentrated at the corners of the square grid. This is why another geometry has been studied in this work.

Circular grid

The shape performs better than the square grid. No stress concentration is observed and the final shape is more aesthetically pleasant. The symmetries of the structure will also make the interpretation of the results more straightforward.

5.2.3 Stabilization

Since the form-finding of grid shells is based on the absence of shear stiffness of the mat, it is clear that a stabilization is necessary once the final shape is obtained.
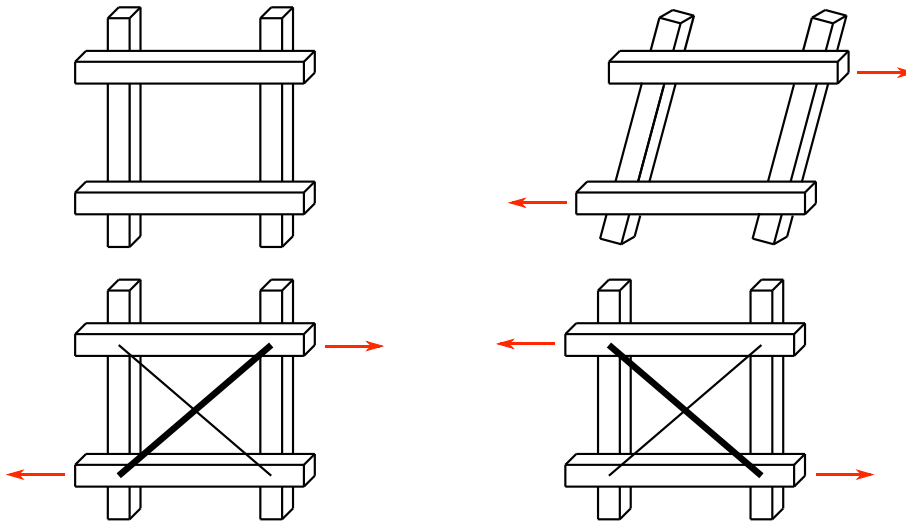
Figure 5.4: Shear deformation of different grid arrangements

Several options can be used, and will be discussed more precisely.

- make the joints rigid after form-finding;

- add cross cables;

- add struts;

- add a third layer;

- a combination of several methods above.

Having rigid joints is an advantage from a visual point of view, since the initial grid can easily be "read". However, it complexifies the design of the connections: creating moment rigid connections for timber or GFRP pipes is a technical challenge by its own. Moreover, this solution is structurally less efficient than a triangulation.

Cables are also a very transparent solution and still allow a good understanding of the initial grid. They have been successfullly used during the Bundesgartenschau in Mannheim. This solution however has two drawbacks. The first is that, since the cables are only efficient in tension, it is necessary to create crosses in order to stabilize the structure in all directions, which eventually doubles the number of connections. Secondly, the cables need to be prestressed in order to be effective, this is an issue for materials subject to bending such as GFRP or timber. Such a solution would require both a control of the tension in the cables during the life of the structure in order to guarantee an effective stabilization and precautions to ensure a good geometric precision during the erection of the grid shell.

Finally, using elements able to carry the loads both in tension and compression is a robust solution that has been chosen for different existing grid shells, such as Downland Gridshell or more recently Solidays' Gridshell. In both cases, the elements were added as a third layer elastically deformed to fit the final shape of the grid. The stiffness of this scheme is likely to be inferior to the one of a solution where straight struts would be mounted on the final shape. However, the montage of straight struts, which are likely to be unique, complexifies the erection sequence: the concept of a third layer is coherent with the first step of the montage and it explains the success of this solution.

For the purpose of this study, and although the practical interest of a third layer has been stated, it seems that using straight elements to triangulate the structure is a good compromise. The behavior of the stabilization is likely to be close to the one of a third layer and it narrows the study to the influence of the initial stresses in the structure to the mat only. If a third layer was introduced, an initial moment in this layer would appear and complexify the parametric study and the interpretation of the results.

In reality, the curvature of the third layer will decrease its "in plane" stiffness. Therefore an equivalent stiffness has to be chosen for the truss elements in ADINA. For this purpose, it is considered that the circular arch is subject to an horizontal load W. The hoizontal stiffness of the arch is given by the ratio of the deflection δ over the applied load W. A theoretical solution of this problem has been derived in [36].
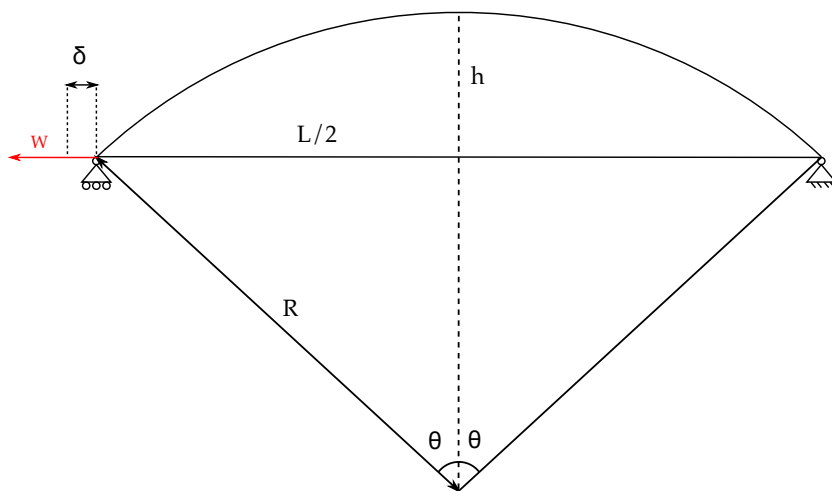
Figure 5.5: Description of the problem of an equivalent truss stiffness

$$k_{arch} = \frac{\delta}{W} = \frac{-R^3}{EI}\left(2\theta c^2 + k_1\left(\theta - sc\right) - 2k_2 sc\right) \tag{5.6}$$

Where $c = cos\left(\theta\right)$, $s = sin\left(\theta\right)$, $\alpha = \dfrac{I}{AR^2}$ $\beta = \dfrac{FEI}{GAR^2}$. The correction factors k_1 and k_2 are defined by $k_1 = 1 - \alpha + \beta$ and $k_2 = 1 - \alpha$. The ratio of the horizontal stiffness and of the axial stiffness of a strut is:

$$r = \frac{k_{arch}}{k_{strut}} = \frac{-AR^3}{IL}\left(2\theta c^2 + k_1\left(\theta - sc\right) - 2k_2 sc\right) \tag{5.7}$$

It is noticed that this ratio depends on the length of the strut as well as of the angle α.

To evaluate realistic values of $\frac{h}{L}$, the case of the subdivisions of a half-circle has been studied. It can be considered as an application of the meshing of the grid presented in Figure 5.2, as seen in Figure 5.6.
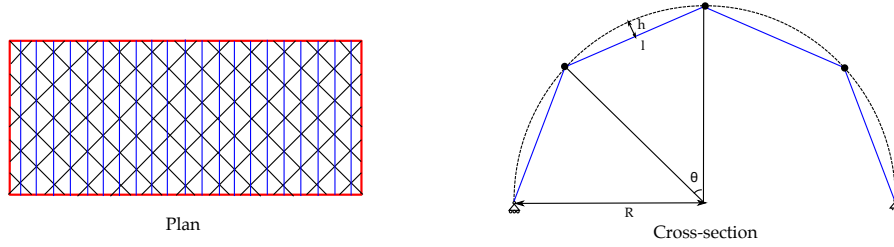
Figure 5.6: Subdivision of a half-circle: stabilization of a cylindrical grid

The geometries studied in this work and the geometries of previous grid shells are more complex, and there are not enough data to estimate the value of $\frac{h}{L}$. However, this small case-study provides the trends on the values of the rise-over-span ratio. We consider a uniform subdivision of the circle with n struts. The length of each strut is given by:

$$l = R\sqrt{2 - 2\cos\theta} \tag{5.8}$$

The rise of the curved element is given by

$$h = R\left(1 - \cos\frac{\theta}{2}\right) \tag{5.9}$$

The rise of the curved element is given by

$$\frac{h}{L} = \frac{1 - \cos\frac{\theta}{2}}{\sqrt{2 - 2\cos\theta}} \tag{5.10}$$

Noticing that $\theta = \frac{\pi}{n}$, we find:

$$\frac{h}{L} = \frac{1 - \cos\frac{\pi}{2n}}{\sqrt{2 - 2\cos\frac{\pi}{n}}} \tag{5.11}$$

The Figure 5.7 is a plot of the equation 5.11. It shows that for relatively coarse meshes (less than 10 subdivisions), the rise-over-span ratio can be of the order of 10%. For finer meshes, it is closer to 1%-2%.
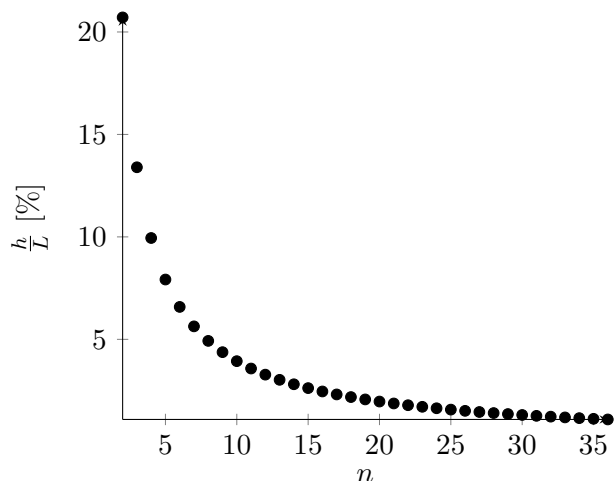
Figure 5.7: Influence of the number of subdivisions on the ratio $\frac{h}{L}$

Typical values for the ratio r defined by equation (5.7) have been investigated. If the first grid shells had fine grids (with a spacing inferior to 1m), the most recent examples have a spacing between 1m [22], [21] and 1.2m [17]. In order to set a unique value of r throughout this work, the cross sections of beams of the prototype GFRP grid shell in *l'Ecole Nationale des Ponts et Chaussées* and of the Savill building have been considered. The real spacing L and a spacing of 2000mm have been used. The Figure 5.8 shows the main results, the ratio r is plotted against the rise-over-span ratio $\frac{h}{L}$ with the notations taken from Figure 5.5.
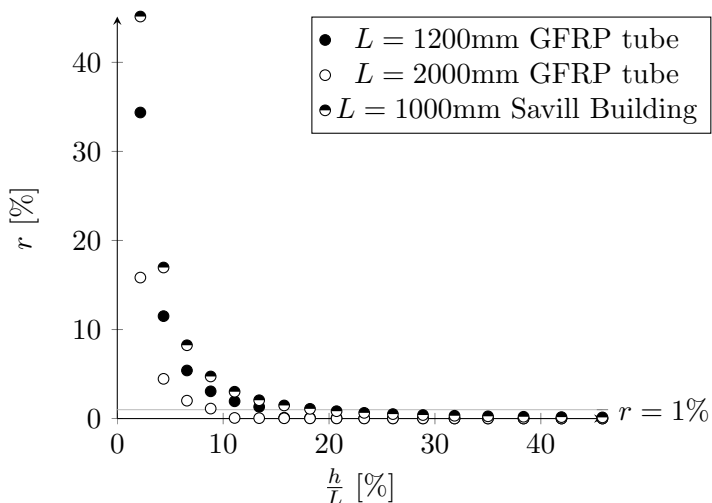
Figure 5.8: Influence of the geometry of the grid on the stiffness of the struts

The Figure 5.8 demonstrates that the stiffness of the truss decreases significantly with the rise-over-span ratio. It is also noticed that the strut of 2000mm is softer than the strut of 1200mm.

This simple study demonstrates the interest of having fine meshes. For fine meshes, the typical value of $\frac{h}{L} = 1\%$ would lead to a much higher stiffness of the bracing compared to a coarse mesh. During the parametric study, the value of $\frac{h}{L}$ can reach 10%. Therefore, this value has been chosen conservatively. As seen in the Figure 5.8, the value of $r = 1\%$ is realistic and had been chosen in the rest of this work.

5.3 Parametric studies

Given the initial geometry of the grid, the buckling of a grid shell can be described by five quantities. In this case, the displacement of the supports δ is not chosen as a parameter. The quantities l (the grid spacing), L (the initial diameter of the grid) and δ are linked together.

For the designer, δ is not an interesting value, but the rise h on the other hand is often an important design parameter. For example, the grid shell of the Odeon in Munich had to be invisible from the outside, implying a restriction on the rise [39]. The five parameters chosen to describe the problem follow:

a) In the reality of a built project, the designer focuses on the final shape and not the initial geometry. Therefore, the final span of the structure $L' = L - 2\delta$ is an interesting dimension;

b) the spacing of the grid l $[m]$;

c) the height of the structure after form-finding h $[m]$;

d) the bending stiffness of the beam EI $[N.m^2]$;

e) the critical line load p_{cr} $[kN.m^{-1}]$.
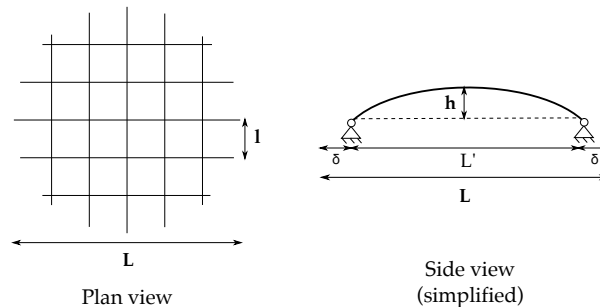
Figure 5.9: Geometric parameters describing the buckling of a circular grid

There are two units (length and force) and five parameters, which means that three dimensionless numbers can be built.

$$\Pi_1 = \frac{h}{L'} \tag{5.12}$$

$$\Pi_2 = \frac{l}{L} \tag{5.13}$$

$$\Pi_3 = \frac{p_{cr}L^3}{EI} \tag{5.14}$$

It has been chosen to study three different values of $\frac{l}{L'}$. These three values correspond to a coarse grid, an intermediate grid and a dense grid. The later one is more likely to be found in real life projects.

Ten different rise-over-span ratios have been studied. It has to be noticed that the the rise-over-span ratio Π_1 is related to the pre-stress in the structure since the bending moment in the structure is proportional to the curvature of the members. Therefore, a high value of the parameter Π_1 means a high "value of pre-stress" in the structure.

(a) Low level of pre-stress   (b) High level of pre-stress
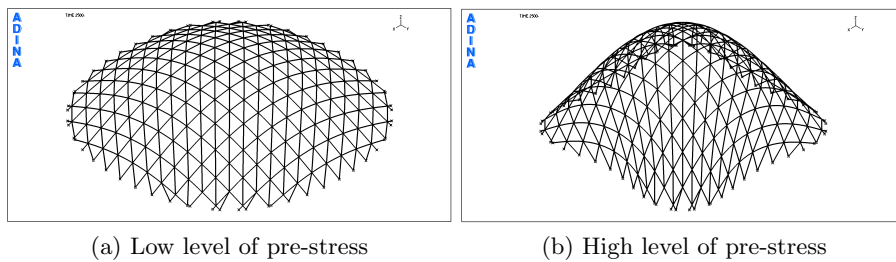
Figure 5.10: The same grid for two different levels of pre-stress

Finally, the elastic grid shells have been compared to grid shells without pre-stress, but the same geometry. For the study of initially flat circular grids, we get 60 values of critical load.
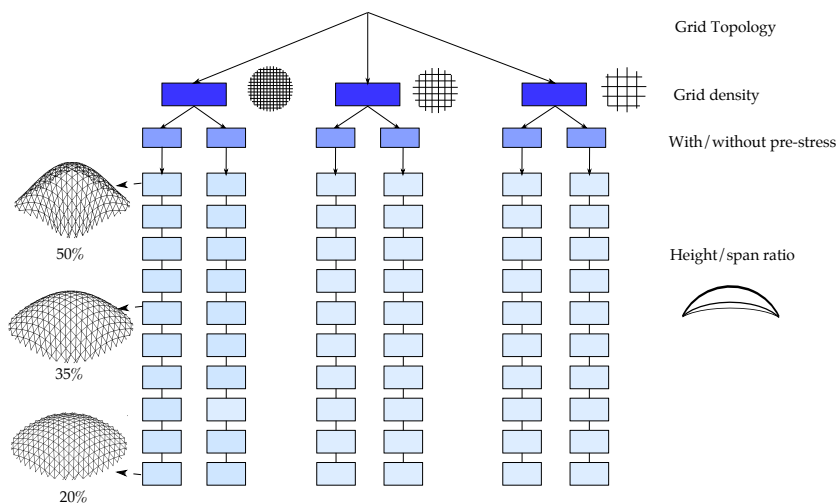
Figure 5.11: Methodology used

The principal values of the parameters are given in the Table 5.1.

Parameter	Value
Cross section	Circular Hollow Section $d_{ext} = 42$mm, $t = 3$mm
Young's modulus	$E = 25$ GPa
Diameter	$L = 15$m
Π_1	$20\% < \dfrac{h}{L'} < 50\%$
Π_2	$\dfrac{l}{L} \in [\dfrac{1}{16}, \dfrac{1}{8}, \dfrac{1}{4}]$

Table 5.1: Design parameters

5.4 Results

5.4.1 Influence of the pre-stress on the mode shapes

The first important consideration was to understand whether or not the pre-stress would have an influence on the buckling modes. It appeared that the buckling modes of the pre-stressed

structures were qualitatively the same as the buckling modes of the unstressed structures.

The dense grid was subject to global modes involving the snap-through of several points and the buckling of several members regardless the level of pre-stress, as seen in Figure 5.12. The first buckling mode is not symmetrical, which can be explained by the non-symmetrical arrangement of the bracing.

(a) Without pre-stress   (b) With pre-stress
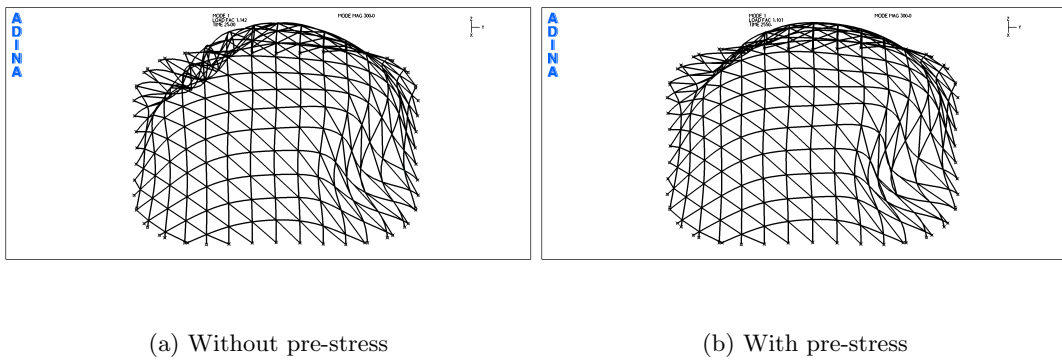
Figure 5.12: Typical first buckling mode for a fine grid (scale factor: 300)

The buckling modes for the intermediate grid were identical, except for one case: the higher level of pre-stress. In this case, the mode of the pre-stressed structure is local whereas the buckling mode of the unstressed structure remains a global mode. In all other cases, the buckling modes remain global for both the pre-stressed and unstressed structures. It can be concluded that the pre-stress has a very little impact on the shape of the buckling modes for the intermediate grid.

(a) Without pre-stress   (b) With pre-stress
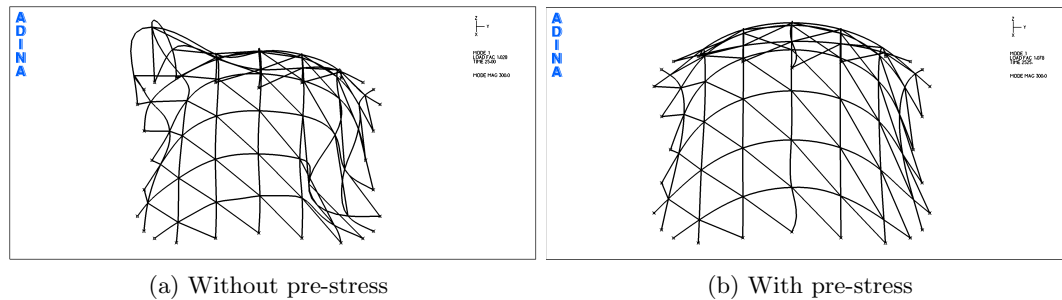
Figure 5.13: First buckling modes for an intermediate grid with a high level of pre-stress (scale factor: 300)

The Figure 5.13 shows the unique difference observed in the qualitative aspect of the first mode. The modes for other levels of pre-stress were similar to 5.13a.

The coarse grid is subject to a much wider variety of modes that would be discussed in part 5.4.2. The modes are member buckling modes, they can be either in-plane (see Figure 5.14) or out-of-plane (see Figure 5.15). The pre-stress does not change the shape of the buckling mode.

(a) Without pre-stress   (b) With pre-stress
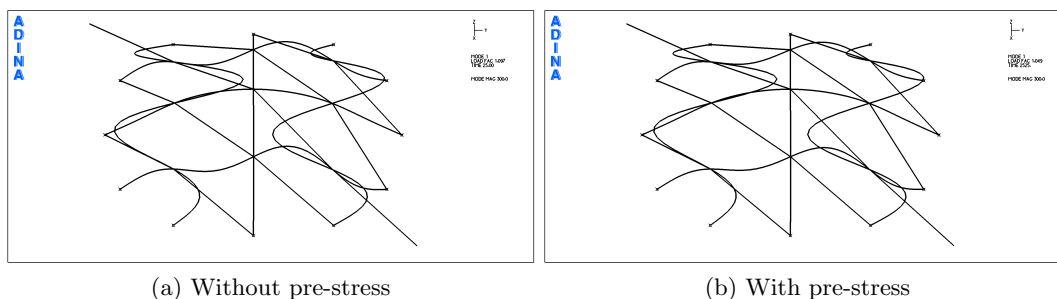
Figure 5.14: In-plane member buckling modes for a coarse grid (scale factor: 300)

(a) Without pre-stress   (b) With pre-stress
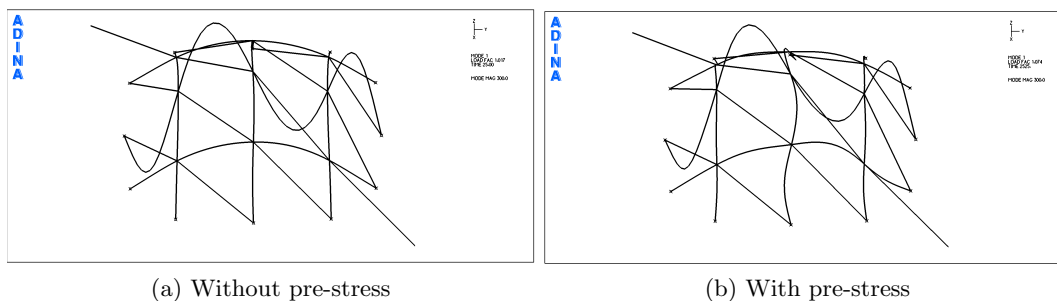
Figure 5.15: Local buckling modes for a coarse grid (scale factor: 300)

The first conclusion that can be made is that the parameters chosen involve different buckling modes and show the complexity of the behavior of grid shells. With only one exception out of the thirty comparisons, the pre-stressed structure always had the same mode shape as the unstressed one. It can thus be concluded that pre-stress has little influence on the mode shapes, which answers the first question asked in the beginning of this chapter. The influence of the pre-stress on the bearing capacity is discussed further.

5.4.2 Influence of the pre-stress on the buckling load

The results of the fine and intermediate grid densities (which are closer to the design examples cited in this work) can be easily compared. Therefore these results are presented together, whereas the coarse grid is presented separately because of a qualitatively different behavior.

Fine and intermediate grids

As for the pre-buckled arch, the buckling capacity of the pre-stressed structure is lower than the unstressed structure. The Figure 5.16 displays the non dimensional load $\frac{p_{cr}L^3}{EI}$ versus the parameter $\frac{L}{h}$. In this case, the first mode is a global mode, and the buckling capacity of elastic grid shell and grid shells decreases when the ratio $\frac{L}{h}$ increases.

Two phenomenons compete in this case: the geometrical stiffness and the forces due to pre-stress increase at the same time. However, the geometrical stiffness increases faster than the negative effect due to pre-stress.

(a) Fine grid   (b) Intermediate grid
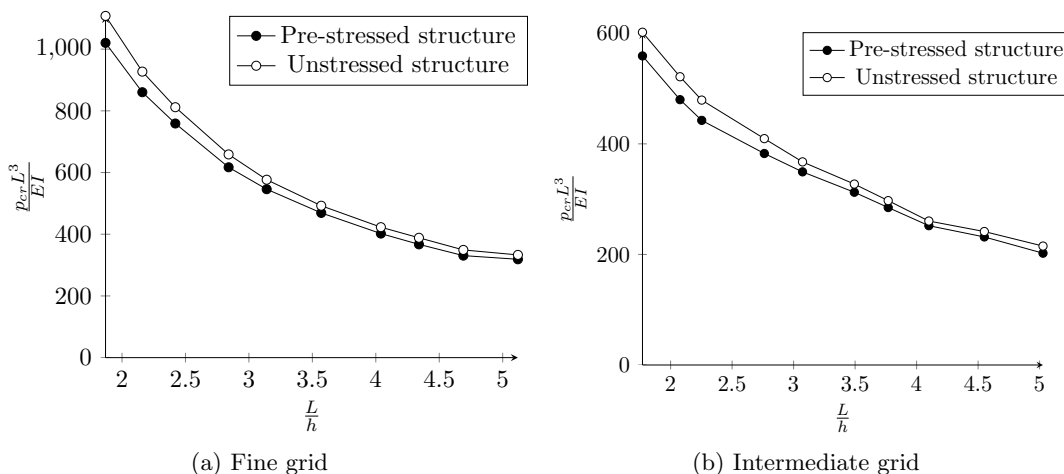
Figure 5.16: Non dimensional critical line load vs. aspect ratio

The trend followed by the ultimate maximal compression force N_{cr} is similar to the one followed by the ultimate line load p_{cr}, as seen in Figure 5.17a. The ultimate maximal compression force N_{cr} increases when $\frac{L}{h}$ decreases. The difference between pre-stressed and rigid structure is less significant than when p_{cr} is considered.
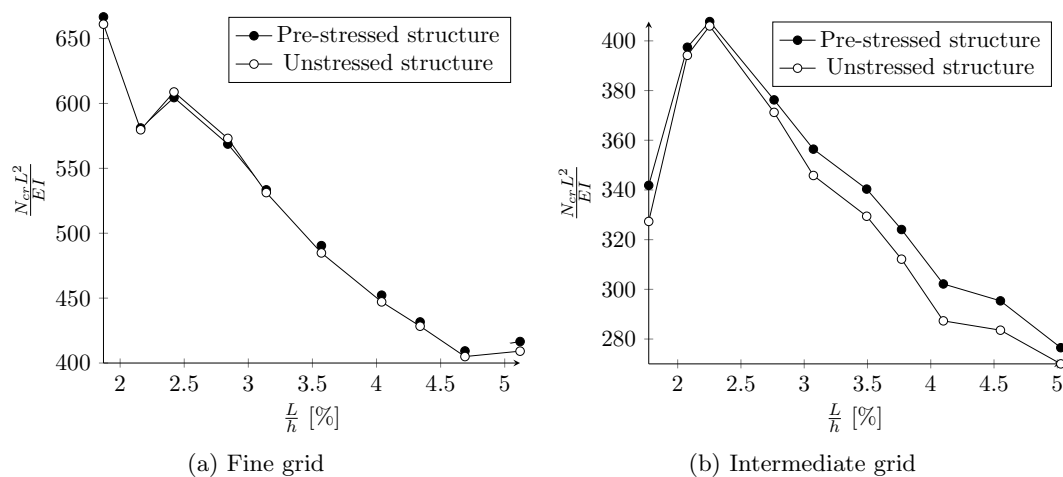
Figure 5.17: Non dimensional axial load vs. aspect ratio

The ratio of the critical loads $\frac{p_{cr,pre}}{p_{cr,uns}}$ and $\frac{N_{cr,pre}}{N_{cr,uns}}$ plotted against $\frac{L}{h}$ can be seen in Figure 5.18. Unlike the pre-buckled beam, the ratio $\frac{p_{cr,pre}}{p_{cr,uns}}$ increases with the ratio $\frac{L}{h}$. The reduction of buckling capacity is much smaller compared to the pre-buckled arch. The mean value of the reduction of bearing capacity is only of 6%, both for the fine and the intermediate grid.

$$\frac{p_{cr,pre}}{p_{cr,uns}}\Big|_{mean} = 94\% \tag{5.15}$$
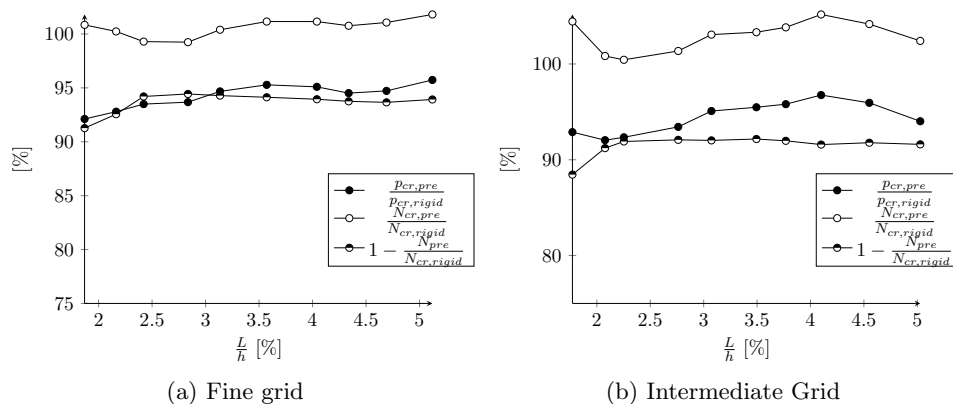
Figure 5.18: Ratio of the critical values

Coarse grid

The results of the parametric study for the coarse grid ($\Pi_2 = \frac{1}{4}$) are qualitatively different and require some comments. First, the increase of buckling capacity with the ratio $\frac{h}{L}$ is not as regular as for the first modes, as seen in Figure 5.19. Actually the shape of the first buckling mode changes with the ratio $\frac{L}{h}$, as seen previously. All the modes involve member buckling, but the modes are in-plane mode for high values of $\frac{L}{h}$ (Figure 5.14) whereas we observed out-of-plan modes for lower levels of $\frac{L}{h}$ (Figure 5.15). More interestingly, the pre-stressed structure seems to have a higher buckling load in certain cases.
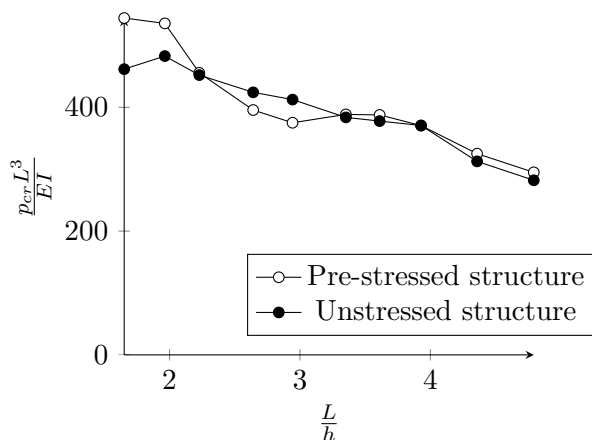
Figure 5.19: Non dimensional critical load vs. aspect ratio - Coarse grid

The same trends can be observed for the critical maximal axial force. The critical maximal force is not a monotonic function, and the variations make it difficult to interpret. It can be related to the mode shape that changes with the ratio $\frac{L}{h}$.
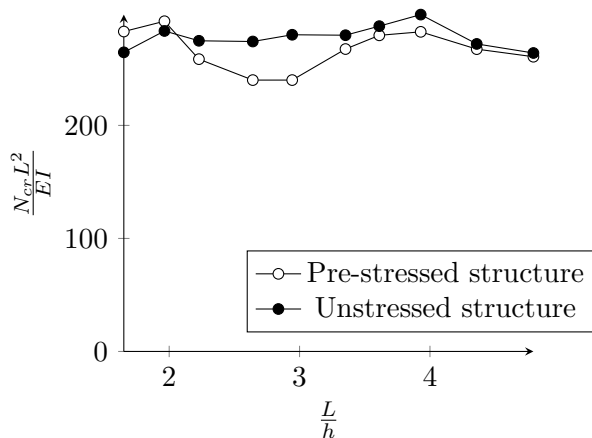
Figure 5.20: Non dimensional axial load vs. aspect ratio - Coarse grid

The ratio $\frac{N_{cr,pre}}{N_{cr,uns}}$ varies between 94% and 117%, whereas the ratio $\frac{p_{cr,pre}}{p_{cr,uns}}$ varies between 85% and 110%. The range of variation is pretty significant and the accuracy of the method of calculation of the buckling load was checked carefully to guarantee that this result is not due to a numerical approximation.
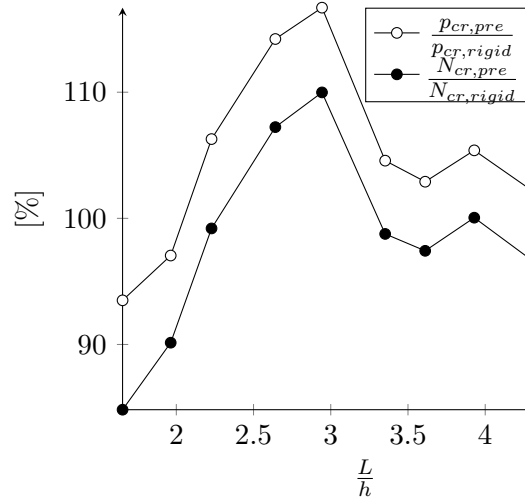
Figure 5.21: Ratio of the critical values - Coarse grid

The increase of the buckling capacity of the pre-stressed structure is discussed in the Section below.

5.5 Discussion

The results show that the buckling capacity of elastic grid shells is inferior to the one of rigid grid shells. The reduction of bearing capacity for the intermediate and fine grids (which are subject to global modes) is between 5% and 10%. Even for a coarse grid with a reach variety of buckling modes, the pre-stress did not have a significant impact on the buckling mode shapes.

As for the pre-buckled arch, we propose to explain the loss of bearing capacity by the effect of the compressive forces coming from the pre-stress. It was indeed observed that for the fine and intermediate grids, the critical maximum compressive force was nearly constant:

$$N_{cr,pre} \simeq N_{cr,uns} \tag{5.16}$$

If we write N_{pre} the maximal compressive force due to the pre-stress, a consequence of equation (5.16) is:

$$\frac{p_{cr,pre}}{p_{cr,uns}} \simeq 1 - \frac{N_{pre}}{N_{cr,uns}} \tag{5.17}$$

With the approximation defined by equation (5.17), the error committed between the formula and the finite element analysis is inferior to 2% for the fine grid, and it is inferior to 5% for the intermediate grid. This shows that the initial axial force in the structure has a significant impact on the ultimate buckling load. It was noticed that the approximation is better as the ratio $\frac{l}{L}$ is smaller, i.e. as the grid is finer. The approximation is also better for lower values of $\frac{L}{h}$, which can be explained by the fact that shallow shells or grid shells have a tendency to experience more bending moment than deep shells or grid shells. However, it does not give satisfying results for the case of the coarse grid, when local buckling occurs. The logical conclusion is that the value of the maximal compression force implied by the pre-stress is not sufficient to explain the behavior of elastic grid shells subject to local buckling.

In order to illustrate the importance of the shape of the buckling mode in the case of local buckling, another geometry with a coarse mesh has been studied. The grid spacing l is equal to the spacing of the coarse grid and the ratio $\frac{L}{l}$ has been set to 16 (like it was for the fine grid). The results of the parametric study are presented in Figure 5.22, where the non-dimensional buckling load $\frac{p_{cr}L^3}{EI}$ is plotted against the ratio $\frac{L}{h}$. Values on the right of the graph correspond to high rise-over-span ratio and to higher pre-stress.
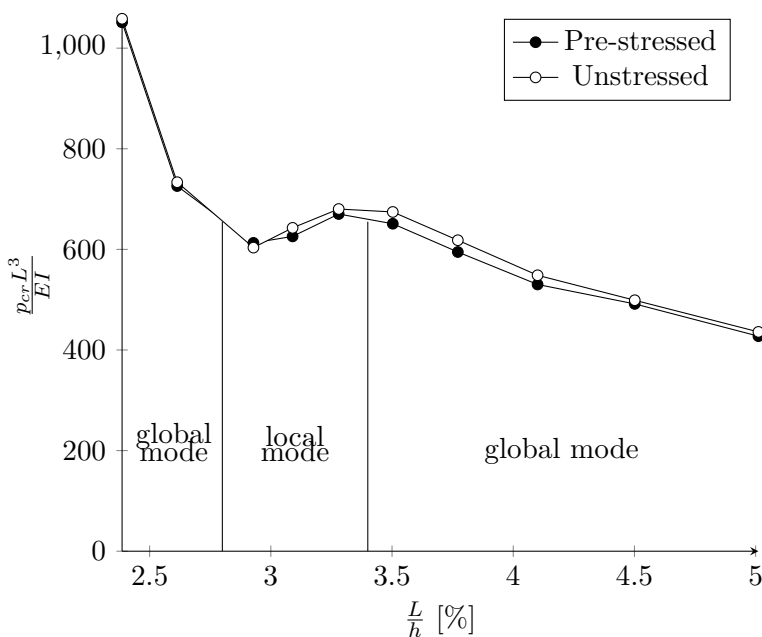
Figure 5.22: Non dimensional critical load vs. aspect ratio - Coarse grid

Unlike the curves obtained for fine grids, the structure does not always gain strength when the rise-over-span ratio increases. The area of loss of strength corresponds to a change from a global buckling mode to a local snap-through of one node.

The snap-through occurs near the supports, as seen in Figure 5.23. In this area, the bending moment due to the pre-stress and the bending moment due to the live load are added. The ratio of the critical loads remain inferior to 100%.
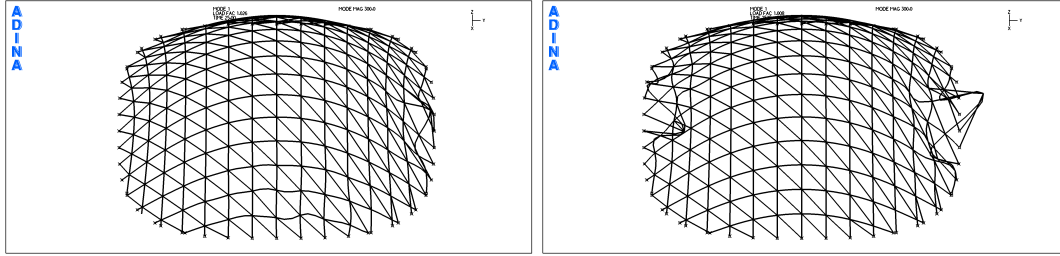
(a) Without pre-stress   (b) With pre-stress

Figure 5.23: First buckling modes for a coarse grid $\frac{L}{h} = 3.1$ (scale factor: 300)

This example illustrates the importance of the mode shape on the relative bearing capacity of elastic and rigid grid shells. Two circular grids with the same spacing l, the same beams, but a different diameter might encounter different mode shapes. When the ratio $\frac{l}{L}$ is small (in this case $\frac{1}{16}$), it seems that the mode is a local snap-through of one node, as seen in Figure 5.23. When the ratio $\frac{l}{L}$ is high (in this case $\frac{1}{4}$) the mode can be more complex and involves the buckling of one or several members (see Figure 5.15).

The fact that the buckling capacity of the elastic grid shell can be superior to a grid shell seems highly counter-intuitive. The buckling mode concerned (Figure 5.15) is very specific: one member buckles entirely, as an arch that would be restrained on five points. It is possible that the bending moment induced by the pre-stress cancels out the moment at the crown, as shown in Figure 5.24.
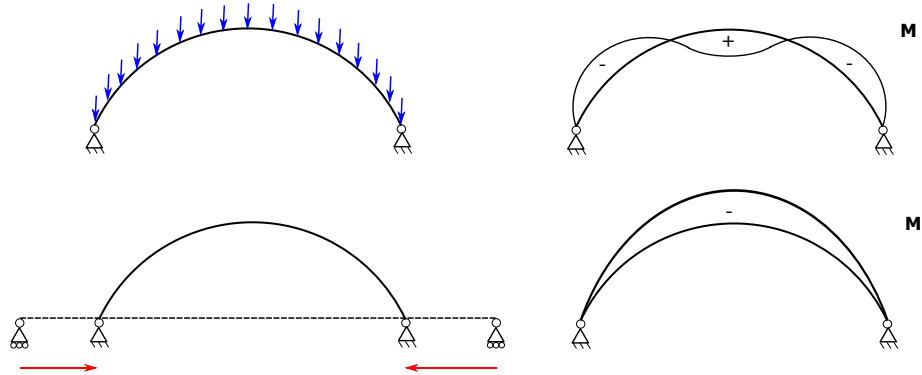
Figure 5.24: Bending moment implied by initial pre-stress and live load

This effect of the moment would explain why the phenomenon does not occur for the grid with $\frac{l}{L} = \frac{1}{16}$. In this case, the local mode occurs at the base of the grid shell, where both axial force and bending moment induced by the pre-stress are added to the existing bending moment and axial forces. However, a finer study on local should be required to clarify that statement, and it is pointed out that the real-life design tend to choose fine grids, as seen in Part A.2.

5.6   Summary

This Chapter presented the results of the parametric studies on the buckling of elastic grid shells. The form-finding of numerous elastic grid shells with a circular grid illustrates the formal possibilities of this solution.

The pre-stress implied by the deformation of the grids decreases the bearing capacity of elastic grid shells. This loss of buckling capacity is reduced compared to a pre-buckled beam, since it is between 5% and 10%. Despite an exploration of different topologies, no difference in the mode shape has been observed in the parametric studies, which led to the conclusion that the pre-stress does not generally influence the shape of the buckling mode of elastic grid shells.

The influence of the initial compressive forces is key to the structural behavior. When the modes are global, the behavior of the elastic grid shell can be inferred by assuming that the critical maximal compressive force is the same for unstressed and prestressed structure. This approximation is better as the grid is finer. Local buckling modes give less consistent results with respect to the critical maximal compressive force. In order to understand them, one needs to look at the local distribution of compressive forces and bending moment.

Chapter 6

Conclusion

6.1 Summary of contribution

The goal of this work was to quantify the influence of the pre-stress due to the deformation of an initially flat grid on the buckling capacity of elastic grid shells. The aim is to understand if the tools and knowledge used for grid shells can be used for elastic grid shells. It was summed up in three questions:

- Does the pre-stress influence the shape of the buckling modes?

- How does the pre-stress affect the bearing capacity of elastic grid shells?

- It is possible to draw parallels between the behavior of elastic grid shells and grid shells?

The strategy proposed to answer these questions was to implement a parametric study involving form-finding and buckling analysis of elastic grid shells. The method was carefully controlled and validated, and can therefore be used again in future works. The method was applied to a pre-buckled arch, where an original correlation between the initial axial force and the critical buckling load was highlighted. It also appeared that the linear buckling analysis of pre-stressed structures is a complex procedure that requires precautions, and more time than the linear buckling of classic grid shells.

The different studies performed as well as comparisons with some theoretical formulæ answered the preliminary questions as follows:

- *Mode shapes:*
  It appeared that even for high levels of pre-stress, elastic grid shells and grid shells have the same buckling mode shapes. This is a considerable factor of simplification for the comparison of these structures.

- *Effect of the pre-stress:*
  This dissertation shows that elastic grid shells are subject to two competing effects: the geometrical stiffness and the loss of stiffness due to pre-stress. The axial force due to the deformation of the structure always leads to a loss of stiffness, the bending moment can eventually have a positive or negative influence following the load case. This phenomenon was also observed clearly on the problem of the stability of a pre-buckled arch.

- *Design considerations:*
  The trend observed suggests that elastic grid shells behave similarly to "rigid" grid shells within a range of 10%, this means that some tools developed for "rigid" grid shells could be adapted to elastic grid shells for preliminary studies. The refined study should however be specific to the pre-stressed structure.

6.2 Future work

The parametric study has been done under restrictive hypothesis in order to find trends in the behavior of elastic grid shells. The first results tend to show that simplified design approaches could be used for elastic grid shells. It also opens new perspectives for future studies. The influence of the imperfections is known to be important for grid shells, but it has to be quantified for elastic grid shells with nonlinear analysis.

This dissertation has set the frame for a parametric study of elastic grid shells. Other geometries could be studied using the same method in order to validate this approach. Another natural continuation of this work would be to identify whether or not the topology optimization of an elastic grid shell can be treated similarly to the topology optimization of a grid shell.

This work only considered uniform symmetrical loadings. Shells and grid shells are known to be more sensitive to unsymmetrical loadings. Therefore some studies should be performed in order to adapt the approximation method proposed in this dissertation. Finally, an experimental procedure could be implemented to complete the studies presented here. If the numerical simulations are a powerful mean to investigate various possibilities, they still remain a numerical approximation of a mathematical representation of a physical phenomenon. Engineers can still learn a lot from experiments, which bring to face to face their analysis to the reality.

Bibliography

[1] ADINA Engineering AB. and ADINA Engineering Inc. *ADINA: Theory and Modeling Guide*. Report AE. ADINA Engineering AB, 1984. 41

[2] M. F. Ashby. *Materials Selection in Mechanical Design*. Butterworth-Heinemann, third edition, 2005. 94

[3] M.R. Barnes. Form-finding and analysis of prestressed nets and membranes. *Computers & Structures*, 30(3):685 – 695, 1988. 27, 95

[4] Klaus-Jurgen Bathe. *Finite Element Procedures*. Prentice Hall, 1st edition, June 1995. 37, 41

[5] Olivier Baverel, Jean-Francois Caron, Frederic Tayeb, and Lionel Du Peloux. Gridshells in Composite Materials: Construction of a 300 m^2 Forum for the Solidays' Festival in Paris. *Structural Engineering International*, 22(3):408–414, 2012. 26, 35, 96

[6] D.P. Billington. *The tower and the bridge: the new art of structural engineering*. Princeton paperbacks. PRINCETON University Press, 1985. 36

[7] Lina Bouhaya. *Optimisation structurelle des gridshells*. PhD thesis, École Nationale des Ponts et Chaussées, 2010. 35, 40

[8] Lina Bouhaya, Olivier Baverel, Jean-François Caron, et al. Mapping two-way continuous elastic grid on an imposed surface: Application to grid shells. In *Proceedings of the International Association for Shell and Spatial Structures (IASS) Symposium 2009, Valencia*, pages 989–998, 2009. 35

[9] E. Buckingham. On physically similar systems; illustrations of the use of dimensional equations. *Phys. Rev.*, 4:345–376, Oct 1914. 52

[10] Th. Bulenda and J. Knippers. Stability of grid shells. *Computers & Structures*, 79(12):1161 – 1174, 2001. 27, 36, 37

[11] J.C. Chilton. *Heinz Isler: The Engineer's Contribution to Contemporary Architecture*. The engineer's contribution to contemporary architecture / series editors Angus Macdonald, Remo Pedreschi. Thomas Telford Limited, 2000. 13, 18, 55

[12] S. Chini and A. Wolde-Tinsae. Buckling test of prestressed arches in centrifuge. *Journal of Engineering Mechanics*, 114(6):1063–1075, 1988. 38, 55

[13] Seyed Chini and Amde Wolde-Tinsae. Effect of prestressing on elastica arches. *Journal of Engineering Mechanics*, 114(10):1791–1800, 1988. 46, 47, 55

[14] A. Delaplace, F. Gatuingt, and F. Ragueneau. *Aide-mémoire de mécanique des structures - Résistance des matériaux: Résistance des matériaux*. Sciences de l'ingénieur. Dunod, 2008. 57

[15] Milos Dimcic. *Structural optimization of grid shells based on genetic algorithms*. PhD thesis, Universität Stuttgart, Holzgartenstr. 16, 70174 Stuttgart, 2011. 18, 33, 36, 40

[16] Nationaler anhang - national festgelegte parameter - eurocode 5: Bemessung und konstruktion von holzbauten - teil 1-1: Allgemeines - allgemeine regeln und regeln für den hochbau, 2012. 33

[17] Cyril Douthe. *Étude de structures élancées précontraintes en matériaux composites: application à la conception des gridshells*. PhD thesis, École Nationale des Ponts et Chaussées, 2007. 25, 34, 42, 61, 68, 94, 95, 96

[18] Cyril Douthe, Olivier Baverel, and Jean-Francois Caron. Form-finding of a grid shell in composite materials. *International Association for Shells and Spatial Structures*, 47(1):53–62, April 2006. 27, 34, 35, 49, 94

[19] James Glymph, Dennis Shelden, Cristiano Ceccato, Judith Mussel, and Hans Schober. A parametric strategy for free-form glass structures using quadrilateral planar facets. *Automation in Construction*, 13(2):187 – 202, 2004. <ce:title>Conference of the Association for Computer Aided Design in Architecture</ce:title>. 22

[20] E. Happold and W.I. Liddell. Timber lattice roof for the mannheim bundesgartenschau. *The Structural Engineer*, 53:99–135, 1975. 14, 21, 30, 87, 88, 89

[21] Richard Harris, S. Haskins, and J. Roynon. The Savill Garden gridshell: design and construction. *The Structural Engineer*, 86(17):27–34, September 2008. 32, 68, 92

[22] Richard Harris, John Romer, Oliver Kelly, and Stephen Johnson. Design and construction of the Downland Gridshell. *Building Research & Information*, 31(6):427–454, 2003. 30, 32, 68, 91

[23] Knippers Helbig. The Theme Pavilion One Ocean. `http://www.knippershelbig.com/press/Pressemeldung_Yeosu_E.pdf`, 2013. 26

[24] A. Holgate. *The Art of the Structural Engineering: The Work of Jörg Schlaich and His Team*. Edition Axel Menges GmbH, 1997. 22

[25] John V Huddleston. Behavior of a steep prestressed arch made from a buckled strut. *Journal of Applied Mechanics*, 37:984, 1970. 38

[26] P. Huovila, United Nations Environment Programme. Sustainable Consumption, and Production Branch. *Buildings and Climate Change: Summary for Decision-makers.* United Nations Environment Programme, Sustainable Consumption and Production Branch, 2009. 35

[27] Amelia Saskia Jülich Saavedra. *Contrôle de forme de passerelle composite.* These, Ecole des Ponts ParisTech, December 2006. 14, 94, 95

[28] D. Noble K. Kensek, J. Leuppi. Plank Lines of Ribbed Timber Shell Structures. In *Acadia 2000: Eternity, Infinity and Virtuality in Architecture*, pages 261–266. 2000. 90

[29] Jan Knippers and Thorsten Helbig. Recent developments in the design of glazed grid shells. *International Journal of Space Structures*, 24(2):111–126, 06 2009. 23, 33

[30] Jan Knippers and Thomas Speck. Design and construction principles in nature and architecture. *Bioinspiration & Biomimetics*, 7(1):015002, 2012. 26

[31] Raph Levien. The elastica: a mathematical history. Technical Report UCB/EECS-2008-103, EECS Department, University of California, Berkeley, Aug 2008. 41

[32] Jian-Min Li and Jan Knippers. Form-finding of grid shells with continuous elastic rods. In *Taller, Longer, Lighter - Meeting growing demand with limited resources.* Proceedings of the International Symposium of the IABSE-IASS Symposium, London, UK, September 2011. 35

[33] Ing K Linkwitz and H-J Schek. Einige Bemerkungen zur Berechnung von Vorgespannten Seilnetzkonstruktionen. *Ingenieur-Archiv*, 40(3):145–158, 1971. 33

[34] Samar Malek. *The Effect of Geometry and Topology on the Mechanics of Grid Shells.* PhD thesis, Massachusetts Institute of Technology, 2012. 27, 36, 62

[35] Johannes Natterer. *Analyse non-linéaire des coques géodésiques multicouches à joints semi-rigides.* PhD thesis, École Polytechnique Fédérale de Lausanne, 2010. 33

[36] R.J. Roark, W.C. Young, and R.G. Budynas. *Roark's Formulas for Stress and Strain.* McGraw-Hill's accessEngineering. McGraw-Hill, 2002. 66

[37] J. Schlaich, R. Bergermann, and A. Bögle. *Leicht Weit.* Prestel, 2003. 23

[38] Jörg Schlaich. Gut genietet ist besser als schlecht geschweißt. Sozialer Brückenbau - die Second Hooghly Bridge in Kalkutta. *DBZ Deutsche Bauzeitschrift*, (58):20–21, August 2010. 25

[39] Hans Schober, Stefan Justiz, and Kai Kuerschner. Opportunities and risks with free-form design. In *Spanning Between Theory and Practice.* Proceedings of the 6th International Conference on Computation of Shell & Spatial Structures, Cornell University, Ithaca, NY, USA, May 2008. 69

[40] Christian Stutzki, Hiroki Tamai, and Joshua Buckholt. Design process, detailing and examples of non-traditional structures. In *Spanning Between Theory and Practice*. Proceedings of the 6th International Conference on Computation of Shell & Spatial Structures, Cornell University, Ithaca, NY, USA, May 2008. 13, 28

[41] J.M.T. Thompson and G.W. Hunt. On the buckling and imperfection-sensitivity of arches with and without prestress. *International Journal of Solids and Structures*, 19(5):445 – 459, 1983. 14, 38, 56, 58

[42] S.P. Timoshenko and J.M. Gere. *Theory of Elastic Stability*. Dover Civil and Mechanical Engineering Series. Dover Publications, 2009. 54

[43] Marguerite Yourcenar. *Mémoires d'Hadrien*. Farrar, Straus and Giroux, 1951. 18

Appendix A

Previous elastic grid shells

This Chapter presents an overview on previous elastic grid shells. First, the characteristics, design procedures and construction of some significant examples are presented. The mechanical and geometrical properties of these structures are summed up in the second part of this Chapter.

A.1 List of previous elastic grid shells

A.1.1 Deubau grid shell in Essen

This grid shell was the German Building Exhibition at Essen and was built in 1962. It is the first elastic grid shell designed by Frei Otto. It lays on a super-elliptical base of 16.82m×16.82m and has a height of 5m [20].

The shape was determined with an hanging chain model. The structure is a single layer grid of timber laths of 60mm×40mm and was lifted with a single crane.

A.1.2 Mannheim Bundesgartenschau

The informations on this building were found in the article written by Edmund Happold [20].

The Multihalle was designed as a temporary building for the *Bundesgartenschau*, a federal horticulture show in Germany in 1976. Given the success of the structure, it is still standing nowadays. By its dimensions (free span of 55m×55m and 9,500m^2), it was a significant change with the previous elastic grid shells, and it remains the biggest elastic grid shells ever built.

The design intent was to create a round free-form structure next to the newly created hill in the park of Mannheim. After the exploration of several lightweight solutions, Frei Otto proposed to build an elastic grid shell. Following the principles he elaborated, he created a hanging chains model in the early steps of the design to determine an acceptable shape (Figure A.1). The final geometry was determined with the technique of stereo photography applied to this model. The *Institut für Anwendung der Geodäsie im Bauwesen* from the University of Stuttgart was responsible of the procedure. Due to small imperfections, some links were not under tensions, and the geometry had to be corrected by Professor Linkwitz with the force density method.
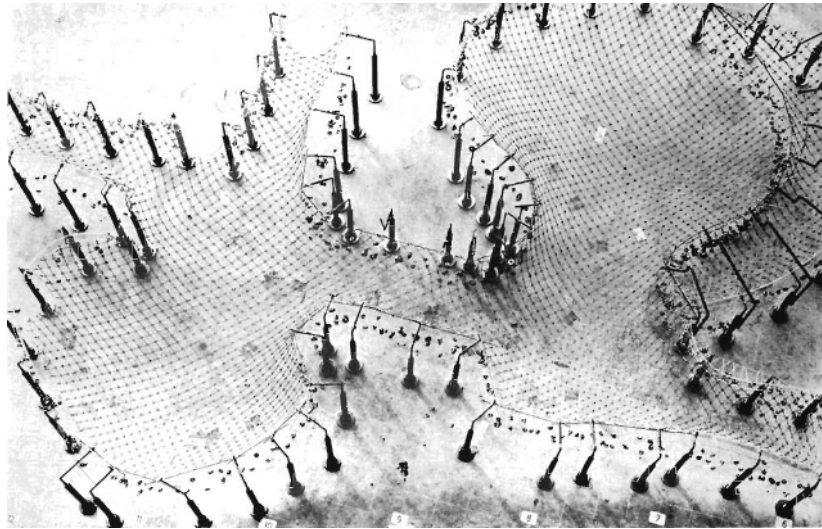
Figure A.1: Early model of the Multihalle - scale 1 : 98 *(photo: [20])*

The loads defined were based on the fact the building is a temporary structure. The snow load was estimated to be $40kg$m$^{-}2$ and the self-weight (including light elements) $20kg$m^{-2}. After some tests on the timber resistance, the designers realized that they had to restrict the cross-section to 50mm×50mm in order to reach the required curvature. The consequence was that they had to use a double layered grid with a spacing of 500mm in order to resist the design load with respect to buckling. The structure is braced with cross-cables every sixth frame.

Since the top layer would have a tendency to elongate and the lower grid to shorten during the mounting process, it was necessary to provide enough flexibility in the connection detail. The solution chosen was to threat a bolt through the laths and drill oblong holes that could allow the sliding of each grid on top of each other, as seen in Figure A.2a and A.2b.

(a) Typical section

(b) Oblong hole
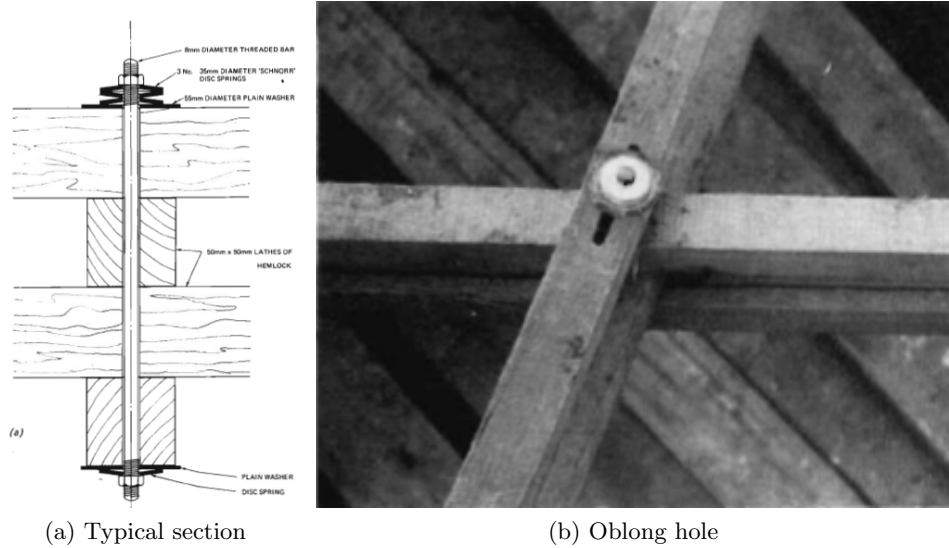
Figure A.2: Connection detail of the Multihalle in Mannheim *(photo: [20])*

The grid was lifted from the ground. For that purpose, scaffolding towers were used, mainly because only very big cranes were able to lift the mass of the grid. The towers were build from the bottom, and as they grew, the lifted the grid. Since points loads were implied by this procedures, the engineers had to analyse carefully the erection sequence. The proposed H-shaped connectors (Figure A.3) that spread the loads and mitigated the risk of punch shearing. The erection sequence only lasted three weeks.
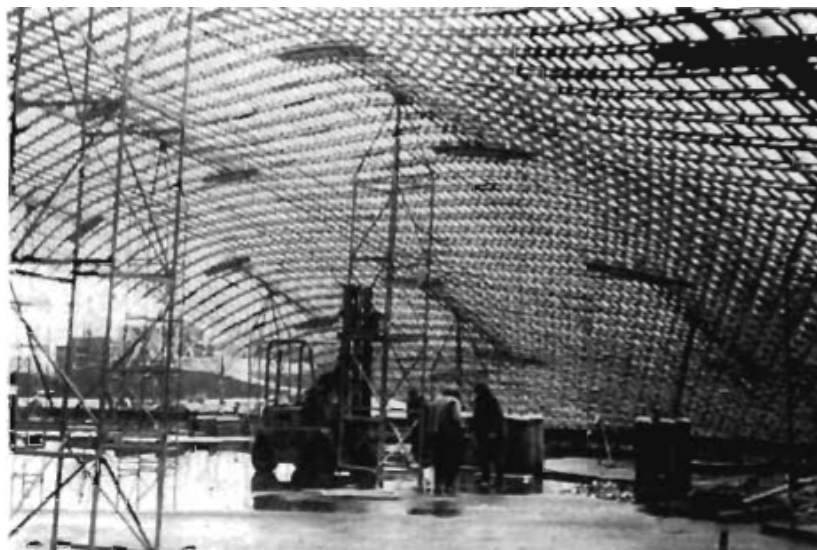
Figure A.3: Lifting of the scaffolding towers *(photo: [20])*

The project is still a reference and a great illustration of the potential of elastic grid shells.

A.1.3 Polydôme, Lausanne

This structure was built in Lausanne (Switzerland) in 1991. The geometry is a portion of a sphere with a radius of 27.5m. It lays on 4 supports and occupies approximately a surface of 25m×25m. The grid follows the geodesic lines. It was designed by the lab *IBOIS* of the l'École Poytechnique Fédérale de Lausanne. [28].
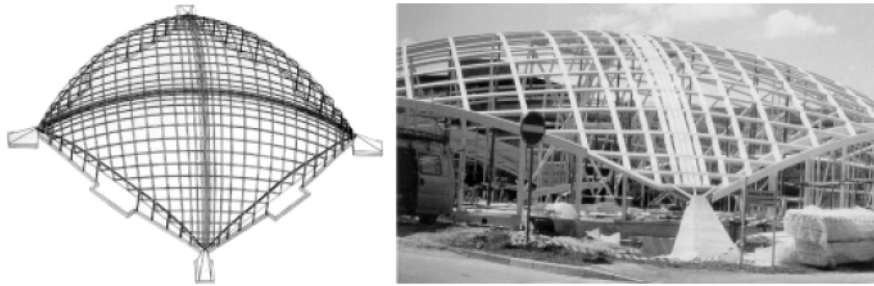
Figure A.4: Drawing and photography of the Polydôme *(BCN Natterer; IBOIS)*

A.1.4 Earth Centre grid shell

The engineers of Buro Happold designed this grid shell which was built in 1998. The structure consists of a single layer grid spanning approximately six meters. The spacing between the laths is relatively small and has been estimated at 200mm from Figure A.5. The structure was lifted with one crane and then adjusted manually to fit the final shape. Important lessons were learnt from it, especially regarding the connections that must allow rotations.

Figure A.5: Earth Centre grid shell

A.1.5 Downland Museum grid shell

The informations on this building were found in an article written by the design team [22].

The "Weald and Downland Open Air Museum" is a centre of excellence for the restoration of timber buildings. A new workshop was needed to display the restoration process to the visitors. An elastic grid shell was an accurate response to the program and had the advantage to show the possibilities of timber (Fig A.6a). Edward Culligan Architects and the engineers of Buro Happold proposed the first double-layered elastic grid shell in the UK.

The structure is a corrugated barrel vault. Several models, including a model at scale 1 : 30 was built in the early stage of the design (Fig A.6b). It guided the engineers for the boundary conditions for the form-finding. It was also a tool to communicate on the feasibility of the project. Unlike the Multihalle in Mannheim, the geometry is not the result of the inversion of an hanging net. The shape was found with the dynamic relaxation method. The physical models helped the engineers define the initial grid geometry. The bending stiffness of the members was considered in the numerical model.
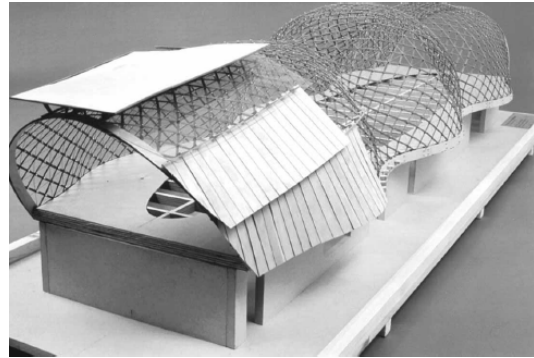
(a) Exterior view   (b) Scale 1 : 30 model *(photo: Harris et al. [22])*

Figure A.6: Downland Museum grid shell: arch. Edward Culligan Architects, Engineer: Buro Happold *(photo: Carpenter Oak & Woodland Limited)*

The grid is made out of four layers of 35mm×50mm oak laths. The spacing of the beams is generally of 1m with a spacing of 0.5m at the corrugation. Shear blocks were inserted upon completion in order to link the different layers and increase the moment of inertia of the structure. The connection detail is different from the one of Mannheim: it does not involve drilling of holes in the timber laths. A patent was submitted by the design team and the contractor (Carpenter Oak & Woodland Limited).

In their paper [22], the design team presented a cost comparison of the elastic grid shell of Downland Museum with other museums built in the same region. With £1097/m^2, the cost of the grid shell is just below the medium cost of typical education or cultural build-

ings (£1140/m^2). It demonstrates that timber elastic grid shells are an economically viable solution.

A.1.6 Savill Building grid shell

The informations on this building were found in an article written by the design team [21].

The biggest elastic grid shell of United Kingdom is located in Windsor, and forms the entry of the Savill Garden. Built in 2006, designed by the engineers of Buro Happold, the structure only constitutes the roof of the building, allowing views on the Garden (Figure A.7). The 28m×90m roof is a three-domed, double-curved structure. The geometry can be described by a sine curve in the longitudinal direction and by a parabola in the transverse direction. The height varies between 4.50m and 8.50m. The shape was defined mathematically and is not pure funicular shape. A grid with uniform length was constructed on this surface. The lateral bracing is not based on cables for aesthetical reasons. The timber roof is used as a diaphragm and provide the in-plane shear stiffness.

Figure A.7: Roof of the Savill Building

The building was designed with an adaptation of the Eurocode 5. Even if the shape is not the perfect result of the inversion of a hanging net, the self-weight of the roof is of 17kg.m^{-2}. This building demonstrates that the techniques and technology developed came to maturity.

A.1.7   Chiddingstone orangery

The informations on this building were found in `http: // fewrightstannergate. wordpress. com/ 2013/ 02/ 04/ structural-inspiration-chiddingstone-castle-orangery-gridshell/ .*

Built in 2007, this grid shell was conceived as an Open Air Wedding Venue. It was designed by Buro Happold and built by Carpenter Oak & Woodland Limited, who worked together on the Downland Museum. Unlike Downland, the grid shell is only a roof sitting on a primary structure, as seen on the general view of the structure A.8. It spans over an elliptical basis of 5m×12m. An elliptical ring beam supports the structure and avoid transfer of the thrust on the ground.

Figure A.8: Chiddingstone orangery: arch. Peter Hulbert, Engineer: Buro Happold *(photo: Carpenter Oak & Woodland Limited)*

The main structure is a four layers grid composed of 40mm× 35mm chestnut beams. The principal innovation of this project is the frameless glass roof. So far, it is the only documented elastic grid shell with a glass covering. The bracing of the structure is guaranteed by 12mm diameter cables. The detail used is an adaptation of the patented detailed developed by Buro Happold and Carpenter Oak & Woodland Limited for Downland. The Figure A.9 shows how this detail has been modified to allow fixation of the glass panels as well as the cables.

Figure A.9: Connection detail *(photo: Carpenter Oak & Woodland Limited)*

Unlike Downland or Savill buildings, no paper has been published on this structure. Based on the different pictures available, it seems that the rise-over-span ratio of the structure is significantly lower than previous elastic grid shells. It can be explained by the smaller span of the structure compared to previous elastic grid shells designed by Buro Happold.

This elastic grid shelll demonstrates that the techniques developed for timber grid shells have come to maturity. It also shows that despite the low stiffness of timber, it is possible to use relatively heavy cladding.

A.1.8   Experimental grid shell in GFRP

This section is based on the thesis and articles published by Cyril Douthe [17],[18].

Built in 2007, this grid shell is the first one to use GFRP (Glass Fiber Reinforced Plastics). It is the result of the research of the *UR Navier* on the use of composite materials in construction. The background of this project is recalled below.

The *UR Navier* lab has applied the material selection method developed by M. Ashby to understand how to use composite materials. This method is based on the reading of maps linking different properties of materials, for example Young Modulus and yield stress [2]. From their research two structural systems seemed to comply with the properties of composite materials, and both are based on the pre-stress of an initial structure.

The first structure developed is a 40m span tied-arch bridge where the arch is made out of a pre-bucked beam [27]. The pre-stress in the arch induces tension forces in the deck and stabilizes it, allowing great slenderness. A prototype at scale 1 : 10 has been built and can be seen in Figure A.10.

Figure A.10: Model of a tied-arch bridge with a pre-stressed arch in GFRP (*photo: Jülich [27]*)

The elastic grid shell presented in this Section is the second application of this principle. Like timber, GFRP have a high yield strain, which allows large deformation of members. However, the higher Young Modulus of composite materials make them more performant as far as buckling is concerned. Moreover, the cost of GFRP remains reasonable [17].

The structure is made out of a two-layers elliptical grid. The GFRP tubes have an external diameter of 42mm and a thickness of 3mm. It covers roughly 150m^2, which is equivalent of an individual house. The structure is used both as roof and facade, an opening has been cut to allow circulation in the structure. The form-finding was performed with AlgoRD, a program developed by Cyril Douthe and inspired by the work of Barnes at the University of Bath [3].

A third layer is used as bracing: it increases the critical buckling load by a factor 15. As seen in Figure A.11, the final pattern is not triangular. Because of the size of the connections (simple scaffolding connections), it was not possible for all the layers to intersect at the same point. It creates a visually interesting pattern. However, it has been shown that a triangular mesh would have increased significantly the buckling capacity of the structure.

Figure A.11: Prototype of an elastic grid shell in GFRP

Measurements of the deflections have been conducted and compared with numerical simulations. Studies on the cost of the prototype have shown that composite grid shells were an economically valid solution. Another prototype of composite elastic grid shell was built on the campus of l'École Nationale des Ponts et Chaussées. The construction, design and cost study are presented in [17].

A.1.9   Solidays' Forum Café grid shell

This section is based on the article published by members of the design team of the grid shell: [5].

The structure is a temporary forum built in 2011 for the festival Soliday's in Paris. It is the first composite grid shell used and designed as a public building. The project is a continuation of the work of *UR Navier* on composite materials and the research on the concept of *flexibility for stiffness*. Other entities were involved in the project, among them students from l'École Nationale des Ponts et Chaussées and the engineering firm T/E/S/S.

The peanut-shaped structure shown on Figure A.12 covered 280m^2 and could hold 500 people. It is 26m long, 7m high and it spans up to 15m. The structure is composed of a double layer grid of 42mm diameter GFRP tubes. As for the experimental prototype built four years before, a third layer is used for bracing. As seen on Figure A.13, the mesh is triangular because of the connection detail used.

Figure A.12: Forum Café - Festival Solidays' (2011) *(photo: Durashell)*

Figure A.13: Forum Café - inside view

Some lessons were learned from this prototype, especially regarding the connection details. The length of the composite extrusions being limited, it is necessary to connect several beams to reach the required span. This problem is solved by the use of fingerjoints in the case of timber structures, but this solution is not valid for GFRP extrusions.

The building confirms the efficiency of elastic grid shells: it took only around ten people and two cranes to lift and stabilize the primary structure. A new composite grid shell has been built by the same design team UR Navier- T/E/S/S in Créteil, some improvements regarding the connections seem to have been used.

A.2 Influence on the choice of the parameters

A.2.1 Mechanical properties of previous elastic grid shells

This Chapter sums up the principal mechanical characteristics of elastic grid shells built so far. The values of height and cross sections were found in the articles cited in this part. The spacing of the grid in the case of Earth Centre grid shell was estimated from pictures.

The values of interest to calibrate the parametric study are recalled in Table A.1. They were used to calibrate the parameters of the parametric study presented in the Chapter 5. The parameters of the parametric study are recalled below:

- $\Pi_1 = \frac{h}{L'}$ the rise-over-span ratio, varies between 30% and 58% in practice;

- $\frac{L'^3}{EI}$ is the softness of the structure (it is expected that for global modes, the critical buckling load is proportional to $\frac{EI}{L'^3}$).

- $\Pi_3 = \frac{l}{L'}$, which defines the refinement of the grid (the smaller this number is, the finer the grid is). It varies between 1% and 18%

In order to calculate the stiffness EI we have considered a Young's modulus of $E = 10$GPa for timber, and of $E = 26.7$GPa for GFRP. The inertia of the double layered grid shells was calculated considering that the different layers were rigidly linked.

Name	Cross section	$\frac{h}{L'}$	$\frac{L^3}{EI}$ [N.m^{-1}]	$\frac{l}{L'}$
Essen	60mm×40mm	$\frac{5}{16.82} = 29.7\%$	$\frac{16.82^3}{3200} = 1.51$	$\frac{0.48}{16.82} = 2.9\%$
Mannheim	50mm×50mm	$\frac{15.5}{55} = 28.2\%$	$\frac{55^3}{135417} = 1.23$	$\frac{0.5}{55} = 0.9\%$
Earth Centre	32mm×15mm	$\frac{3}{6} = 50\%$	$\frac{6^3}{90} = 2.40$	$\frac{0.2}{6} = 3.3\%$
Downland	50mm×35mm	$\frac{9.50}{16.5} = 57.6\%$	$\frac{16.5^3}{46448} = 0.1$	$\frac{1}{16.5} = 6.0\%$
Savill	80mm×50mm	$\frac{8.50}{28} = 30.4\%$	$\frac{28^3}{216667} = 0.10$	$\frac{1}{28} = 3.6\%$
GFRP Grid shell	$d_{ext} = 42$mm; $t = 3$mm	$\frac{3.77}{6.6} = 57.1\%$	$\frac{6.6^3}{1502} = 0.19$	$\frac{1.2}{6.6} = 18.2\%$

Table A.1: Properties of previous elastic grid shells

A.2.2   Consequence on the choice of parameters

Some values of $\frac{h}{L'}$ are superior to 50%, however in the prototype in GFRP and the Downland museum, the grid is not aligned with the span direction. From a practical, all the elements have individually a rise-over-span ratio inferior to 50%. Since the elements follow the lines of principal curvature in the case of circular grids, it has been chosen to restrain the ratio $\frac{h}{L'}$ to 50%. The varying height of Savill building is not shown in the previous table, the ratio $\frac{h}{L'}$ can be inferior to 30%. Finally it has been chosen:

$$20\% < \Pi_1 < 50\% \tag{A.1}$$

The value of $\frac{L'^3}{EI}$ has evolved during the years. The first grid shells of Frei Otto have a value of $\frac{L'^3}{EI}$ between 1 and 2. The Earth Centre grid shell which is pavilion and therefore does not have to fulfil all the requirements of building codes has a higher value, the spacing of the elements is also considerably smaller for this elastic grid shell (200 mm) compared to the other grid shells, which had a spacing between (500 mm and 1200 mm)

The last elastic grid shells designed by Buro Happold and the GFRP prototype have much lower values (inferior to 0.2). It can be understood by the fact that these structures were designed with modern building codes as permanent buildings. Therefore, they require a higher stiffness. We proposed following value in the parametric study:

$$0.1 < \frac{L'^3}{EI} < 2 \tag{A.2}$$

Finally, the typical spacing of the grids varies between 200mm and 1200mm whereas the ratio $\Pi_3 = \frac{l}{L'}$ varies 0.9% and 18.2%. We proposed following variations for Π_3:

$$6\% < \frac{l}{L} < 25\% \tag{A.3}$$

Appendix B

Design of elastic grid shells

This Chapter presents some informations on the design of the elastic grid shells presented in the parametric study. The form-finding procedure is detailed. The ultimate stress and critical pressure are given and compared to common design values.

B.1 Form-finding

The form-finding is an important procedure in the design of an elastic grid shell. It is one of the most computationally expensive phases of the design. The Figure B.1 illustrates different steps calculated with ADINA. The principal steps are described below:

- Step 0 corresponds to the initial state: the circular grid is planar, the supports are free to move in the plane (XY), except one which restrains the three rigid body modes in the plane (XY). This point was added manually after the automatic generation of the grid.

- Steps 1 to 5 describe different stages of the form-finding *per se*: an increasing vertical load is applied to the grid, which implies the deformation. These steps illustrate the variety of shapes that can be obtained with a same grid: from the regular dome of Step 2 to a free-form reminding blob-architecture at Step 5.

- The vertical load is maintained between Step 5 and Step 6 in order to guarantee the numerical stability of the algorithm.

- The motion of the supports in the plane (XY) are restrained at Step 7. In this work, springs with a considerable stiffness are introduced, it was verified on several models that they did not affect the buckling load with the stiffness chosen. Because in practice, the bracing is added to the structure subject to its self-weight, he self-weight of the structure is applied.

- The self-weight is maintained between Step 7 and Step 8, here again to guarantee numerical stability of the procedure

- Finally, the bracing is introduced at Step 9. The stiffness of the structure is been multiplied several times thanks to this procedure. Step 10 corresponds to the last stabilization of the structure.
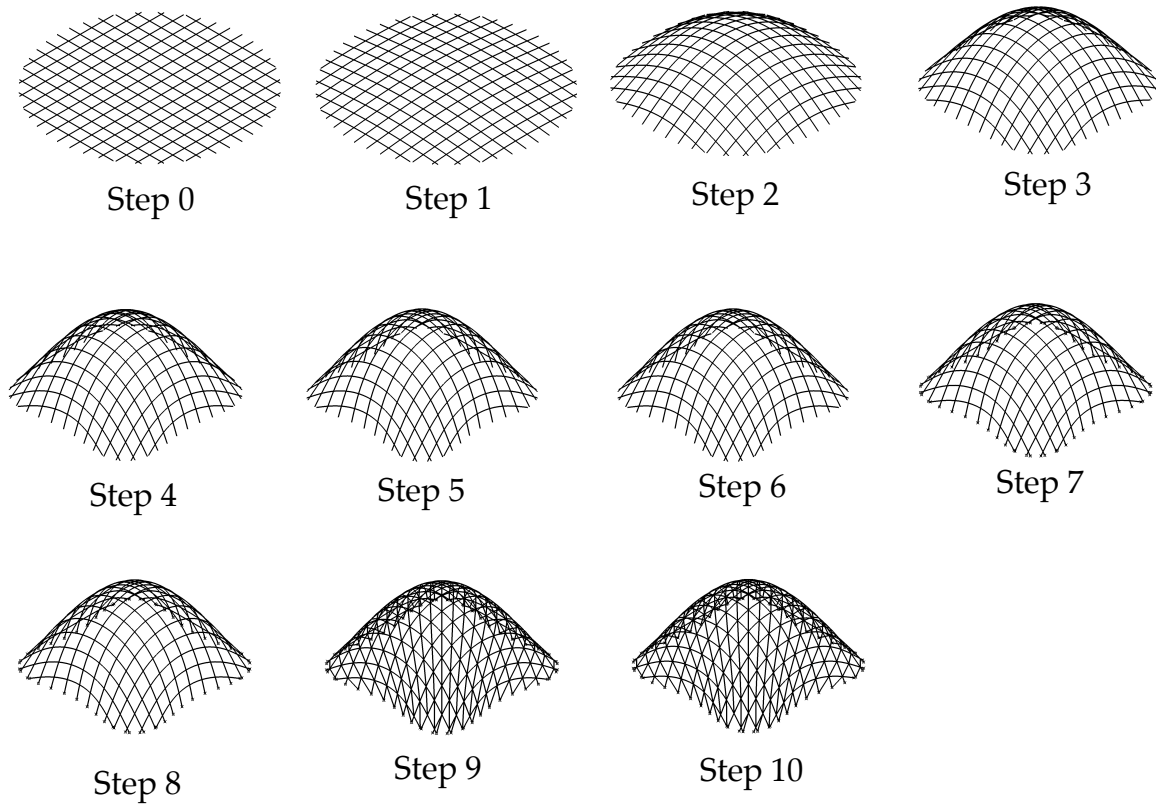
Figure B.1: Different steps of the form-finding

B.2 Maximal stress

The maximal stress after form-finding for the load case combination self-weight+pre-stress was calculated for all the elastic grid shells. With one exception, they all had a stress below the design stress considered, as seen in Figure B.2.
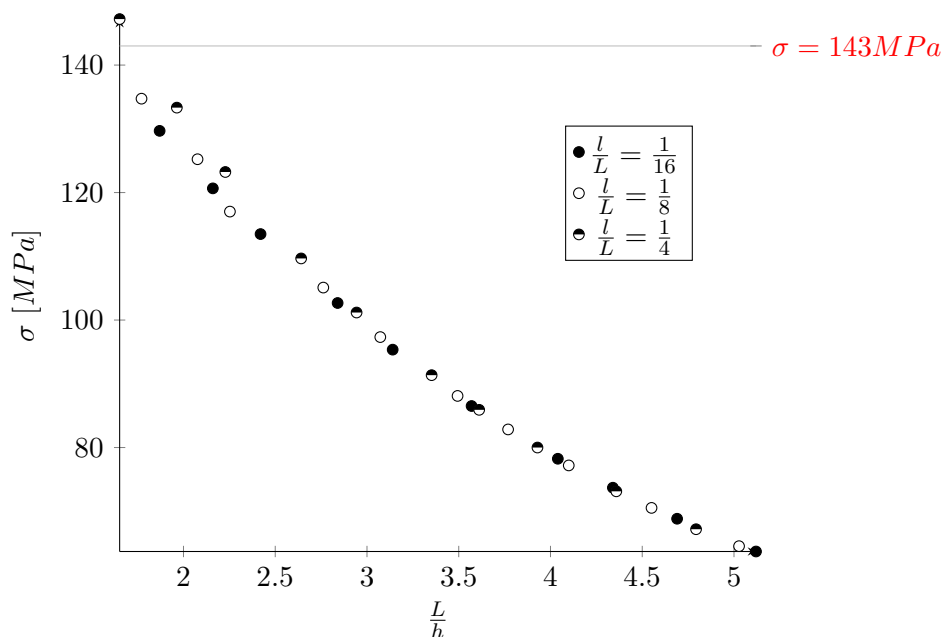
Figure B.2: Stress under self-weight and pre-stress for the different models

Even though this does not constituts a real design with respect to stress, it shows that the models considered in the parametric studies are reasonable.

B.3   Critical pressure

In order to get a sense of whether a design is realistic or not, the critical line load calculated was converted into a critical pressure with following equation, with the same notations as in Chapter 5:

$$q_{cr} = \frac{2p_{cr}}{l} \tag{B.1}$$

The equivalent critical pressure is displayed on Figure B.3. It appears that some design (for the fine grid) provide quite high critical pressures. The design with the fine grid seems to be a quite realistic design, given typical values for snow loads (for example a characteristic value of $q_{snow} = 600Pa$ is fairly common in western Europe).
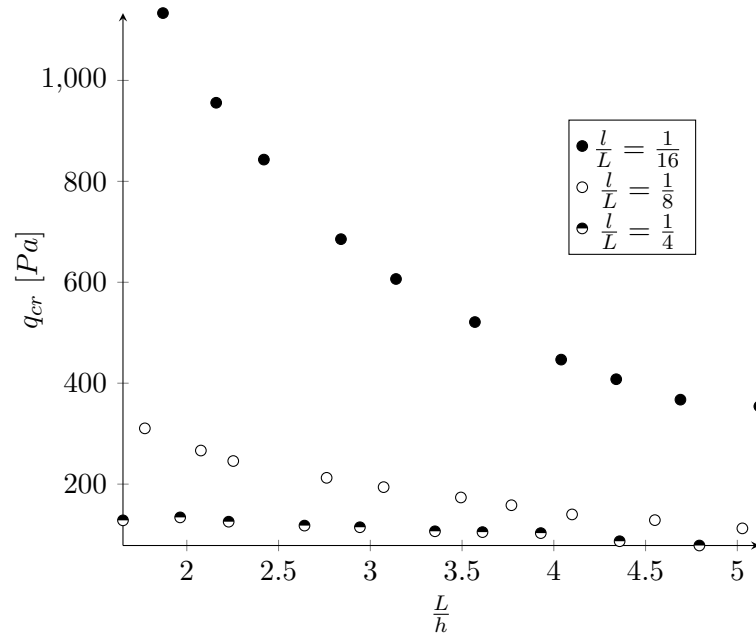
Figure B.3: Critical pressure for the different models

Once again, this study does not provide the design of elastic grid shells, but gives the main trends followed by the different options. It can be seen that the coarse grid calculated is non realistic in this particular design situation. However, it has been chosen to consider it because it showed different local buckling modes that are susceptible to occur in elastic grid shells with complex geometries.

Appendix C

MATLAB Code

C.1   Generation of a circular grid

```matlab
%This program creates a flat circular grid with no shear stiffness (the
%members of the grid are connected with links. A third "grid" is created.
%For the sake of simplicity, this grid is modelled with truss elements


clear all
hold on

%% INPUT IN METER, NEWTON

    Nodes=[]; % contains the nodes each line refers to the number of the ...
        point and the coordinates X Y Z
    Members=[]; %contains the members of the square grid
    Links=[]; %contains the links
n=input('Please insert the number of bars in each direction, n: ');
l=input('Please insert the span of the grid, l [m]: ');
h=input('Please insert the offset in Z-direction, h [m]: '); % this will ...
    offset the beams oriented on the Y axis

Blocked_nodes=zeros(4*n,1);
Blocked_nodes_1=zeros(4,1);
Deleted_nodes=[];

%% Parameters for the ellipse
% The parameters can be changed provided the ellipse fits into the contour
% Equation of the ellipse (x-x0)^2/a^2+(y-y0)^2/b^2=1

a=l/2; %length of the half axis in x
b=l/2; %lenghth of the half axis in y
x0=l/2; %center of the ellipse (in x)
y0=l/2; %center of the ellipse (in y)
```

```matlab
30
31
32  %————————————————————————————————
33  %————————————————————————————————
34  %————————————————————————————————
35
36  %% I—CREATION OF THE MESH TOPOLOGY
37
38  c1=1;
39  for k=1:n
40      Nodes=vertcat(Nodes, [c1,k*l/(n+1),0,h]);
41      c1=c1+1;
42  end
43  for k=1:n
44      Nodes=vertcat(Nodes, [c1,0,k*l/(n+1),0]);
45      c1=c1+1;
46      for j=1:n
47          Nodes=vertcat(Nodes, [c1,j*l/(n+1),k*l/(n+1),0]);
48          c1=c1+1;
49          Nodes=vertcat(Nodes, [c1,j*l/(n+1),k*l/(n+1),h]);
50          c1=c1+1;
51      end
52      Nodes=vertcat(Nodes, [c1,l,k*l/(n+1),0]);
53      c1=c1+1;
54  end
55  for k=1:n
56      Nodes=vertcat(Nodes, [c1,k*l/(n+1),l,h]);
57      c1=c1+1;
58  end
59  Nodes=vertcat(Nodes, [c1,0,0,0],[c1+1,0,l,0],[c1+2,l,0,0],[c1+3,l,l,0]);
60
61  c2=1;
62  %% CREATION OF BOUNDARIES
63
64  for k=1:n
65      Blocked_nodes(c2)=k;
66          c2=c2+1;
67  end
68  for k=1:n
69      Blocked_nodes(c2)=(2*k−1)*(n+1);
70      c2=c2+1;
71      Blocked_nodes(c2)=(2*k+1)*(n+1)−1;
72      c2=c2+1;
73  end
74  for k=1:n
75      Blocked_nodes(c2)=2*n^2+3*n+k;
76          c2=c2+1;
77  end
78  Blocked_nodes_1(1)=c1;
79  Blocked_nodes_1(2)=c1+1;
80  Blocked_nodes_1(3)=c1+2;
81  Blocked_nodes_1(4)=c1+3;
82
83  % On the first and last line, there are n nodes, on the n other lines in
```

105

```matlab
84  % the middle, there are 2*n+2 nodes. In the end, there are n*(2*n+2)+2*n
85  % nodes, which can be simplified to 2*n^2+4*n
86
87  %% CREATION OF THE MEMBERS IN THE Y-DIRECTION
88
89  c=1; %help numbering the members
90
91  for k=1:n
92      Members=vertcat(Members, [c,k,((n+1)+2*k-1)]);
93          c=c+1;
94      for j=1:(n-1)
95          Members=vertcat(Members, [c,(2*j-1)*(1+n)+2*k-1,(2*j+1)*(1+n)+2*k-1]);
96          Links=vertcat(Links, [(2*j-1)*(1+n)+2*k-1,(2*j-1)*(1+n)+2*k]);
97          c=c+1;
98      end
99      Members=vertcat(Members, [c,(2*n-1)*(1+n)+2*k-1,2*n^2+3*n+k]);
100     Links=vertcat(Links, [(2*n-1)*(1+n)+2*k-1,(2*n-1)*(1+n)+2*k]);
101     c=c+1;
102 end
103
104 %% CREATION OF THE MEMBERS IN THE X-DIRECTION
105 for k=1:n
106     Members=vertcat(Members, [c,(n+1)*(2*k-1),(n+1)*(2*k-1)+2]);
107         c=c+1;
108             for j=1:(n-1)
109         Members=vertcat(Members, [c,(n+1)*(2*k-1)+2*j,(n+1)*(2*k-1)+2*(j+1)]);
110         c=c+1;
111             end
112         Members=vertcat(Members, [c,(n+1)*(2*k+1)-2,(n+1)*(2*k+1)-1]);
113         c=c+1;
114 end
115 %% CREATION OF THE MEMBERS FOR TRIANGULATION
116
117 % First the longest member is created, then two loops will be used to
118 % create the other diagonals, this will provide a single triangulation
119
120 Members_truss=[]; % contains the "truss" elements for stabilization ony
121
122     Members_truss=vertcat(Members_truss, [c,2*n^2+4*n+1,n+2]);
123         c=c+1;
124     for j=1:(n-1)
125     Members_truss=vertcat(Members_truss, ...
126         [c,(2*j-1)*(n+1)+(2*j-1),(2*j+1)*(n+1)+(2*j+1)]);
126         c=c+1;
127     end
128     Members_truss=vertcat(Members_truss, [c,2*n^2+3*n-2,2*n^2+4*n+4]);
129         c=c+1;
130
131 for k=1:(n-1)
132     Members_truss=vertcat(Members_truss, [c,(2*k-1)*(n+1),(2*k+1)*(n+1)+1]);
133         c=c+1;
134         for j=1:(n-k-1)
135             Members_truss=vertcat(Members_truss, ...
                    [c,(2*(k+j)-1)*(n+1)+2*j-1,(2*(k+j)+1)*(n+1)+2*j+1]);
```

```
136         c=c+1;
137         end
138         Members_truss=vertcat(Members_truss, ...
                [c,(2*(n-1)+1)*(n+1)+2*(n-k-1)+1,2*n^2+4*n-(k-1)]);
139         c=c+1;
140 end
141
142 for k=1:(n-1)
143     Members_truss=vertcat(Members_truss, [c,k,(n+1)+2*(k+1)-1]);
144         c=c+1;
145         for j=1:(n-k-1)
146             Members_truss=vertcat(Members_truss, ...
                    [c,(2*j-1)*(n+1)+2*(k+j)-1,(2*j+1)*(n+1)+2*(k+j+1)-1]);
147         c=c+1;
148         end
149         Members_truss=vertcat(Members_truss, ...
                [c,(2*(n+1-k)-1)*(n+1)-3,(2*(n+2-k)-1)*(n+1)-1]);
150         c=c+1;
151 end
152
153 % in following code, member_truss is updated to have a double triangulation
154
155 %     c=c+1;
156 %     for j=1:(n-1)
157 %     Members_truss=vertcat(Members_truss, ...
          [c,(2*j-1)*(n+1)+2*(n+1-j),(2*j+1)*(n+1)+2*(n-j)]);
158 %         c=c+1;
159 %     end
160 %     Members_truss=vertcat(Members_truss, [c,2*n^2+n+1,2*n^2+4*n+2]);
161 %         c=c+1;
162
163 %         for k=1:(n-1)
164 %             Members_truss=vertcat(Members_truss, [c,n+1-k,(n+1)+2*(n-k)]);
165 %             c=c+1;
166 %             for j=1:(n-k-1)
167 %             Members_truss=vertcat(Members_truss, ...
          [c,(2*j-1)*(n+1)+2*(n-k+1-j),(2*(j+1)-1)*(n+1)+2*(n-k-j)]);
168 %             c=c+1;
169 %             end
170 %             Members_truss=vertcat(Members_truss, ...
          [c,(2*(n-k)-1)*(n+1)+2,(2*(n-k+1)-1)*(n+1)]);
171 %             c=c+1;
172 %         end
173
174  %         for k=1:(n-1)
175  %             Members_truss=vertcat(Members_truss, ...
          [c,(2*k+1)*(n+1)-1,(2*k+1)*(n+1)+2*n]);
176  %             c=c+1;
177  %             for j=1:(n-k-1)
178  %             Members_truss=vertcat(Members_truss, ...
          [c,((2*(k+j)-1)*(n+1)+2*(n+1-j)),(2*(k+j+1)-1)*(n+1)+2*(n+1-j-1)]);
179  %             c=c+1;
180  %             end
```

```matlab
181   %            Members_truss=vertcat(Members_truss, ...
          [c,(2*n-1)*(n+1)+2*(k+1),2*n^2+3*n+k]);
182   %            c=c+1;
183   %        end
184   %-----------------------------------
185   %-----------------------------------
186   %-----------------------------------
187
188   %% Adaptation of the contour
189
190   for k=1:n
191       xk=k*l/(n+1);
192       y1=y0-b*sqrt(1-(xk-x0)^2/a^2);
193       y2=y0+b*sqrt(1-(xk-x0)^2/a^2);
194       n1=floor(y1/(l/(n+1)));
195       n2=floor(y2/(l/(n+1)));
196           if (n1==0)
197           Nodes(k,3) = y1;
198
199           elseif(n1>0)&&(n1<n)
200           Deleted_nodes=vertcat(Deleted_nodes,[k]);
201               for j=1:(n1-1)
202               Deleted_nodes=vertcat(Deleted_nodes,[(2*j-1)*(n+1)+2*k-1]);
203               end
204           Nodes(((2*n1-1)*(n+1)+2*k-1),3) = y1;
205           Blocked_nodes=vertcat(Blocked_nodes,(2*n1-1)*(n+1)+2*k-1);
206
207           elseif (n1==n)
208          Deleted_nodes=vertcat(Deleted_nodes,[k]);
209               for j=1:(n1-1)
210               Deleted_nodes=vertcat(Deleted_nodes,[(2*j-1)*(n+1)+2*k-1]);
211               end
212           Nodes((2*n1-1)*(n+1)+2*k-1,3)=y1;        %-1 au lieu de +1
213           Deleted_nodes=vertcat(Deleted_nodes,[(2*n*n+3*n+k)]);
214           else
215
216               end
217
218           if (n2==n)
219               Nodes((2*n*n+3*n+k),3) = y2;
220           elseif(n2<n)&&(n2>1)
221           Deleted_nodes=vertcat(Deleted_nodes,[(2*n*n+3*n+k)]);
222               for j=1:(n-n2-1)
223               Deleted_nodes=vertcat(Deleted_nodes,[(2*(n+1-j)-1)*(n+1)+2*k-1]);
224               end
225           Nodes(((2*(n2+1)-1)*(n+1)+2*k-1),3)=y2;
226           Blocked_nodes=vertcat(Blocked_nodes,[(2*(n2+1)-1)*(n+1)+2*k-1]);
227           else
228           end
229   end
230
231   for k=1:n
232
233       yk=k*l/(n+1);
```

```
234      x1=x0-a*sqrt(1-(yk-y0)^2/b^2);
235      x2=x0+a*sqrt(1-(yk-y0)^2/b^2);
236      n1=floor(x1/(l/(n+1)));
237      n2=floor(x2/(l/(n+1)));
238
239      if (n1==0)
240          Nodes((2*k-1)*(n+1),2) = x1;
241      end
242
243      if (n1>0)&&(n1<n)
244          Deleted_nodes=vertcat(Deleted_nodes,[(2*k-1)*(n+1)]);
245          for j=1:(n1-1)
246              Deleted_nodes=vertcat(Deleted_nodes,[(2*k-1)*(n+1)+2*j]);
247          end
248          Nodes((2*k-1)*(n+1)+2*n1,2)=x1;
249          Blocked_nodes=vertcat(Blocked_nodes,[(2*k-1)*(n+1)+2*n1]);
250      end
251
252      if (n2==n)
253           Nodes((2*(k+1)-1)*(n+1)-1,2) = x2;
254      end
255      if (n2<n)
256          Deleted_nodes=vertcat(Deleted_nodes,[(2*(k+1)-1)*(n+1)-1]);
257          for j=1:(n-n2-1)
258              Deleted_nodes=vertcat(Deleted_nodes,[(2*(k+1)-1)*(n+1)-2*j]);
259          end
260          Nodes((2*(k+1)-1)*(n+1)-2*(n-n2),2)=x2;
261          Blocked_nodes=vertcat(Blocked_nodes,[(2*(k+1)-1)*(n+1)-2*(n-n2)]);
262      end
263  end
264
265  %The connection involving deleted nodes are deleted
266  Deleted_Truss=[];
267
268  for k=1:size(Members_truss)
269       if (ismember(Members_truss(k,2),Blocked_nodes))&& ...
             (ismember(Members_truss(k,3),Blocked_nodes))
270          Deleted_Truss=vertcat(Deleted_Truss,[Members_truss(k,1)]);
271       end
272  end
273
274  for k=1:size(Deleted_nodes)
275      A1 = sort(find(Members(:,2)==Deleted_nodes(k)),'descend');
276              for j=1:size(A1,1)
277              Members(A1(j,1),:)=[];
278              end
279      A2 = sort(find(Members(:,3)==Deleted_nodes(k)),'descend');
280              for j=1:size(A2,1)
281              Members(A2(j,1),:)=[];
282              end
283      A3 = sort(find(Members_truss(:,2)==Deleted_nodes(k)),'descend');
284              for j=1:size(A3,1)
285              Members_truss(A3(j,1),:)=[];
286              end
```

```matlab
287     A4 = sort(find(Members_truss(:,3)==Deleted_nodes(k)),'descend');
288             for j=1:size(A4,1)
289             Members_truss(A4(j,1),:)=[];
290             end
291     A5 = sort(find(Blocked_nodes==Deleted_nodes(k)),'descend');
292             for j=1:size(A5,1)
293             Blocked_nodes(A5(j,1),:)=[];
294             end
295     A6 = sort(find(Nodes(:,1)==Deleted_nodes(k)),'descend');
296             for j=1:size(A6,1)
297             Nodes(A6(j,1),:)=[];
298             end
299     A7=sort(find(Links(:,1)==Deleted_nodes(k)),'descend');
300      for j=1:size(A7,1)
301             Links(A7(j,1),:)=[];
302      end
303     A8=sort(find(Links(:,2)==Deleted_nodes(k)),'descend');
304      for j=1:size(A8,1)
305             Links(A8(j,1),:)=[];
306      end
307 end
308
309 for k=1:size(Blocked_nodes)
310     A1 = sort(find(Links(:,1)==Blocked_nodes(k)),'descend');
311         for j=1:size(A1,1)
312             Links(A1(j,1),:)=[];
313         end
314     A2 = sort(find(Links(:,2)==Blocked_nodes(k)),'descend');
315          for j=1:size(A2,1)
316             Links(A2(j,1),:)=[];
317         end
318 end
319 for k=1:size(Deleted_Truss)
320     A1 = sort(find(Members_truss(:,1)==Deleted_Truss(k)),'descend');
321     for j=1:size(A1,1)
322         Members_truss(A1(j,1),:)=[];
323     end
324 end
325
326 %% CREATION OF THE ADINA INPUT FILE %%
327
328
329 %% INPUT OF DATA
330
331 d1=input('Please insert the external diameter of the pipe, d[m]: ...
        ');%diameter in meter
332 t1=input('Please insert the thickness of the pipe t [m]: ');% thickness in ...
        meter
333 p1=input('Please insert the line load used for the form-finding [N/m]: ...
        ');% Used for form-finding, multiplication factor
334 Area=pi*(d1^2/4-(d1-t1)^2/4);
335 density=floor(50/(n+1));
336 %% ENTETE
337 fid=fopen('linecheck15.in','at');
```

```matlab
338  fprintf(fid, 'DATABASE NEW SAVE=NO PROMPT=NO\nFEPROGRAM ADINA\nCONTROL ...
         FILEVERSION=V88\n*');
339  fclose(fid);
340  %% DEFINE POINTS
341
342  fid=fopen('linecheck15.in','at');
343  fprintf(fid, '\n*\nCOORDINATES POINT SYSTEM=0\n@CLEAR');
344  fprintf(fid, '\n%d %d %d %d 0',Nodes');
345  fprintf(fid, '\n@');
346  fclose(fid);
347
348  %% DEFINE FIXITIES
349  fid=fopen('linecheck15.in','at');
350  fprintf(fid, '\n*\nFIXITY NAME=IN—PLANE\n@CLEAR\n ''Z—TRANSLATION''\n ...
         ''OVALIZATION''\n@');
351  fprintf(fid, '\n*\nFIXITY NAME=PINNED\n@CLEAR\n ''X—TRANSLATION''\n ...
         ''Y—TRANSLATION''\n ''Z—TRANSLATION''\n ''OVALIZATION''\n@');
352  fclose(fid);
353
354  %% APPLY BOUNDARY CONDITIONS TO POINTS
355  fid=fopen('linecheck15.in','at');
356  fprintf(fid,'\n*\n FIXBOUNDARY POINTS FIXITY=IN—PLANE\n@CLEAR');
357  fprintf(fid,'\n%d ''IN—PLANE''', Blocked_nodes');
358  fprintf(fid,'\n%d ''PINNED''', Blocked_nodes_1');
359  fprintf(fid,'\n@');
360  fclose(fid);
361
362  %% DEFINE LINKS
363  fid=fopen('linecheck15.in','at');
364  fprintf(fid, '\n*');
365  for k=1:size(Links)
366  fprintf(fid, '\n*\nRIGIDLINK NAME=%d SLAVETYP=POINT SLAVENAM=%d ...
         MASTERTY=POINT MASTERNA=%d,\n    DISPLACE=DEFAULT OPTION=0 SLAVEBOD=0 ...
         MASTERBO=0 DOF=ALL,\n    DOFSI=123',k,Links(k,1),Links(k,2));
367  end
368  fclose(fid);
369  %% CREATION OF THE MATERIAL
370  fid=fopen('linecheck15.in','at');
371  fprintf(fid, '\n*\nMATERIAL ELASTIC NAME=1 E=2.50000000000000E+10 ...
         NU=0.300000000000000,\nDENSITY=1.00000000000000 ALPHA=0.00000000000000 ...
         MDESCRIP=''GFRP''');
372  fprintf(fid, '\n*\nMATERIAL ELASTIC NAME=2 E=2.50000000000000E+09 ...
         NU=0.300000000000000,\nDENSITY=1.00000000000000 ALPHA=0.00000000000000 ...
         MDESCRIP=''GFRP—2''');
373  fclose(fid);
374
375  %% DEFINITION OF THE MODEL PROPERTIES
376  fid=fopen('linecheck15.in','at');
377  fprintf(fid,'\n*\nKINEMATICS DISPLACE=LARGE STRAINS=SMALL UL—FORMU=DEFAULT ...
         PRESSURE=NO,\nINCOMPAT=AUTOMATIC RIGIDLIN=NO BEAM—ALG=CURRENT ...
         KBEAM—EI=NO');
378  fclose(fid);
379
380  %% WRITE CROSS SECTION BLOCK
```

```matlab
381  fid=fopen('linecheck15.in','at');
382  fprintf(fid,'\n*\nCROSS—SECTIO PIPE NAME=1 DIAMETER=%d,\n      THICKNES=%d ...
         SC=0.00000000000000,\n       TC=0.00000000000000 ...
         TORFAC=1.00000000000000,\n      SSHEARF=0.00000000000000 ...
         TSHEARF=0.00000000000000 SOLID=NO',d1,t1);
383  %fprintf(fid,'\n*\nPROPERTYSET NAME=1 K=1.00000000000000E+08 ...
         M=0.00000000000000,\nC=0.200000000000000 S=0.00000000000000 NONLINEA=NO');
384  fclose(fid);
385  %% DEFINE ELEMENT TYPE
386  fid=fopen('linecheck15.in','at');
387  fprintf(fid,'\n*\nEGROUP BEAM NAME=2 SUBTYPE=THREE—D DISPLACE=DEFAULT ...
         MATERIAL=1 RINT=5,\nSINT=DEFAULT TINT=DEFAULT RESULTS=STRESSES ...
         INITIALS=NONE,\nCMASS=DEFAULT RIGIDEND=NONE MOMENT—C=NO ...
         RIGIDITY=1,\nMULTIPLY=1000000.00000000 RUPTURE=ADINA ...
         OPTION=NONE,\nBOLT—TOL=0.00000000000000 DESCRIPT=''NONE'' ...
         SECTION=1,\nPRINT=DEFAULT SAVE=DEFAULT ...
         TBIRTH=0.00000000000000,\nTDEATH=0.00000000000000 SPOINT=4 ...
         BOLTFORC=0.00000000000000,\nBOLTNCUR=0 TMC—MATE=1 BOLT—NUM=0 ...
         BOLT—LOA=0.00000000000000,\nWARP=NO ENDRELEA=ACCURATE');
388  fprintf(fid,'\n*\nEGROUP TRUSS NAME=3 SUBTYPE=GENERAL DISPLACE=DEFAULT ...
         MATERIAL=2,\nINT=DEFAULT GAPS=NO INITIALS=NONE ...
         CMASS=DEFAULT,\nTIME—OFF=0.00000000000000 OPTION=NONE RB—LINE=1 ...
         DESCRIPT=''STABILIZATION'',\nAREA=%f PRINT=DEFAULT ...
         SAVE=DEFAULT,\nTBIRTH=1000.00000000000 TDEATH=0.00000000000000 ...
         TMC—MATE=1,\nRUPTURE=ADINA GAPWIDTH=0.00000000000000', Area);
389  fprintf(fid,'\n*\nPSET—6DOF NAME=1 K1=1.00000000000000E+13 ...
         K2=1.00000000000000E+13,\n      K3=1.00000000000000E+13 ...
         K4=1.00000000000000E+01 K5=1.00000000000000E+01,\n      ...
         K6=0.00000000000000 NK1=0 NK2=0 NK3=0 NK4=0 NK5=0 NK6=0,\n      ...
         C1=0.00000000000000 C2=0.00000000000000 C3=0.00000000000000,\n      ...
         C4=0.00000000000000 C5=0.00000000000000 C6=0.00000000000000');
390  fprintf(fid,'\n*\nEGROUP SPRING NAME=1 PROPERTY=1 RESULTS=FORCES ...
         NONLINEA=NO,\n      SKEWSYST=NO OPTION=NONE DESCRIPT=''NONE'' ...
         PRINT=DEFAULT,\n      SAVE=DEFAULT TBIRTH=0.00000000000000 ...
         TDEATH=0.00000000000000,\n      6DOF—SPR=YES');
391  fclose(fid);
392
393
394  %% DEFINE LINE
395
396  fid=fopen('linecheck15.in','at');
397  fprintf(fid,'\n*\nLINE STRAIGHT NAME=%d P1=%d P2=%d',Members');
398  fprintf(fid,'\n*\nLINE STRAIGHT NAME=%d P1=%d P2=%d',Members_truss');
399  fclose(fid);
400
401  %% DEFINE TIME FUNCTION and TIME STEP
402
403  fid=fopen('linecheck15.in','at');
404  fprintf(fid,'\n*\nTIMESTEP NAME=DEFAULT\n@CLEAR\n20 50.00000000000\n3 ...
         500.00000000000\n@');
405  fprintf(fid,'\n*\nTIMEFUNCTION NAME=1 IFLIB=1 FPAR1=0.00000000000000,\n ...
           FPAR2=0.00000000000000 FPAR3=0.00000000000000,\n      ...
         FPAR4=0.00000000000000 FPAR5=0.00000000000000,\n      ...
         FPAR6=0.00000000000000');
```

```
406  fprintf(fid,'\n@CLEAR\n0.00000000000000 0.00000000000000\n400.000000000000 ...
         1.00000000000000\n700.00000000000 1.00000000000000\n800.00000000000 ...
         0.00000000000000\n1.00000000000000E+20 0.00000000000000\n@\n*');
407  fprintf(fid,'\n*\nTIMEFUNCTION NAME=2 IFLIB=1 FPAR1=0.00000000000000,\n ...
            FPAR2=0.00000000000000 FPAR3=0.00000000000000,\n     ...
         FPAR4=0.00000000000000 FPAR5=0.00000000000000,\n     ...
         FPAR6=0.00000000000000');
408  fprintf(fid,'\n@CLEAR\n0.00000000000000 0.00000000000000\n700.00000000000 ...
         0.00000000000000\n800.00000000000 ...
         1.00000000000000\n1.00000000000000E+20 1.00000000000000\n@\n*');
409  fclose(fid);
410
411  %% DEFINE MESH (SUBDIVISION OF THE BEAMS)
412  index=2*n*(n+1)+1;
413
414  fid=fopen('linecheck15.in','at');
415  fprintf(fid,'\n*\nSUBDIVIDE LINE NAME=%d MODE=DIVISIONS NDIV=%d ...
         RATIO=1.00000000000000,\n     PROGRESS=GEOMETRIC ...
         CBIAS=NO\n@CLEAR',Members(1,1),density);
416  fprintf(fid,'\n%d', Members(:,1)');
417  fprintf(fid,'\n@');
418  fprintf(fid,'\n*\nSUBDIVIDE LINE NAME=%d MODE=DIVISIONS NDIV=1 ...
         RATIO=1.00000000000000,\n     PROGRESS=GEOMETRIC ...
         CBIAS=NO\n@CLEAR',Members_truss(1,1));
419  fprintf(fid,'\n%d', Members_truss(:,1)');
420  fprintf(fid,'\n@');
421  fclose(fid);
422  %% CREATION OF THE ELEMENTS
423  Aux_point=c1+2;
424  %springs
425  fid=fopen('linecheck15.in','at');
426  fprintf(fid,'\n*\nSPRING-6DOF POINTS\n@CLEAR\n');
427  for k=1:size(Blocked_nodes)
428  fprintf(fid,'%d %d 0 0.0000000000 0.0000000000 0.0000000000 0 0  ...
         ,\n''DEFAULT''  ''DEFAULT'' 600.00000000000 ...
         0.00000000000000\n',k,Blocked_nodes(k,1)');
429  end;
430  fprintf(fid,'@');
431  fclose(fid);
432
433  %truss and beams
434  fid=fopen('linecheck15.in','at');
435  fprintf(fid,'\n*\nGLINE NODES=2 AUXPOINT=%d NCOINCID=ENDS NCENDS=12,\n     ...
         NCTOLERA=1.00000000000000E-05 SUBSTRUC=0 GROUP=2 MIDNODES=CURVED,\n ...
            XO=0.00000000000000 YO=0.00000000000000 ZO=0.00000000000000,\n     ...
         XYZOSYST=SKEW\n@CLEAR',Aux_point);
436  fprintf(fid,'\n%d', Members(:,1)');
437  fprintf(fid,'\n@');
438  fprintf(fid,'\n*\nGLINE NODES=2 NCOINCID=ENDS NCENDS=12 ...
         NCTOLERA=1.00000000000000E-05,\n     SUBSTRUC=0 GROUP=3 ...
         MIDNODES=CURVED XO=0.00000000000000,\n     YO=0.00000000000000 ...
         ZO=0.00000000000000 XYZOSYST=SKEW\n@CLEAR',(Aux_point));
439  fprintf(fid,'\n%d', Members_truss(:,1)');
440  fprintf(fid,'\n@');
```

```matlab
441  fclose(fid);
442
443  %% LOADS
444  fid=fopen('linecheck15.in','at');
445  fprintf(fid,'\n*\nLOAD MASS-PROPORTIONAL NAME=2 ...
        MAGNITUD=9.81000000000000,\n     AX=0.00000000000000 ...
        AY=0.00000000000000 AZ=-1.00000000000000,\n     INTERPRE=BODY-FORCE\n*');
446  fprintf(fid, '\n*\nLOAD LINE NAME=1 MAGNITUD=%d\n*',p1);
447  fprintf(fid, '\nAPPLY-LOAD BODY=0\n@CLEAR\n%d');
448  for k=1:(size(Members))
449      fprintf(fid, '\n%d',k);
450  fprintf(fid, '  ''LINE'' 1  ''LINE'' %d 0 1 0.00000000000000 13 1 %d 0 0  ...
        ''NO'',\n    0.00000000000000 0.00000000000000 1 0  ...
        ''MID''',Members(k,1),Aux_point);
451  end
452  fprintf(fid,'\n%d  ''MASS-PROPORTIONAL'' 2  ''MODEL'' 0 0 2 ...
        0.00000000000000 0 -1 0 0 0  ,\n''NO'' 0.00000000000000 ...
        0.00000000000000 1 0  ''MID''',(2*n*(n+1)+1));
453  fprintf(fid, '\n@');
454
455
456  fclose(fid);
457  %% SOLVER ETC.
458  fid=fopen('linecheck15.in','at');
459
460  fprintf(fid,'\n*\nAUTOMATIC TIME-STEPPING MAXSUBD=10 ACCURACY=NO,\n    ...
        DISTOL=0.00100000000000 DTMAX=3.00000000000000,\n    ...
        RESTORE=AUTOMATIC RESPS=YES RESFAC=0.000100000000000000,\n    ...
        DIVFAC=2.00000000000000 LSMASSF=1.00000000000000\n');
461  fprintf(fid, '\n*\nMASTER ANALYSIS=STATIC MODEX=EXECUTE ...
        TSTART=0.00000000000000 IDOF=0,\n    OVALIZAT=NONE FLUIDPOT=AUTOMATIC ...
        CYCLICPA=1 IPOSIT=STOP,\n    REACTION=YES INITIALS=NO FSINTERA=NO ...
        IRINT=DEFAULT CMASS=NO,\n    SHELLNDO=AUTOMATIC AUTOMATI=ATS ...
        SOLVER=SPARSE,\n    CONTACT-=CONSTRAINT-FUNCTION ...
        TRELEASE=0.00000000000000,\n    RESTART-=NO FRACTURE=NO LOAD-CAS=NO ...
        LOAD-PEN=NO SINGULAR=YES,\n    STIFFNES=0.000100000000000000 ...
        MAP-OUTP=NONE MAP-FORM=NO,\n    NODAL-DE='''' POROUS-C=NO ADAPTIVE=0 ...
        ZOOM-LAB=1 AXIS-CYC=0,\n    PERIODIC=NO VECTOR-S=GEOMETRY EPSI-FIR=NO ...
        STABILIZ=NO,\n    STABFACT=1.00000000000000E-10 RESULTS=PORTHOLE ...
        FEFCORR=NO,\n    BOLTSTEP=1 EXTEND-S=YES CONVERT-=NO DEGEN=YES ...
        TMC-MODE=NO,\n    ENSIGHT-=NO IRSTEPS=1 INITIALT=NO TEMP-INT=NO ...
        ESINTERA=NO,\n    OP2GEOM=NO INSITU-D=NO');
462
463  fclose(fid);
```